Design and Evaluation of a Slit Die Rheometer to Study Wall Slip

By

Martin Lamar Sentmanat

Department of Chemical Engineering
McGill University, Montreal

March 1992

A Thesis submitted to the Faculty of Graduate Studies and Research in partial fulfillment of the requirements of the degree of Masters of Engineering.

ABSTRACT

Extrudate distortion is a problem that often limits production rates in certain commercial processes such as film blowing and it has been suggested that slip in the die land plays an important role in this phenomena. It has been hypothesized that during slip flow in a die neither the wall shear stress nor the slip velocity is constant along the length of the die. For this reason, a slit die rheometer was developed to monitor directly the shear stress distribution of a molten polyethylene by means of two shear stress transducers mounted at different axial locations along the length of the slit. Previous transducers used at McGill do not perform well at high pressures. Therefore, a new disk-bar shear stress transducer was designed for use at high pressure. However, experimental evaluation of the slit die rheometer suggests that the large pressure gradient present in the slit affects the operation of this transducer. It is hypothesized that the pressure gradient across the active face of the shear stress transducer and the disk element impose a torque opposite to that of the applied shear stress on the active face. This pressure gradient effect was unanticipated because no shear stress transducer has ever been used in a pressure driven flow. Before the research on wall slip can proceed a new shear stress transducer that is unaffected by either high pressure or large pressure gradients must be developed. Possible ways of meeting this need are proposed

RÉSUMÉ

La distortion d'un échantillon extrudé est un problème qui limite souvent les taux de production dans certains procédés commerciaux comme le soufflage de film. Cet inconvénient semble essentiellement dû au phénomène de glissement dans la filière En effet, on suppose que, pendant l'écoulement d'un polymère dans une filière, ni la contrainte de cisaillement, ni la vitesse de glissement n'est constante sur toute la longueur de la filière C'est pourquoi, un rhéomètre pour filière à fente a été développé. Le contrôle s'effectue grâce à deux capteurs de contrainte de cisaillement montés à différents endroits le long de l'axe de la fente. Les capteurs utilisés auparavant à l'Université McGill ne sont pas performants aux pressions élevées ce qui entraine l'utilisation d'un nouveau capteur a disque-barre, résistant à haute pression. Cependant, l'évaluation experimentale du rhéomètre semble indiquer que l'ampleur du gradient de pression dans la fente altere les performances de ce capteur. On suppose que le gradient de pression le long de la face active du capteur et d'un disque crée un couple de torsion opposé à celui engendré par la contrainte de cisaillement Ce problème dû au gradient de pression était imprévu car aucun capteur de contrainte de cisaillement n'a jamais été utilisé lors d'un écoulement provoque par une différence de pression. Avant de développer une recherche sur le glissement de surface contre un mur, un nouveau capteur, insensible aux hautes pressions et aux gradient de pression élevés doit être développé. Pluieurs solutions répondant à ces besoins sont proposées.

DEDICATION

To my parents, José Manuel and Caridad Pelayo Sentmanat:
Gracias por todo, Mami y Papi.

This material is based upon work supported under a National Science Foundation (U.S.A.) Graduate Fellowship. Any opinions, findings, conclusions or recommendations expressed in this publication are those of the author and do not necessarily reflect the views of the National Science Foundation.

ACKNOWLEDGEMENTS

I would like to first of all express my enormous gratitude to my supervisor Professor John M. Dealy. Through his wisdom, I had the incite to understand my goals; through his support, I had the confidence to strive for my goals; through his patience, I had the time to realize my goals; and through his decency, I never had to hear the words, "What have I gotten myself into?" Thank you Professor Dealy. I can only hope he will be as excellent a PhD supervisor as he was a M.Eng. supervisor.

Secondly, I would like to acknowledge the tremendous amount of support I received from my colleague and great friend Dr. Savvas G. Hatzikiriakos Through his presence, I was given the opportunity to benefit from his genius. Savvas is the best.

Next, I would like to acknowledge the gentleman who made this all possible, Dr. A. Jeffrey Giacomin. It was Jeff who challenged me to expand my horizons and 'bravely go were no Texas A & M Aggie had gone before.' I am forever indebted to him for all he has done for me. He is a great mentor and even greater friend.

Mr Walter Greenland must be acknowledged for his masterful skill in fabricating the slit die rheometer. I would also like to thank my good friends Paul Lageraaen and John and Anita Campanelli for being such great friends and providing the moral support throughout the fourteen months here at McGill. They have made my stay here in Montreal an enjoyable one.

Likewise, I would like to thank my best friend back home in Conroe, Texas, Mark D Cook and the rest of the Cook family (Doug, Dale, and Todd) for their long distance moral support. They are my second family, and I've really missed them.

Finally, I would like to thank my family back home: Mom, Dad, Joe, Jacqui, Kary and Mark. Without their support and understanding, I would have never made it. I love them and miss them all tremendously.

TABLE OF CONTENTS

LIST OF FIGURES AND TABLES

NOMENCLATURE

a = disk outside radius

A = slip coefficient

b = cross sectional bar width dimension

c = temperature constant in reaction rate

c_1, c_2 = slip velocity equation constants

c_3 = energy constant for E_w

C_2, C_5 = constants dependent on the ratio r_0/a

C_1^0, C_2^0 = fitted constants of the function f_1

d = disk deflection parameter

D = capillary diameter

e = equivalent L/h value used in the Bagley correction

E = activation energy

E_M = elastic modulus

E_w = activation energy barrier between bonded and free states

F = force

f_1, f_2 = slip coefficient functions

G = shear modulus

h = slit channel height

H = cross sectional bar height dimension

I = polydispersity

I_b = moment of inertia of bar

K = power law coeffient of a polymer

k_1, k_2 = reaction rates

L = slit channel length

L_3, L_6, L_{11}, L_{14}= constants dependent on the ratio r_0/a

L_b = rectangular bar length

m = slip power law parameter

M = magnitude of imposed moment, or torque

M_f = mass flowrate

M_n = number average molecular weight

M_w = weight average molecular weight

n = power law exponent of a polymer

N_1 = first normal stress difference

N_2 = second normal stress difference

P = pressure

P_1 = capacitance probe 1

P_2 = capacitance probe 2

ΔP = pressure drop across length of slit channel

P_{dr} = driving pressure of rheometer

P_{en} = entrance pressure loss due to entrance into slit channel

q = magnitude of uniformly distributed pressure

Q = volumetric flow rate

r = capillary radius

R = universal gas constant

r_0 = disk inside radius

t = disk thickness

T = temperature

T_0 = reference temperature

u_s = slip velocity

w = magnitude of concentrated load
W = slit channel width
$(\ )_w$ = value at the wall
x,y,z = Cartesian coordinates
Y = magnitude of axial deflection
Z_1 = upstream axial position in slit shannel
Z_2 = downstream axial position in slit channel

α = constant dependent on the ratio r_0/a
β = compressibility
$\dot{\gamma}_A$ = apparent wall shear rate
$\dot{\gamma}_{A,s}$ = apparent wall shear rate corrected for slip
θ = magnitude of angular deflection
ν = poisson's ratio
ξ, ξ_0 = slip velocity constants
ρ_0 = reference density
σ = stress
σ_n = magnitude of wall normal stress
σ_w = magnitude of wall shear stress
σ_{xx} = principal stress in the x direction
σ_{xy} = shear stress
σ_{yy} = principal stress in the y direction
σ_{zz} = principal stress in the z direction
σ_{c1} = first critical shear stress
σ_{c2} = second critical shear stress
ϕ_A = ratio of torque produced by pressure gradient acting on the active face to the torque

produced by shear stress

Φ_D = ratio of torque produced by pressure gradient acting on the disk element to the torque produced by shear stress

CHAPTER 1

INTRODUCTION

1.1. Background

1.1.1. Extrudate Distortion

A major problem that can arise in polymer melt processing is the phenomenon of extrudate distortion, which is manifested in a variation of shape along the direction of flow and is often the factor that limits production rates in certain commercial processes such as film blowing. This effect, often termed melt fracture, can vary in intensity from a loss of surface gloss, commonly referred to as surface melt fracture, to severe distortion, commonly referred to as gross melt fracture. This issue has spurred many investigators to study and attempt to describe the mechanisms involved in extrudate distortion.

1.1.2. Apparent Flow Curve of Linear Polymers

In order to understand the rheology of a particular polymer, an apparent flow curve obtained by means of a capillary rheometer is often used in which wall shear stress is plotted as a function of the apparent shear rate, $\dot{\gamma}_A$, defined as $4Q/\pi r^3$. Figure 1.1 is a typical apparent flow curve for a linear polymer such as high density polyethylene. At very low apparent shear rates (typically below 1 s^{-1}) the wall shear stress is proportional to the apparent shear rate, and the viscosity is thus constant. This is followed by a transition region where the viscosity starts to decrease and then approaches power law behavior.

Beyond a certain average critical shear stress, σ_{c1}, a change of slope is observed in

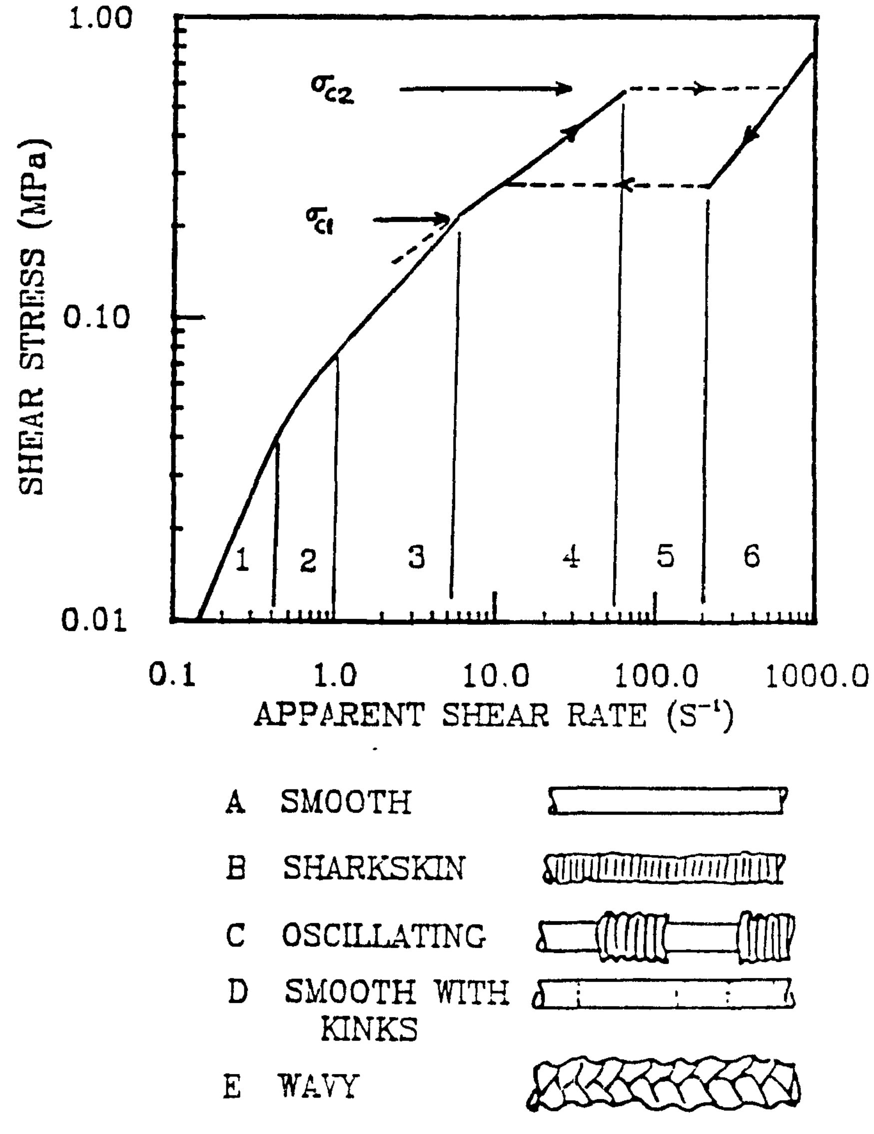

Fig. 1.1: Typical Apparent Flow Curve for a Linear Polymer (HDPE or LLDPE) and Various Extrudate Distortions

the flow curve for some polymers. In 1967, Vinogradov and Ivanova (1) observed this change of slope in the flow curve for shear stresses greater than σ_{c1} and noted that the slope was dependent on the diameter of their capillaries. In his capillary and slit die experiments with several linear and branched polyethylenes, Ramamurthy (2) found this critical wall shear stress, σ_{c1}, to be around 0.1 MPa and concluded that this value is independent of the molecular structure (molecular weight, molecular weight distribution, and branching), melt temperature, and the detailed design of the capillary.

At a second critical wall shear stress value, σ_{c2}, and within a certain range of apparent shear rates the flow ceases to be stable and oscillating flow is observed at a constant plunger speed. Ramamurthy (2) reported this second critical wall shear stress, σ_{c2}, to be about 0.43 MPa, and noted the onset of oscillating flow. Atwood and Schowalter's (3) 1989 slit die experiments with hot film probe anemometers yielded similar results. Bagley and co-workers (4) observed that under these flow conditions the pressure drop oscillates between two extreme values, causing a discontinuity in the flow curve resulting in a hysteresis effect. At shear stresses beyond the second critical wall shear stress, σ_{c2}, another change of slope in the flow curve occurs and flow again becomes stable.

1.1.3. Extrudate Appearance

The appearance of the extrudate varies considerably as the flow rate is increased. The extrudate is smooth at the lowest shear rates but begins to exhibit small-scale roughness, often called sharkskin, as the flow rate increases. Ramamurthy (2) associated the onset of sharkskin with the change of slope in the flow curve at σ_{c1}. However, other investigators such as Beaufils (5) and Becker (6) have noted extrudate distortion at lower flow rates

In the case of oscillatory flow at constant plunger speed, the extrudate appearance varies in a cyclical manner in accordance with the periodicity of the reservoir pressure. The extrudate obtained during one cycle in the oscillatory extrusion of linear polyethylenes consists of two segments of distinctly different appearance. Lupton and Regester (7) and

Ramamurthy (2) reported that a relatively smooth segment exhibiting sharkskin is associated with the ascending portion of the pressure waveform, and a rougher segment is associated with the descending portion of the waveform

Stresses just above σ_{c2} are associated with extrudates that exhibit a large swell ratio and are relatively smooth with some kinks. At somewhat higher stresses, the onset of gross melt fracture is observed accompanied with a decrease in the swell ratio.

1.1.4. Wall Slip

As mentioned before, when wall shear stress is plotted as a function of apparent shear rate for various die diameters, the data do not fall onto a single curve beyond the region of the first critical wall shear stress, σ_{c1}. This has led investigators to suspect slip in the die land region, in which the melt no longer adheres to the die wall, as a possible cause of melt fracture. It was Vinogradov and Ivanova (1) who proposed that in the case of polymers displaying melt fracture, wall slippage occurs and that it increases with increasing shear stress. In 1980, Kraynik and Schowalter (8) conducted experiments to study slip behavior with hot film probe anemometers. From their heat flux measurements, they inferred wall slippage and concluded that this slippage decreases the momentum transfer and increases the heat flux. It is important to note that when slip occurs, it renders the usual steady flow equations invalid; the velocity of the melt at the wall interface is not zero but equal to a value termed the slip velocity A technique referred to as the Mooney analysis can be used to determine the slip velocity as a function of wall shear stress By correcting the apparent wall shear rate, the stresses above the first critical wall shear stress, σ_{c1}, collapse onto a single curve that often follows a power law model Ramamurthy (2), following Lupton and Regester (7), used a Mooney analysis to estimate wall slip velocities for various die geometries in the stress versus strain rate curve region beyond the average critical wall shear stress for the onset of surface melt fracture. Although there are dissimilarities in these reported values, this is most likely due to the fact that different polymers were used as well as different experimental methods.

It has been found that with increasing channel length to height ratio, the slip velocity becomes invariant with any further increase of this ratio. Vinogradov and Ivanova (9) first noticed this in their study of elastomer capillary flows in 1968. Recently, Hatzikiriakos and Dealy (10) have presented similar results based on their capillary die experiments with high density polyethylenes. Thus, beyond a certain critical length to diameter ratio, Hatzikiriakos and Dealy found that the slip velocity remained approximately constant. It is important to note that Hatzikiriakos and Dealy modified the Mooney technique to take into account that neither the wall shear stress nor the slip velocity are constant along the length of the die.

1.1.5. Local Phenomena

Although several attempts have been made to understand the phenomenon of wall slip, most studies have considered wall slip to be a global phenomenon in the die land region as opposed to a local phenomenon that varies along the length of the channel. In 1967, Vinogradov and Ivanova (1) proposed that wall slippage of viscoelastic media in capillaries depends on the pressure within the die land so that the slip velocity increases with the length of the channel; however, their experimental test of this hypothesis yielded inconclusive results.

In 1991, White et al. (11), performed experiments on various elastomers between rotating plates under varying levels of applied pressure. They concluded that slip occurred to a higher degree under lower applied pressures but that the incremental effect of pressure on slip diminished above a certain applied pressure. Thus, the original hypothesis proposed by Vinogradov and Ivanova (1) in 1967 merits further consideration in the study of wall slip phenomena. Hatzikiriakos and Dealy (10) assumed a pressure-dependent slip in their capillary flow model and to analyze the results of their capillary flow experiments with high density polyethylene.

Most observations of extrudate distortion have been made with capillary flows generated by a piston moving at a constant speed in a reservoir above the capillary. The shear stress at the wall can be indirectly calculated as a function of the pressure gradient within the die channel. This is quite straight forward if the pressure gradient along the die channel is constant, i.e., if there is a linear pressure profile along the channel. But, it has been suggested by some investigators that the pressure profile within the die land is nonlinear. In 1983, Laun (12) suggested a nonlinear longitudinal pressure profile within the flow channel. He concluded that the deviation from the linear pressure profile is significant at high shear rates or high pressure ranges, and that the pressure profile within the channel best fits a parabolic profile; he attributed the variation in the pressure gradient to the effect of pressure on viscosity.

It has been suggested by Hatzikiriakos and Dealy (10) after Vinogradov and Ivanova (1) that the slip velocity is actually a function of the pressure within the die. They have proposed that the slip velocity increases with increasing distance along the die, so that the local shear stress at the wall decreases along the length of the die. However, the only way to verify this hypothesis is to measure directly the local wall shear stress along the die

1.2. Objectives

The primary objective of this research was to design and construct a slit die rheometer to study the wall shear stress distribution of a molten high density polyethylene. This was to be accomplished by mounting two shear stress transducers in contact with the polymer melt flow so that they could monitor directly the shear stress at two axial locations. The second objective was to evaluate the performance of the newly developed slit die rheometer especially the shear stress transducers.

CHAPTER 2

THEORY

Before the development of any experimental apparatus, it is important to obtain a fundamental understanding of the elements involved. For this reason, this chapter presents the fundamental concepts and theories of polymer flow through a channel It should be pointed out that the verification of the slip model proposed by Hatzikiriakos and Dealy (10) and discussed at the end of this chapter was the primary motivation behind the development of the new slit die rheometer

2.1. Fluid Flow Through a Channel

One of the simplest fluid flow problems is steady, pressure driven flow through a straight channel under no-slip conditions This situation is of central importance in polymer melt processing since it arises in processes such as extrusion and injection molding In this type of flow, the velocity field is generated by applying an external pressure to the fluid while the flow boundaries of the system are rigid and stationary In most rheological studies this type of flow is generated with the use of a piston-driven, capillary melt rheometer in which melt is forced through a capillary or slit die. We consider here the flow in a slit with the geometry shown in Fig 2.1

2.1.1. Shear Stress at the Wall

A force balance on a rectangular element of fluid of the slit neglecting acceleration yields a relationship between the shear stress and the pressure gradient:

$$\sigma(y) = \sigma_{xy}(y) = y\left(\frac{dP}{dz}\right) \tag{2.1}$$

The magnitude of the shear stress at the wall, σ_w, is then:

$$\sigma_w = -\sigma(y = h/2) = \frac{h}{2}\left(-\frac{dP}{dz}\right) \tag{2.2}$$

noting that the pressure gradient within the channel is negative. Further, under these conditions the pressure gradient along the channel is constant, so that:

$$\sigma_w = -\frac{h}{2}\frac{\Delta P}{L} \tag{2.3}$$

where **ΔP** is the pressure drop for a length, **L,** of the channel.

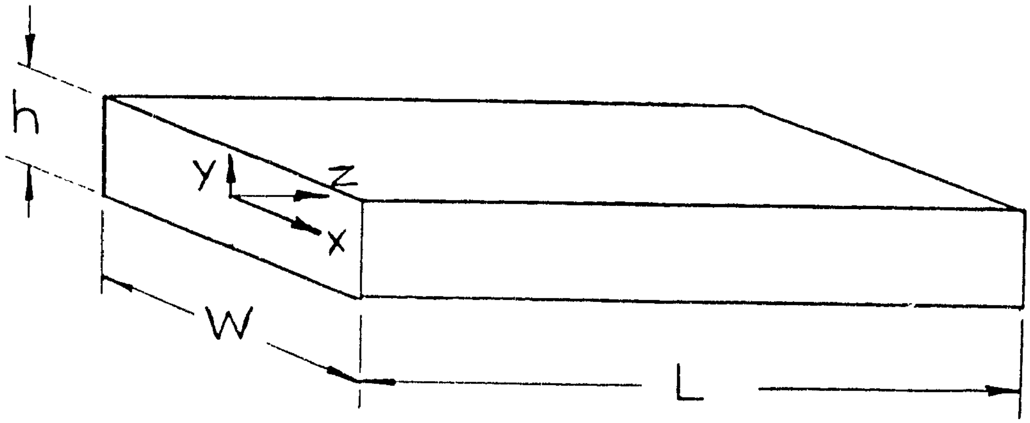

Fig. 2.1: Slit Flow Geometry

In a capillary or slit rheometer, the quantities usually measured are the driving pressure and the piston speed To determine the apparent flow curve, the end correction, or entrance pressure loss from the rheometer reservoir into the die, must be determined as a function of the apparent shear rate by making use of a Bagley plot. This involves plotting the driving pressure (plunger force over reservoir area) as a function of the **L/h** ratio for several values of the apparent shear rate, which is defined as follows:

$$\dot{\gamma}_A = \frac{6Q}{h^2 W} \tag{2.4}$$

where **Q** is the volumetric flow rate, **h** is the channel height and **W** is the channel width. By extrapolating to zero **L/h** or to zero driving pressure, the Bagley correction can be determined in terms of either an entrance pressure loss, $\mathbf{P}_{en}$, or an equivalent **L/h** value, **e**, as follows:

$$\sigma_w = \frac{P_{dr} - P_{en}}{2L/h} = \frac{P_{dr}}{2(L/h + e)} \tag{2.5}$$

It should be noted that at lower shear rates, the data usually follow straight lines, whereas at higher apparent shear rates the data follow curved lines Laun (12) and Laun and Schuch (13) observed these curved lines in their Bagley plots for LDPE melts and attributed this occurrence to the effect of pressure on viscosity at the higher apparent shear rates. Hatzikiriakos and Dealy (10) also observed such curved lines in their capillary experiments with HDPE but at apparent shear rates an order of magnitude less than those observed by Laun and Shuch. However, the apparent shear rates observed by Hatzikiriakos and Dealy (14) are above those in which slip was observed in their sliding plate rheometer studies. They also reported that the pressures in which they performed their capillary experiments were below those at which a significant effect of pressure on viscosity would be expected. Thus, they concluded that the curvature of their Bagley plots at higher apparent shear rates was due primarily to the effect of pressure on the slip velocity of the melt, a topic that will be discussed further in the following sections.

2.1.2 The Wall Shear Rate

If the fluid exhibits power law behavior, in which:

$$\sigma_w = K\left(\frac{2n+1}{3n}\right)(\dot{\gamma}_A)^n \tag{2.6}$$

where **n** and **K** are the power law parameters, then a plot of the logarithm of the apparent wall shear rate versus the logarithm of the wall shear stress, σ_w, will result in a straight line with a slope equal to **n**, assuming no-slip conditions.

2.1.3. The Mooney Technique for Determining the Slip Velocity

As mentioned in Chapter 1, beyond a critical wall shear stress, σ_{c1}, a change of slope occurs in the flow curve which is attributed to slip in the die land region. It was Mooney (15) who first developed a technique to determine the slip velocity when $\sigma_w > \sigma_{c1}$. The basis for the Mooney technique is the following equation:

$$\dot{\gamma}_{A,s} = \dot{\gamma}_A - 6\frac{u_s}{h} \tag{2.7}$$

where $\dot{\gamma}_{A,s}$ is the apparent wall shear rate corrected for slip, and $\mathbf{u_s}$ is the slip velocity. This equation is based on the assumption that the wall shear stress, slip velocity and pressure gradient are constant along the length of the channel. When this is true, a plot of $\dot{\gamma}_A$ versus **1/h**, using data at a constant shear stress, will give a straight line whose slope is equal to $6\mathbf{u_s}$.

2.1.4. Dependence of Flow Curve on Pressure

Hatzikiriakos and Dealy (10) in their capillary experiments with polyethylene melts reported that beyond the critical shear stress $\sigma_{c1,}$ the flow curve depended on both the diameter of the capillary and on the length to diameter ratio. They said that this implies that slip occurs in the die land region and that the slip velocity depends on pressure as well as wall shear stress. They hypothesized that this dependence was not directly on pressure, which was defined as the mean normal stress, but on the stress acting normal to the wall, which can be defined as:

$$\sigma_n \equiv \left(-\sigma_{yy}\right)_w \tag{2.8}$$

Thus, since this normal stress varies with axial distance in the channel, it would follow that the slip velocity and wall shear stress also vary with axial distance. If this is indeed true, then Equation (2.3) as well as the conventional Mooney technique would no longer be valid. Hatzikiriakos and Dealy (10) modified the Mooney technique taking into account the effect of wall normal stress on slip velocity to interpret their capillary flow data.

2.2. Slip Velocity Model

In their development of a slip velocity model for a high density polyethylene, Hatzikiriakos and Dealy (10,14) found the slip velocity to be a function of wall shear stress, temperature, pressure, and molecular weight distribution. The following sections will describe these effects in greater detail.

2.2.1. Temperature Dependence

The effect of temperature on the slip velocity of a high density polyethylene was studied by Hatzikiriakos and Dealy in their sliding plate rheometer studies. They found that for a given temperature for shear stresses beyond the critical shear stress, $\sigma_{c1,}$ the slip velocity could be represented by a power law relationship:

$$u_s = A\sigma_w^m \tag{2.9}$$

The slip coefficient, **A**, was found to depend strongly on temperature, while the power law parameter, **m**, was virtually independent of temperature. Data for capillary flow of the same high density polyethylene were also found to follow such a power law. While the power law parameter, **m**, was practically the same in both studies, the values for the slip coefficient, **A**, for the capillary experiments were about an order of magnitude lower than those found with the sliding plate. To account for this difference, Hatzikiriakos and Dealy proposed that the slip coefficient depends on the wall normal stress:

$$A = \xi f_1(T) f_2(T, \sigma_n/\sigma_w) \tag{2.10}$$

where ξ is a constant that depends on the molecular structure of the polymer, and σ_n is the magnitude of the wall normal stress. The function $f_1(T)$ includes most of the temperature dependency, while f_2 is a relatively weak function of temperature. They then found that the form of the WLF equation, which is often used to describe the temperature dependence of viscosity of many polymers at or above glass transition temperature, gave a good fit to describe the temperature dependence of the function f_1:

$$\log\left(f_1(T)\right) = \frac{C_1^o(T - T_0)}{C_2^o + (T - T_0)} \tag{2.11}$$

where C_1^0 and C_2^0 are constants to be fitted to data and T_0 is a reference temperature.

2.2.2. Pressure Dependence

In 1986, Lau and Schowalter (16) modeled the slip velocity as a function of wall shear stress and temperature by applying the concept of junctions at the polymer-wall interface. Their model was combined with a kinetic equation describing a reaction between bonded and free macromolecules at the interface to give:

$$u_s = c_1 \sigma_w^{m} \left[1 - c_2 \frac{k_2 - k_1}{k_1 + k_2} \right] \tag{2.12}$$

where c_1 and c_2 are constants and k_1 and k_2 are the specific rate constants for the bonded state to free state reaction and free state to bonded state reactions, respectively. Hatzikiriakos and Dealy (10), following Lau and Schowalter, proposed a model on the basis of an activation rate theory and introduced the effect of pressure on the activation energy. They proposed that when the quantity σ_n is elevated, the activation energy for the bonded state to free state reaction is increased by an amount E_w and the activation energy for the transition from the free state to the bonded state is decreased by the same amount, E_w, arguing that in order for a molecule to jump from a bonded state to a free state at a higher value of σ_n, it needs to overcome a higher energy barrier. However, a higher shear stress at a constant σ_n should cause a decrease in the activation energy, because the energy barrier for one molecule to jump from a bonded state to a free state under the action of a higher shear stress should be lower. Thus, they hypothesized that:

$$E_w = c_3 \frac{\sigma_n}{\sigma_w} \tag{2.13}$$

where c_3 is a constant with units of energy. Therefore the specific reaction rates can be written:

$$k_1 = c(T) \exp\left[-\frac{E + E_w}{RT} \right] \tag{2.14}$$

$$k_2 = c(T)\exp\left[\frac{E+E_w}{RT}\right] \tag{2.15}$$

where **c(T)** is a function of temperature taken to be the same for both specific reaction rates, **T** is the absolute temperature, and **R** is the universal gas constant. Combining these relationships, Hatzikiriakos and Dealy proposed a slip velocity model of the following form:

$$u_s = \xi f_1(T)\left[1 - c_2\tanh\left(\frac{E+c_3\sigma_n/\sigma_w}{RT}\right)\right]\sigma_w^{\,m} \tag{2.16}$$

2.2.3. Dependence on Molecular Characteristics

In their capillary rheometer studies, Hatzikiriakos and Dealy noted that beyond the **L/D** ratio of 60 there is no further effect of **L/D** ratio, i.e. pressure, on slip velocity. Thus, using capillaries with **L/D** ratios greater than 60, they found that the slip velocity increases with molecular weight while the critical shear stress for the onset of slip, σ_{c1}, decreases. They also found that increasing the polydispersity of the polymer suppresses slip. Vinogradov, et al. (17) in 1984 and Lin (18) in 1985 presented similar results in which they reported that monodisperse polymers are more likely to fracture and slip. Based on these observations, Hatzikiriakos and Dealy modified Equation (2.16) to give the following slip velocity model:

$$u_s = \xi_0 f_1(T)\left[1 - c_2\tanh\left(\frac{E+c_3\sigma_n/\sigma_w}{RT}\right)\right]\left(\frac{\sigma_w}{\sigma_{cl}I^{1/4}}\right)^m \tag{2.17}$$

where ξ_0 is a constant with dimensions of velocity, σ_{c1} is the critical shear stress for the onset of slip which depends on the molecular weight of the polymer, and **I** is the polydispersity of the polymer (M_w/M_n).

2.3. Model for Slit Die Flow Under Slip Conditions

It is important in experimental research to develop a theoretical model that will guide the study of the system under consideration. As is often the case in complex flow problems, an analytical solution is unattainable, and the use of numerical techniques is necessary to obtain a solution to the governing differential equations The model presented in this section is based on one previously developed by Hatzikiriakos and Dealy (10) for capillary die flow, but it has been modified for slit die flow. The results they obtained were generated by a Galerkin finite element program; thus with minor modification of the governing differential equations and boundary conditions, results comparable to those of Hatzikiriakos and Dealy could be obtained.

2.3.1. Momentum and Mass Balances

If we assume steady, creep flow and an inertial control volume, the momentum equation in integral form reduces to:

$$0 - 2\int_0^{H/2} \frac{\partial \sigma_{yz}}{\partial y} W\,dy + 2\int_0^{H/2} \frac{\partial \sigma_{zz}}{\partial z} W\,dy \qquad (2.18)$$

Now, recognizing that the stresses σ_n and σ_{zz} have been introduced in the slip velocity and momentum equations, respectively, it would be preferable to put these stresses in terms of some measurable quantities, specifically, the wall shear stress, σ_w, and pressure, **P**. Therefore, we must introduce the following definitions:

$$P \equiv -\frac{(\sigma_{xx} + \sigma_{yy} + \sigma_{zz})}{3} \tag{2.19}$$

$$N_1 \equiv \sigma_{zz} - \sigma_{yy} \tag{2.20}$$

$$N_2 \equiv \sigma_{yy} - \sigma_{xx} \tag{2.21}$$

If we recall Eq.(2.8),

$$\sigma_n \equiv \left(-\sigma_{yy}\right)_w \tag{2.8}$$

σ_n can then be defined in terms of pressure and the first and second normal stress differences, $\mathbf{N_1}$ and $\mathbf{N_2}$, respectively.

$$\sigma_n = P + \frac{N_1 - N_2}{3} \tag{2.22}$$

In order to reduce this further, the dependence of $\mathbf{N_1}$ and $\mathbf{N_2}$ on σ_w must be determined. However, these values are very difficult to obtain especially at high values of σ_w. For this reason, two approximations with somewhat uncertain validity must be used. In 1983, Ramachandran and Christiansen (19) proposed, as a first approximation, that:

$$N_2 = -\frac{1}{4}N_1 \tag{2.23}$$

Moreover, in 1976, Han (20), based on his studies of high density polyethylenes at shear stresses greater than 0.1 MPa, proposed that:

$$N_1 = 10\,\sigma_w \tag{2.24}$$

Thus, based on these empirical relationships we can arrive at an expression for the magnitude of the wall normal stress, σ_n in terms of pressure, **P**, and the magnitude of the wall shear stress, σ_w:

$$\sigma_n = P + \frac{50\sigma_w}{12} \tag{2.25}$$

Therefore, the momentum and slip velocity equations can be expressed in terms of the wall shear stress, σ_w and pressure, **P**.

From conservation of mass, assuming the lubrication approximation, we obtain the following relationship:

$$\frac{M}{\rho_0(1+\beta P)} = \left(\frac{h^2W}{2}\right)\left(\frac{1}{2+1/n}\right)\left(\frac{\sigma_w}{K}\right)^{\frac{1}{n}} + Whu_s \tag{2.26}$$

where the right hand side of the equation is merely the volumetric flow rate obtained by integrating the velocity profile over the cross sectional area of the slit channel, and the left hand side of the equation is the mass flow rate, **M**, calculated from the plunger speed of the rheometer, divided by the density as a function of pressure.

2.3.2. Simulation Results

The slip velocity model, the momentum equation and the mass balance equation can now be solved numerically for a fluid exhibiting power law behavior through a rectangular channel or slit die. It is important to note that this model predicts that σ_w varies markedly with z when there is slip. Fig. 2.2 shows the pressure, wall shear stress and slip velocity as functions of channel length, as calculated using this model for the specified parameters. These results were used in determining the positioning of the shear stress transducers in the slit flow channel, as will be explained further in Chapter 3.

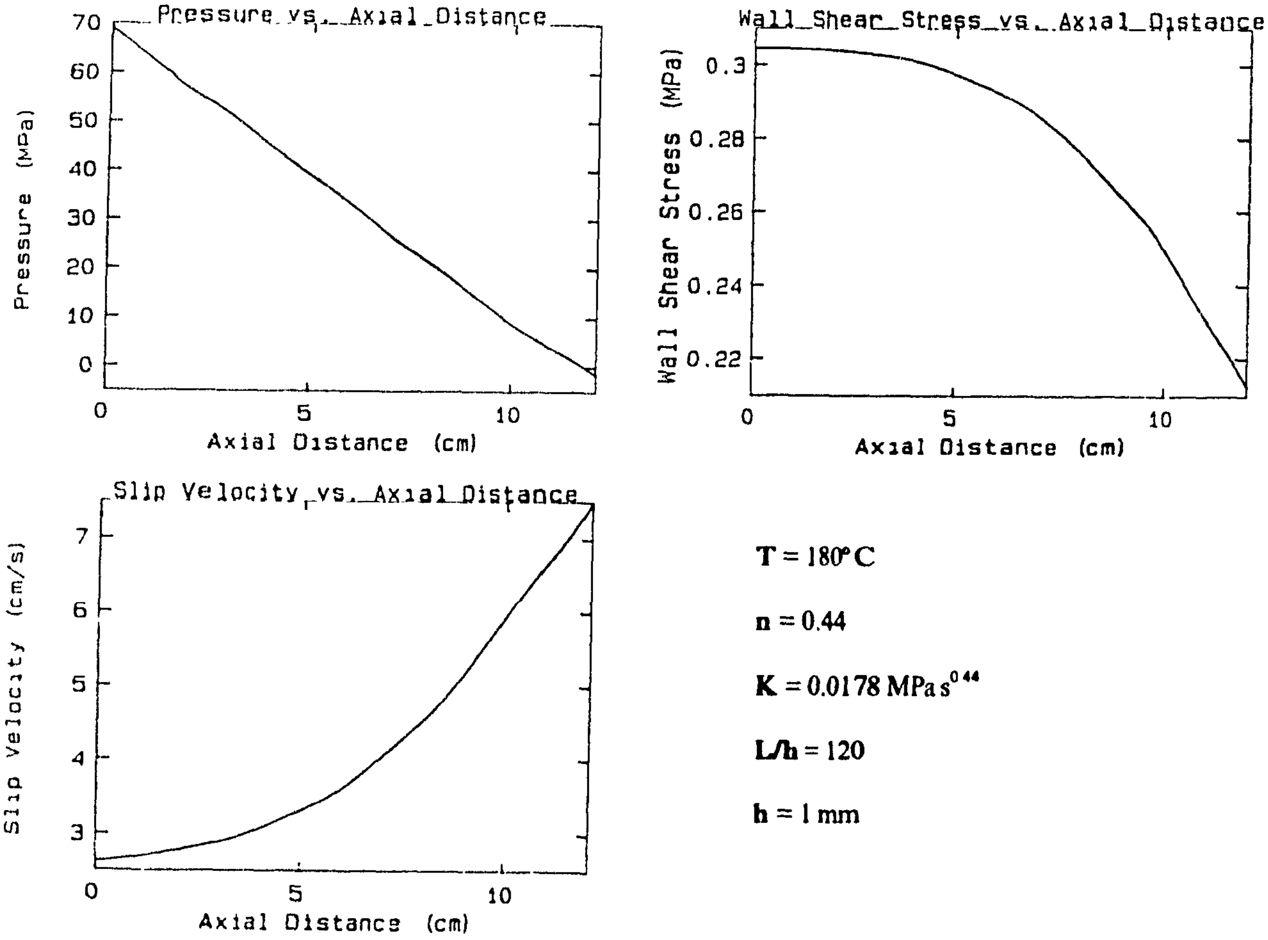

$T = 180°C$

$n = 0.44$

$K = 0.0178\ \mathrm{MPa\,s}^{0.44}$

$L/h = 120$

$h = 1$ mm

Fig. 2.2: Slip Model Results and Specified Model Parameters

CHAPTER 3

EQUIPMENT

In this chapter we will describe the slit die rheometer designed for the study of wall slip of a molten high density polyethylene. The operation of the equipment will be discussed in Chapter 4.

3.1. The Slit Die

The reason a slit die rather than a capillary was chosen for this research is the fact that the flat wall surface makes it possible to incorporate flush mounted shear stress and pressure transducers in the rheometer. In addition, this geometry makes it easy to coat one or both side walls and to clean these surfaces.

3.1.1. Slit Channel Dimensions

A relative disadvantage of the slit geometry is that, unlike a capillary die, a slit die has edges where the velocity is dependent on the **x** and **y** coordinates. But, if the width to height ratio of the slit, **W/h**, is sufficiently large, the effect of these edges can be assumed negligible with respect to the bulk flow. For this reason, Hatzikiriakos developed a two-dimensional steady flow model for flow in a slit [$\mathbf{u}_z = f(\mathbf{x},\mathbf{y})$] to determine the width to height ratio, **W/h**, at which edge effects are negligible. For a **W/h** of 10, the model predicts that 95% of the bulk flow is not affected by edge effects. For a **W/h** of 20, the model predicts that 97% of the bulk flow is not affected by edge effects. Therefore, to ensure negligible edge effects during flow, a **W/h** of 20 was selected for the design of the slit die in the present work.

Based on Hatzikiriakos and Dealy's capillary slip velocity results (10), a length to height ratio (**L/h**) of 120 was chosen, since in their experiments they determined that beyond this ratio the slip velocity remains approximately unchanged. By having selected a slit gap height, **h**, of 1 mm, the remaining slit dimensions were determined from the above criteria; the slit width, **W**, was 20 mm, and the slit length, **L**, was 120 mm.

3.1.2. Positioning of the Shear Stress Transducers

One of the most important aspects of the design of the slit die rheometer was the location of the shear stress transducers along the channel. According to the slip model results presented in Chapter 2, the farther apart the two transducers are along the length of the channel the greater the difference in the local shear stress values measured at the wall. Based on this rationale, the locations of the two shear stress transducers should be at the very entrance and exit of the slit channel. However, this reasoning does not take into account entrance or exit effects. In addition to these factors, there were physical limitations due not only to the size of the transducers but to the space required for the pressure transducer, heaters, and temperature probes.

After the basic dimensions of the shear stress transducers (which are described in the following sections) were decided upon, the axial locations of the transducers within the channel, $\mathbf{Z}_1$ and $\mathbf{Z}_2$, were then determined. Fig. 3.1 shows the location of the transducers with respect to the wall shear stress distribution as predicted by the model of section 2.3.3. Represented as multiples of the slit length, **L**, these positions correspond to axial locations of 0.225 **L** and 0.8 **L**.

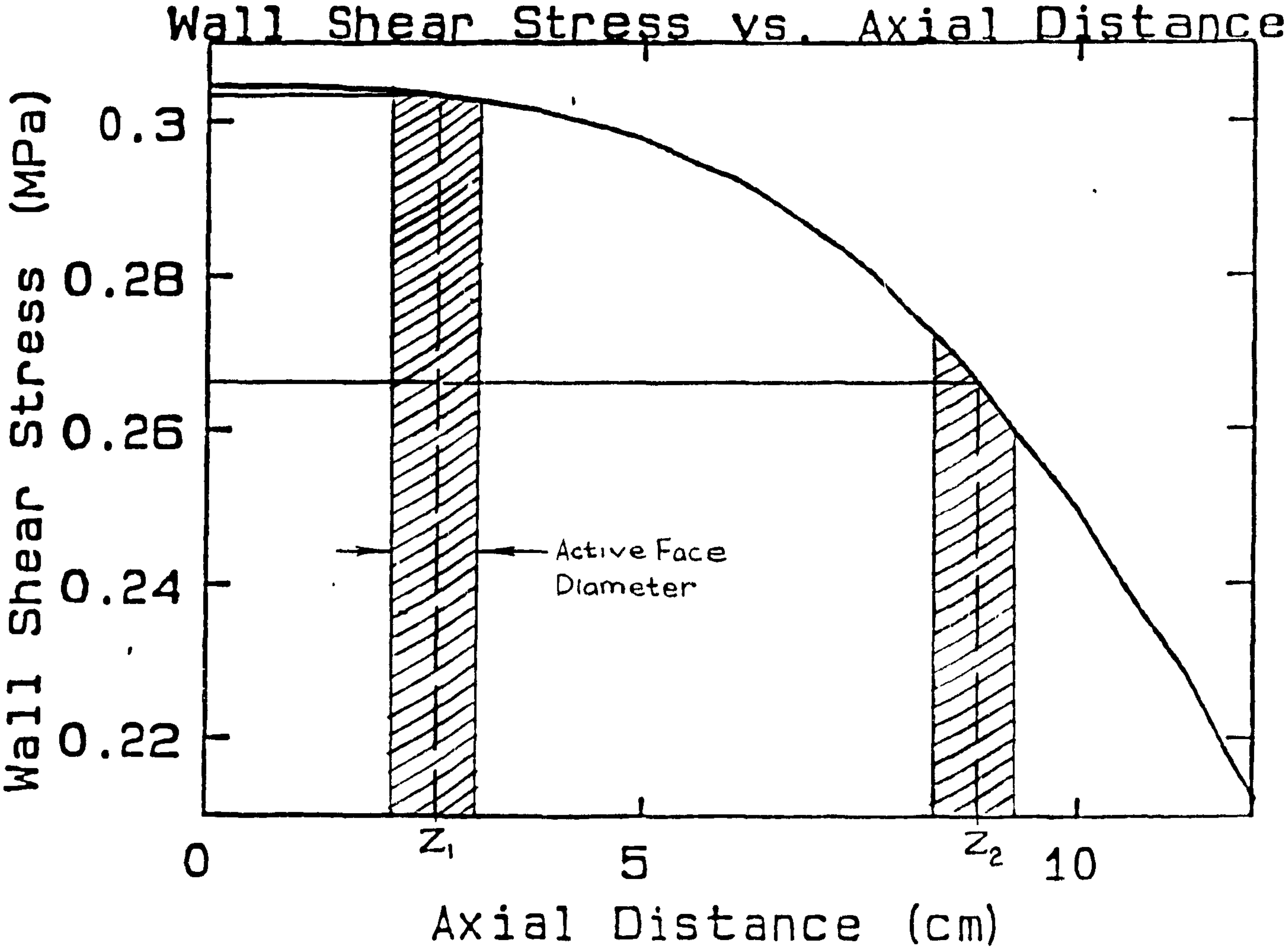

Fig. 3.1. Position of Transducers with Respect to the Wall Shear Stress Distribution from Fig. 2.2

3.1.3. Design and Construction of the Slit Die

The die consists of four major components (refer to Fig. 3.2): the top half **(A)**, the bottom half (**B**), and two identical spacers "sandwiched" in between the two halves (**C**). AISI 420 Stainless Steel was the material of construction for the slit die as well as the shear stress transducers, which are described in Section 3.2. Stainless steel is highly resistant to corrosion and oxidation at high temperatures and maintains considerable strength at these temperatures. AISI 420 is a martensitic steel which can be heat treated to a high hardness.

Construction of the die consisted of milling, from the base stock, the general form of the slit die to within an eighth of an inch of all major dimensions. Characteristics of all coldworked material include not only the strain hardening that can be achieved by this type

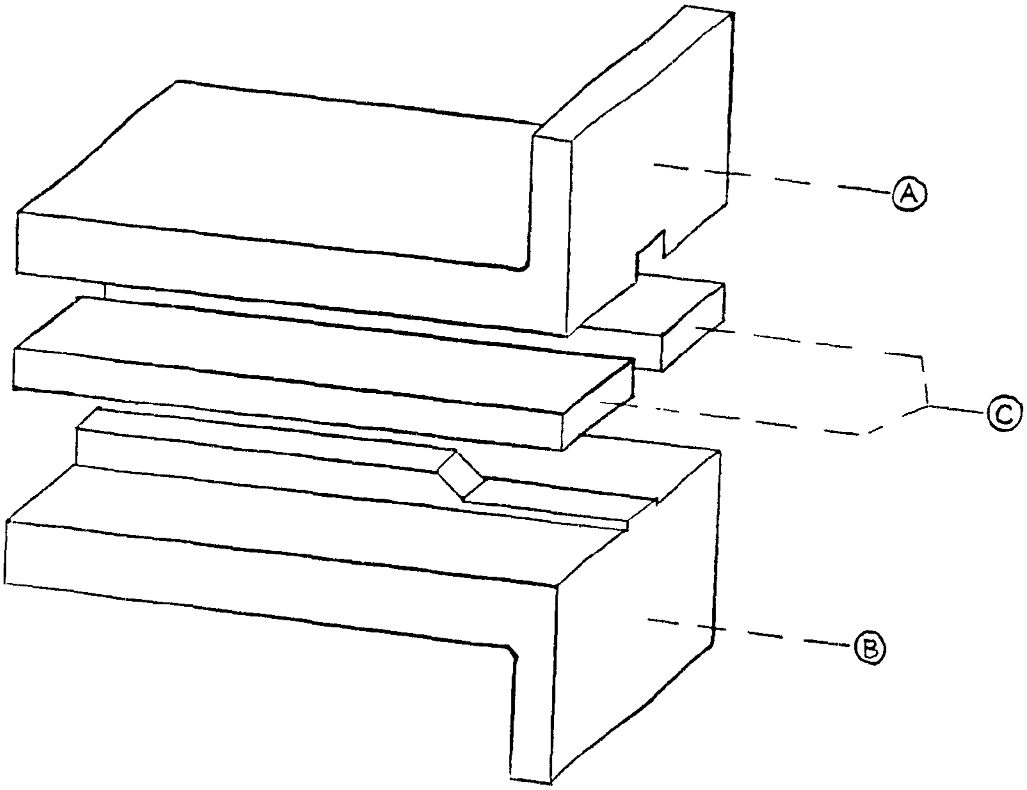

Fig. 3.2: Exploded Schematic Assembly of Slit Die

of processing but the residual stresses that are also inherent in this type of processing. To relieve these stresses within the material, heat treatment is most often used For steel, this involves placing the machined pieces in an oven at temperatures around 500°C for about one week. Heat treatment also results in a hardening of the AISI 420 material It is for this reason that the bulk of machining is accomplished before heat treatment when the material is soft and that the precision machining is carried out after heat treatment when the material has been hardened. It goes without saying then that cold working and heat treatment greatly enhance the strength properties of the material. Refer to Appendix A for the detailed design of the slit die.

3.2. The Shear Stress Transducer

The shear stress transducer developed at McGill University involves the deflection of a stiff beam member in contact with a molten polymer or polymer solution that is undergoing shear. Three different transducer designs are currently being used at McGill University. This thesis introduces a new design, which was developed to address the shortcomings of its predecessors. These designs will be described in the following sections.

3.2.1. The Cantilever Design

The cantilever design (refer to Fig. 3.3) was first introduced for work done on the sliding plate rheometer developed at McGill University (21). The design involves the use of a cylindrical beam member that is fixed at one end to a flat flange plate. The free end of the beam is circular, flat, flush with the rheometer wall, and makes contact with the liquid polymer. The flat surface of this free end is termed the active face of the shear stress transducer. Thus, the beam deflects due to a shear stress imposed on its active face by the liquid polymer flow. If the deflection of the stiff beam is small, and the amount of deflection is known, then a proportional relationship exists between the shear stress acting on the active face and the magnitude of the beam deflection. The simple design of the cantilever beam allows for easy fabrication on a conventional steel-working lathe.

Several methods for measuring this minute deflection (usually on the order of less than 1 mil) have been used, but to date the most successful has been the use of a capacitance proximity probe which is often used in measuring very small linear displacements in precision machinery. The method of capacitance is most effective when air (or any gas) is used as the dielectric medium, since its dielectric properties are not strongly dependent on temperature; any other medium greatly detracts from its measuring capabilities. This topic will be discussed further in the description of the capacitance probes in the following sections.

Note that in the cantilever design the transducer cavity is not sealed, and there is the possibility of liquid polymer entering the cavity and thus rendering the capacitance system

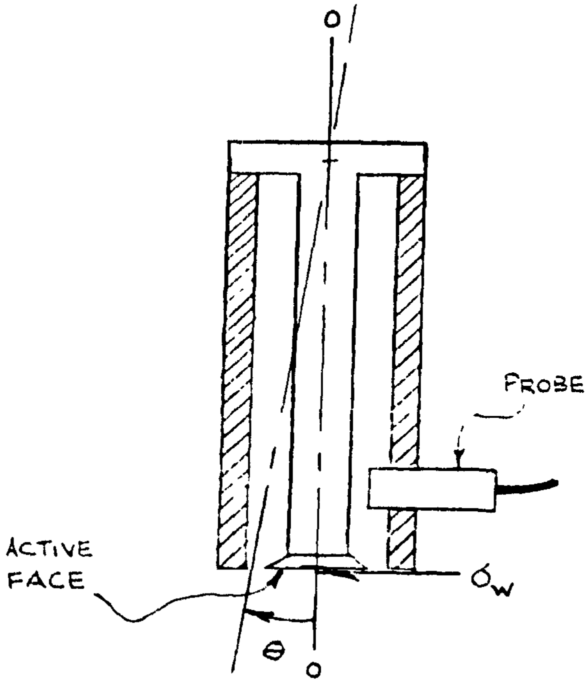

Fig. 3.3: Cantilever Design SST

ineffective. However, this particular design has met with good success in the sliding plate rheometer where there is no pressure driven flow that would cause the polymer to enter the cavity (22). The amount of polymer that does enter the cavity due to normal stress effects is very small in the absence of an externally applied pressure. In the presence of a pressure driven flow, polymer would enter and fill the cavity thus rendering this design unsuitable. Attempts at sealing the active face from the transducer cavity with O-rings have met with limited success at the expense of transducer performance (23).

3.2.2. The Disk Spring Design

The disk spring design (refer to Fig. 3.4) was developed at McGill to keep liquid polymer away from the capacitance probe. The design is a simple disk integrated with a stiff beam through its center. The disk acts as a torsional spring and allows two degrees of freedom about its center. Again, if the beam deflections are small then a proportional relationship exists between the shear stress acting on the active face of the shear stress transducer and the magnitude of the beam deflection.

Note that the beam in the disk spring design has a non-uniform cross section. This is intended to place the mass center of the beam at the geometric center of rotation (the center of the disk) to prevent vibrations in the beam, relative to the housing, as a result of apparatus vibrations. The design, although somewhat more complex than the cantilever design, can still be turned on a steel-working lathe.

The disk serves a two-fold purpose: it acts as the torsional spring member of the beam, and it acts as a seal to keep polymer from making contact with the proximity probe A major shortcoming of the disk design is that the disk must be thin to allow sufficient beam flexibility, and under high pressure it will bow to permit the axial deflection of the beam. This is due to the normal thrust imposed by the polymer on the active face end and

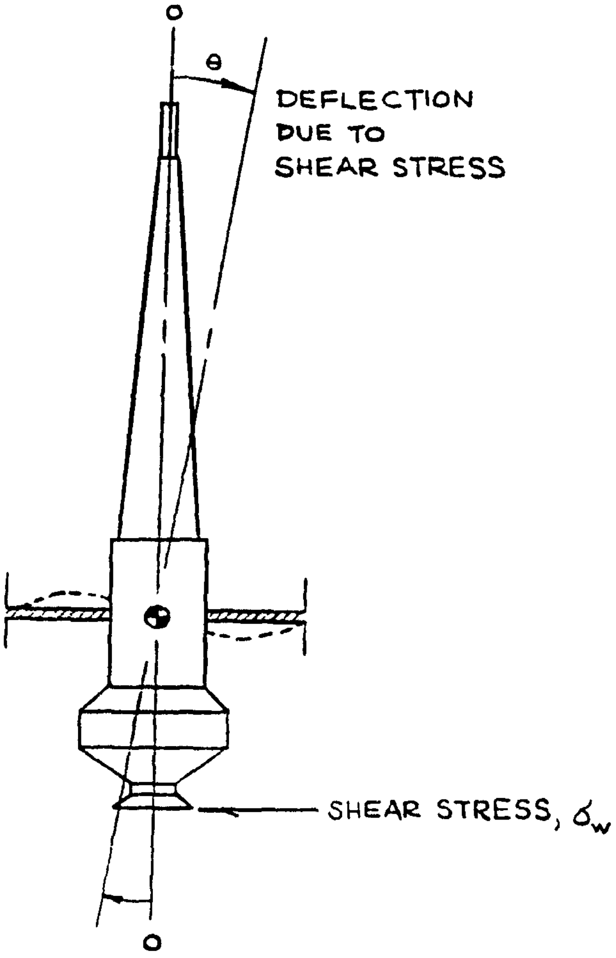

Fig. 3.4: Disk Spring Design SST

on the underside of the disk. If the disk contains any asymmetry due to variations in thickness after machining, asymmetrical bowing will occur under high pressure which will lead to a spurious indication of shear stress. The torsion-bar transducer was designed to eliminate this effect.

3.2.3. The Torsion Bar Transducer with Membrane Seal

The torsion bar design involves the use of a rectangular cross section beam, integrated with the transducer beam to act as the torsional spring member of the transducer (refer to Fig. 3.5). Unlike the disk design, the torsion bar design has only one degree of freedom and allows only uni-directional rotation about the center axis of the torsion beam member. Thus, the transducer must be properly aligned to ensure that its axis of rotation is perpendicular to the direction of flow. The torsion beam suppresses the axial deflection of the transducer beam due to the normal thrust of pressure. The design, although simple from a mechanical point of view, is much more difficult to fabricate than the two previous designs, since the torsion beam member must be milled out.

The major shortcoming of a simple torsion bar design is that nothing prevents polymer from reaching the upper transducer cavity. Whereas the disk in the disk spring design serves not only as the torsional spring member but as the seal to the upper transducer cavity, the torsion bar-membrane design requires the use of a seperate seal Nelson (24) has described a transducer incorporating such a seal. The membrane seal is composed of an annular steel disk (much like a steel washer) and two thin annular brass shims. The steel disk acts as a pressure plate to absorb the load from the applied pressure To prevent the disk from affecting the deflection of the transducer beam, a thin gap is left between the inner edge of the disk and the transducer beam. The inner edge of one brass shim is clamped by two nuts on the transducer beam and the outer edge of the other is clamped by the transducer housing; together, they prevent liquid polymer from reaching the upper transducer cavity.

In total, the torsion bar-membrane design introduces five separate elements to serve as a sealing element. By introducing five individual parts to the basic design, the overall reliability of the design is reduced due to new possibilities for error. A major aspect of

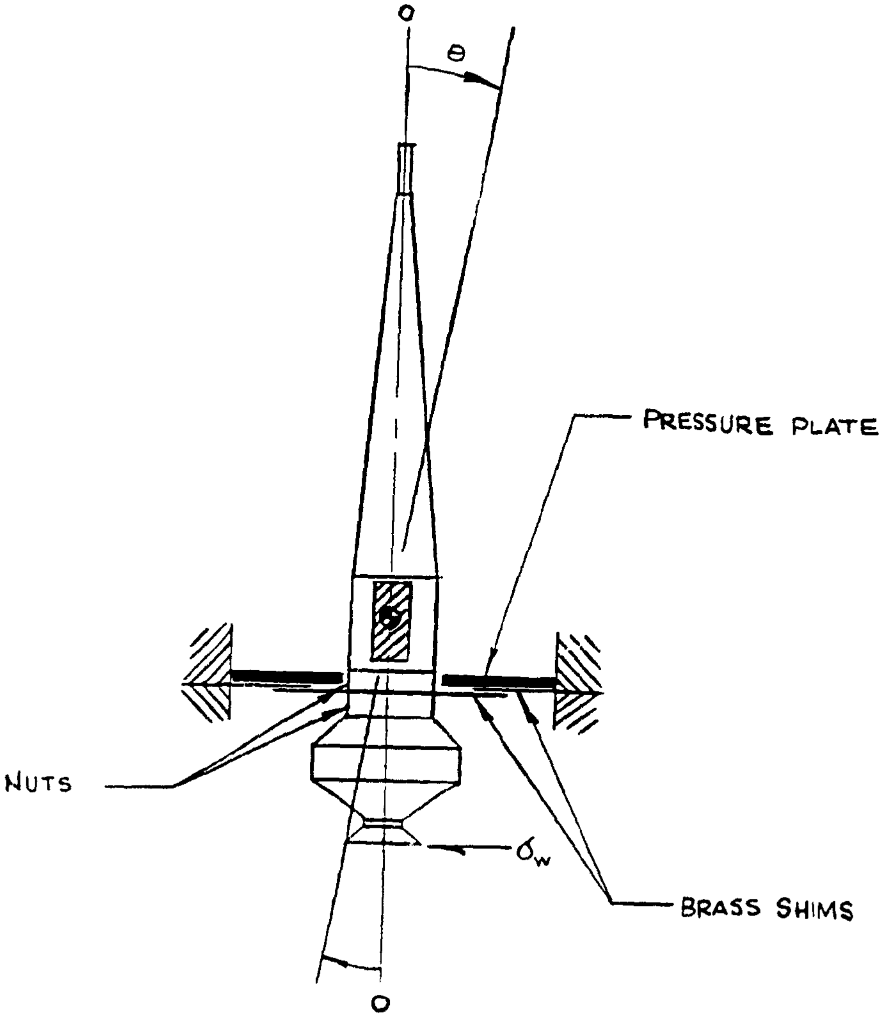

Fig. 3.5: Torsion Bar-Membrane Design SST

conceptual design deals with realizing the assets of each proposed design and integrating them into a single design. This realization provided the basis for developing a new shear stress transducer design, which was a major focus of this project.

3.2.4. The Disk-Bar Design

By combining the positive features of both the disk spring and torsion bar-membrane designs, the disk-bar design was developed. The major asset of the disk spring design, as mentioned earlier, is that the problem of sealing the polymer from the capacitance system is eliminated. The major asset of the torsion bar design is that the problem of axial displacement of the transducer beam due to the normal thrust of the pressure is eliminated. By combining both of these aspects into a single integrated design, an optimized design is obtained.

However, the detailed design of this type of transducer was not a trivial task. The major difficulty was that since the disk is combined with the torsion bar, a more complex spring element is involved. The development of a design model was therefore necessary to simulate the performance of the new transducer. To achieve this, the models for a disk spring and for a torsion bar were superposed to approximate the behavior of the disk-bar design.

The model equations used for each elastic element were taken from Roark's Formulas for Stress & Strain (25). Three modes of loading were considered The first was a torque or coupling mode imposed about the axis of rotation of each member due to the shear stress acting on the active face of the shear stress transducer. The second mode considered was a concentrated load normal to the axis of rotation of each member due to the normal thrust associated with the pressure acting on the active face of the shear stress transducer. Finally, the third mode considered was a uniformly distributed pressure normal to the axis of rotation of each member due to the normal thrust of pressure imposed by the polymer that enters and fills the lower transducer cavity.

After establishing the modes of loading, the next step was to assume a schematic representation of each member for the purpose of using the design equations. The disk was represented as a flat annular plate with its outer edge fixed and its inner edge guided for the second and third modes of loading. For the first mode, the torque mode, the disk was represented as a flat circular plate with a fixed outer edge and a trunnion fixed to the center of the plate. For all three modes of loading, the torsion bar was represented as a straight beam with one edge fixed and one edge guided. Thus, six loading cases were developed to model the two superposed designs.

The two deflections of interest to us are the axial deflection normal to the axis of rotation of each member and the angular deflection about the axis of rotation of each member. With this in mind, the six representative cases and the corresponding deflection equations are as follows.

Case 1: (Disk) Central Couple on Flat Circular Plate with a Fixed Outer Edge and a Trunnion Fixed to the Center of the Plate

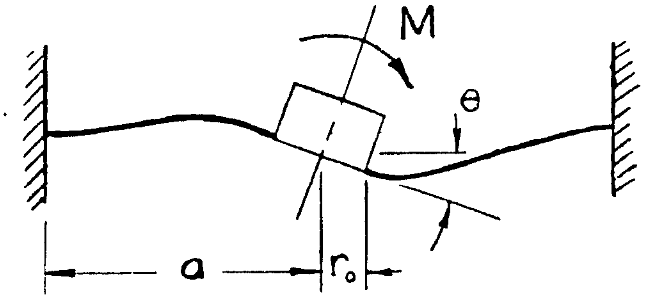

Fig. 3.6

$$\theta = \frac{\alpha M}{E_M t^3} \tag{3.1}$$

where,

θ = magnitude of angular deflection
α = a constant dependent on the ratio $\mathbf{r_0/a}$
M = magnitude of the imposed moment, or torque
$\mathbf{E_M}$ = elastic modulus of the plate material
t = thickness of the plate

Case 2: (Disk) Annular Plate with a Uniform Annular Line Load

Outer Edge Fixed, Inner Edge Guided

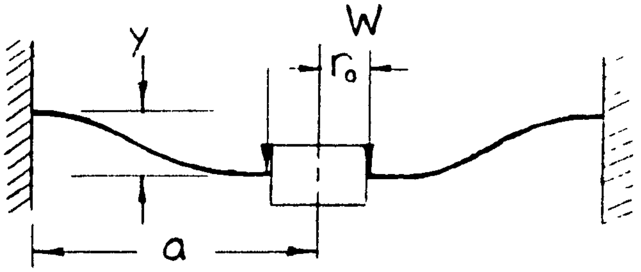

Fig. 3.7

$$Y = -\frac{wa^3}{d}\left(\frac{C_2 L_6}{C_5} - L_3\right) \qquad (3.2)$$

where,

Y = magnitude of axial deflection

w = magnitude of uniform annular line load

and,

$$d = \frac{E_M\, t^3}{12(1 - \nu^2)} \qquad (3.3)$$

$$C_2 = \frac{1}{4}\left[1 - \left(\frac{r_0}{a}\right)^2\left(1 + 2\ln\frac{a}{r_0}\right)\right] \qquad (3.4)$$

$$C_5 = \frac{1}{2}\left[1 - \left(\frac{r_0}{a}\right)^2\right] \qquad (3.5)$$

$$L_3 = \frac{r_0}{4a}\left[\left(\left(\frac{r_0}{a}\right)^2 + 1\right)\ln\frac{a}{r_0} + \left(\frac{r_0}{a}\right)^2 - 1\right] \qquad (3.6)$$

$$L_6 = \frac{r_0}{4a}\left[\left(\frac{r_0}{a}\right)^2 - 1 + 2\ln\frac{a}{r_0}\right] \qquad (3.7)$$

and ν is Poisson's ratio.

Case 3: (Disk) Annular Plate with a Uniformly Distributed Pressure

Outer Edge Fixed, Inner Edge Guided

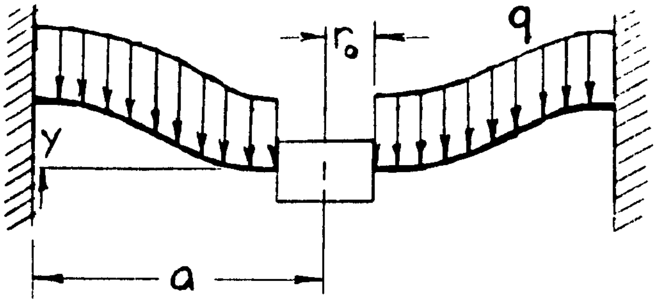

Fig. 3.8

$$Y = -\frac{qa^4}{d}\left(\frac{C_2 L_{14}}{C_5} - L_{11}\right) \tag{3.8}$$

where,

q = magnitude of the uniformly distributed pressure

and,

$$L_{11} = \frac{1}{64}\left[1 + 4\left(\frac{r_0}{a}\right)^2 - 5\left(\frac{r_0}{a}\right)^4 - 4\left(\frac{r_0}{a}\right)^2\left[2 + \left(\frac{r_0}{a}\right)^2\right]\ln\frac{a}{r_0}\right] \tag{3.10}$$

$$L_{14} = \frac{1}{16}\left[1 - \left(\frac{r_0}{a}\right)^4 - 4\left(\frac{r_0}{a}\right)^2 \ln\frac{a}{r_0}\right] \tag{3.10a}$$

Case 4: (Torsion Bar) Torsional Deformation of Solid Rectangular Section

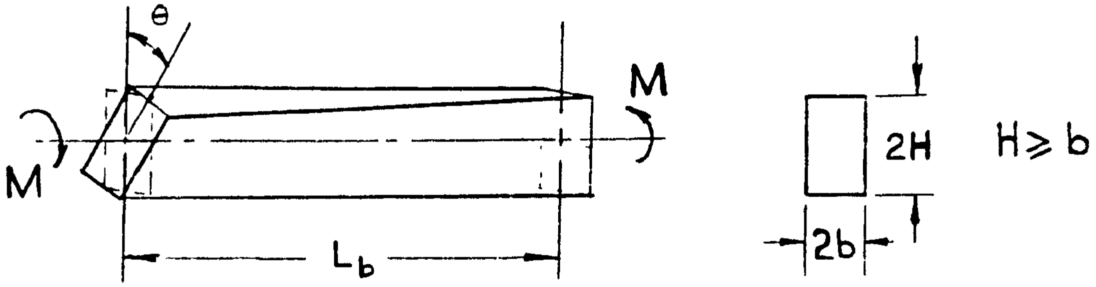

Fig. 3.9

$$\theta = \frac{ML_b}{kG} \tag{3.11}$$

where,

M = magnitude of the imposed torque
L_b = length of the rectangular section
G = shear modulus of the torsion bar material

and,

$$k = Hb^3\left[\frac{16}{3} - 3.36\frac{b}{H}\left(1 - \frac{b^4}{12H^4}\right)\right] \tag{3.12}$$

Case 5: (Torsion Bar) Concentrated Load on a Solid Rectangular Section Straight Beam One End Guided, One Edge Fixed

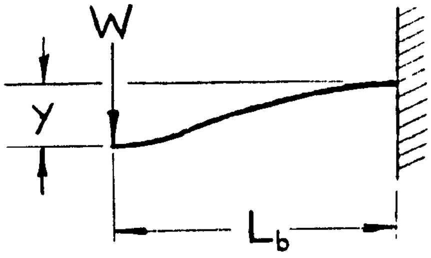

Fig. 3.10

$$Y = -\frac{wL_b^{\,3}}{12E_M I_b} \tag{3.13}$$

where,

w = magnitude of the concentrated load

and,

$$I_b = \frac{1}{12}2b(2H)^3 \tag{3.14}$$

Case 6: (Torsion Bar) Uniformly Distributed Pressure Over a Solid Rectangular Beam One Edge Guided, One Edge Fixed

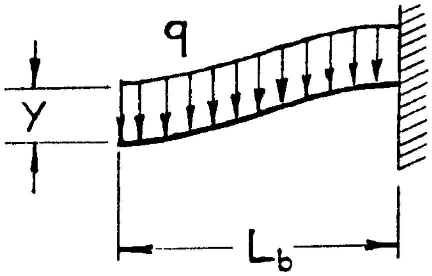

Fig. 3.11

$$Y - \frac{q}{24}\frac{2bL_b^4}{E_M I_b} \tag{3.15}$$

After the models of the beam and disk were established, they were superposed to obtain an approximation of the operation of the disk-bar design. Superposition is thought to be valid here because of the very small deflections expected during operation of the transducer.

Since both the beam and the disk are integrated into a single element, the magnitude of the axial deflections of the beam and the disk under normal thrust loading must be equal. Similarly, the magnitude of the rotational, or angular, deflection due to torsion of both the beam and the disk must be equal. In other words:

$$Y_{total} - Y_{beam} - Y_{disk} \tag{3.16}$$

and,

$$\theta_{total} = \theta_{beam} = \theta_{disk} \tag{3.17}$$

The relationships between the modes of loading were then determined by the use of free body diagrams. For the first mode, torsion due to the shear stress, the free body diagram is shown in Fig. 3.12.

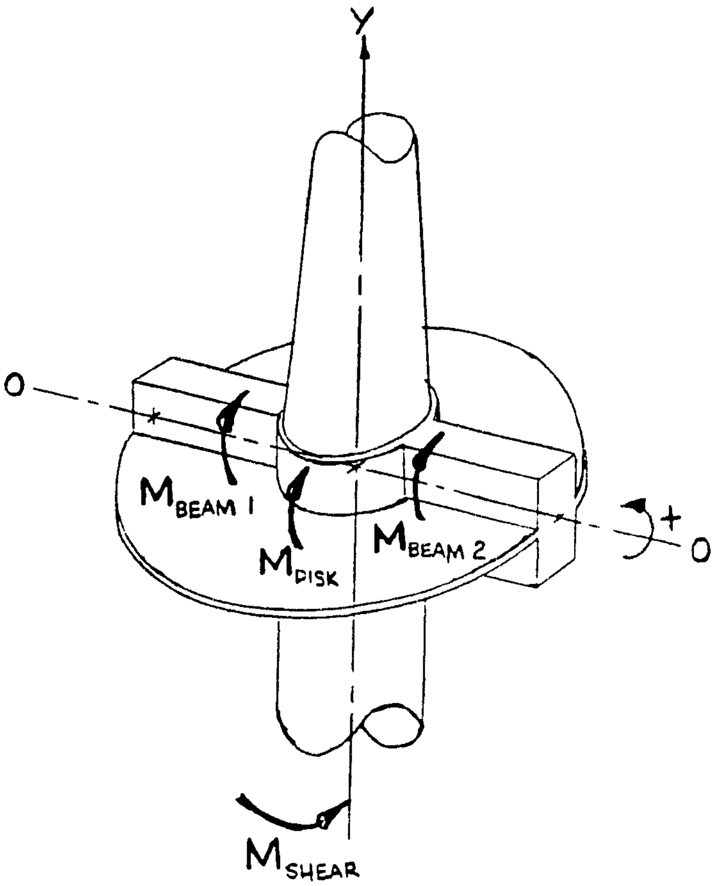

Fig. 3.12: Free Body Diagram of Disk-Bar SST - Torsion

The sum of the moments about axis 0-0 yields,

$$\Sigma\ M_{00} - 0 - M_{shear} - M_{disk} - M_{beam\,1} - M_{beam\,2} \tag{3.18}$$

since beam 1 and beam 2 are one and the same, this yields,

$$M_{shear} - M_{disk} + 2M_{beam} \tag{3.19}$$

For the second mode, a concentrated load due to the normal thrust on the active face, the free body diagram is shown in Fig. 3.13.

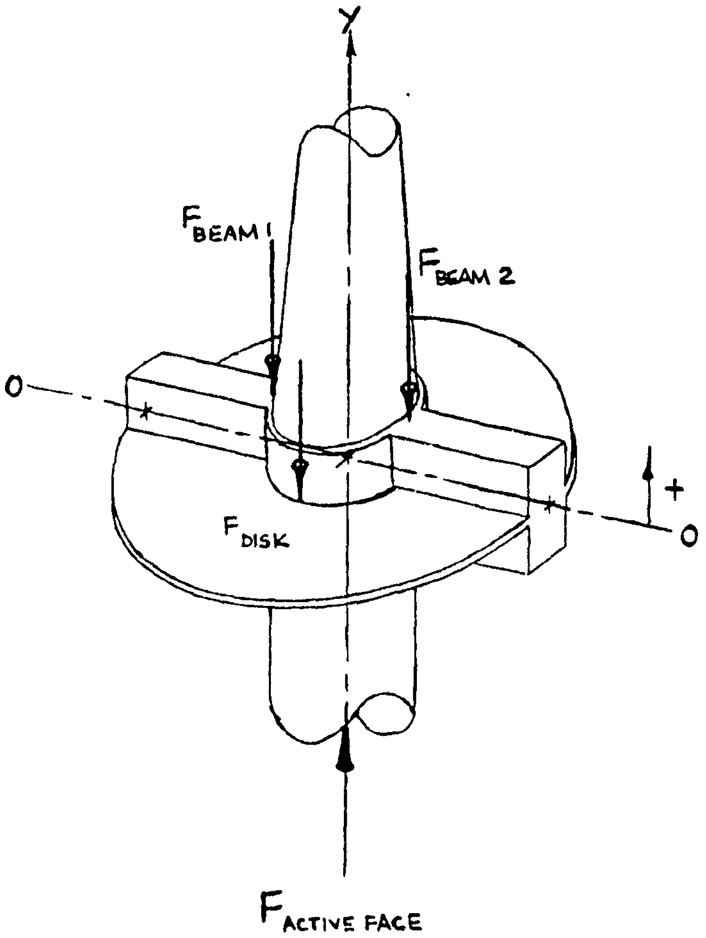

Fig. 3.13: Free Body Diagram of Disk-Bar SST - Concentrated Load

The sum of the forces in the y-direction is:

$$\Sigma F_y = 0 = F_{active face} - F_{disk} - F_{beam\,1} - F_{beam\,2} \qquad (3.20)$$

and since beam 1 and beam 2 are the same,

$$F_{active face} = F_{disk} + 2F_{beam} \qquad (3.21)$$

The third mode does not require a free body diagram, since the pressure acting over the disk and the beam is assumed to be uniform.

It should be mentioned at this time that the primary objective of developing this model was to determine the dimensions of the disk-bar shear stress transducer, specifically, the dimensions of the rectangular section of the bar and the thickness of the disk. The following is a summary of the procedure used to design the disk-bar system.

Case #	Element	Loading Mode	Deflection
1	Disk	Torque about axis of rotation	$\theta(t)$
2	Disk	Concentrated load	$Y(t)$
3	Disk	Uniformly distributed pressure	$Y(t)$
4	Bar	Torque about axis of rotation	$\theta(b,H)$
5	Bar	Concentrated load	$Y(b,H)$
6	Bar	Uniformly distributed pressure	$Y(b,H)$

Table 3.1: Summary of Deflection Cases

The first step in developing the design model was to combine the deflection equation of the disk with that of the bar for each loading mode. Table 3.1 is a review of the cases presented earlier. If the disk element and bar element are integrated into a single system, then for a given loading mode the resulting deflection is the same for both the disk and bar elements. Therefore, the rotational deflection calculated for Case 1 was set equal to the rotational deflection calculated for Case 4; the axial deflection calculated for Case 2 was set equal to the axial deflection calculated for Case 5; and the axial deflection calculated for Case 3 was set equal to the axial deflection calculated for Case 6. In this way the load on the disk element could be represented in terms of the load on the bar element, or vice versa. For example, the load on the bar can be expressed as a fraction of the load on the disk element. Using the appropriate load equation, the load on the disk element can be determined in terms of the applied load and substituted back into the appropriate deflection equation. Thus, by making the magnitude of the axial and rotational deflections input parameters, the deflection equations can be expressed in terms of the input parameters and the dimensions of the disk and bar elements. These dimensions can then be found by solving the system of equations. Appendix B contains a listing of the computer program that was written in GW-BASIC to solve the final design equations and also contains a list of the final disk-bar shear stress transducer design specifications generated by the program. Detailed design drawings of the disk-bar shear stress transducer are presented in Appendix C.

As compared to the construction of the disk spring and torsion bar types of transducer, construction of the disk-bar design proved to be a more difficult task. The transducer was roughed out on a lathe from AISI 420 stainless steel stock and then stress relieved The detailed features of the transducer (e.g. the cutting of the bar into the disk) were formed by precise milling of the transducer body. The most cumbersome aspect of construction was that the transducer had to be milled out on **both** sides of the body. This involved flipping the piece and milling out a mirror image of the form already milled out on the opposite side. Due to the size of the milling bits used, the resulting rounds of the detailed features were larger than desired, which produced an increase in the rigidity of the shear stress transducer; this was believed to be the primary factor contributing to a decrease of flexibility of almost 33% as compared with the design specifications. Other factors are the approximations used in the model.

3.3. The Capillary Rheometer

An Instron rheometer was used in this thesis work to drive the molten polymer through the slit die rheometer. The advantage of using the rheometer as opposed to an extruder is that the flowrate can be better controlled. The rheometer incorporates the use of an insulated, cylindrical reservoir whose temperature is controlled by means of band heaters regulated by temperature controllers. The heated reservoir is filled with polymer resin, which then melts and must be packed to prevent cavities from forming within the molten polymer pool. A plunger is then forced down in the reservoir expelling the molten polymer much like a syringe. A load cell above the plunger monitors the force transmitted through the plunger, which moves at preset speeds.

The melt reservoir used in this project was one that was previously constructed at McGill (26) and has a diameter of 19mm. At the exit of the reservoir, a flange was constructed to adapt the slit die rheometer to the end of the reservoir; the details of the flange design are given in Appendix A

3.4. The Capacitance System

Capacitive proximity sensors have been used in industrial applications for over 25 years A linear capacitive reactance technique for non-contact measurements has been used at McGill University in shear stress transducers since the mid 1980's (22).

3.4.1. Principle of Operation

A sensor plate of a fixed area is surrounded by a larger guard ring. Both are isolated from each other, with the conductor wire of a shielded coaxial cable electrically connected to the sensor and the coaxial shield connected electrically to the ring guard. The combination when positioned relative to an earth ground or conductive target, creates a capacitance proportional to the gap (refer to Fig. 3.14). When this capacitor is incorporated into the circuit of a specialized instrumentation amplifier, the output voltage is proportional to the gap spacing between the target and the capacitive sensor. The dielectric medium of this gap is most commonly air, since its deielectric properties are constant over a wide range

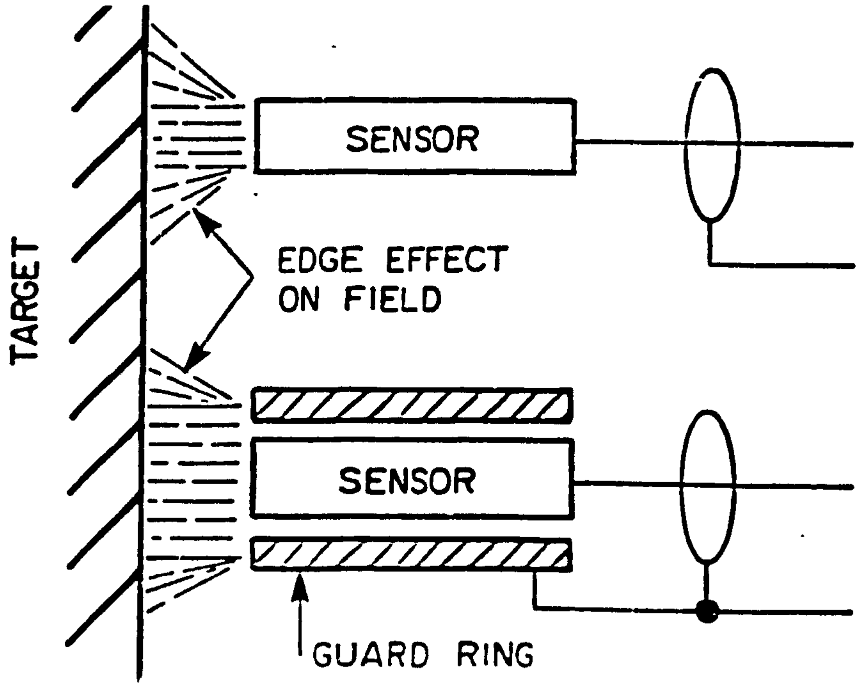

Fig.3.14: Schematic Diagram of a Target and Capacitive Sensor with and without a Guard Ring

of temperatures. The guard ring serves the purpose of alleviating degrading fringing effects that would greatly degrade the performance of the sensor. These fringing effects occur due to the electrical field that exists near the edge of two parallel capacitive plates (refer to Fig. 3.15).

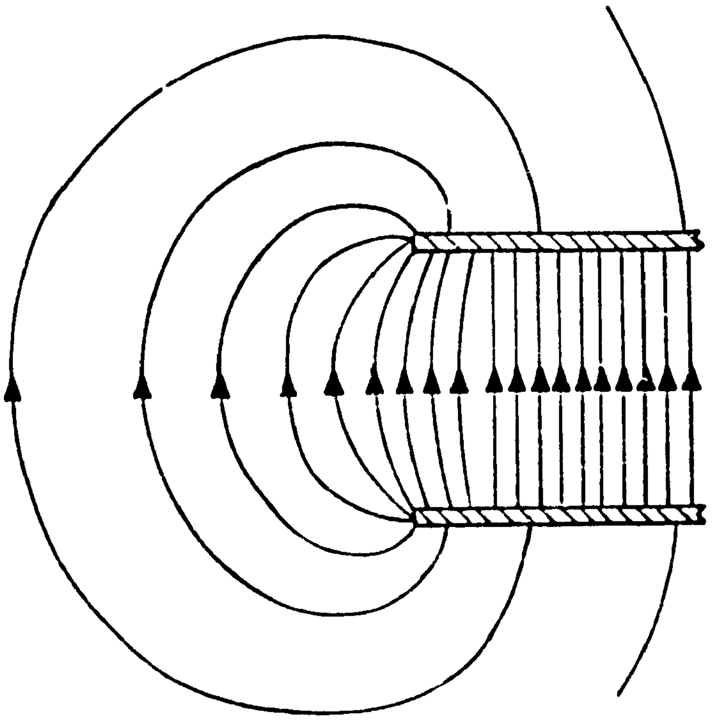

Fig.3.15: The Electrical Field Near the Edge of Two Parallel Plates

Capacitive reactance is established through a special amplifier design. The basic theory of capacitive proximity measurement dictates that when the area of a probe is decreased, so is the capacitance and thus the sensitivity But with capacitive reactance the inverse effect results. When the sensor is made smaller, the sensitivity actually increases, which is a benefit when high resolution is needed as in the case of measuring minute displacements of a shear stress transducer beam.

3.4.2. Capacitec Capacitence Probes

Capacitance probes used in previous shear stress transducer research at McGill University were sold under the commercial name Accumeasure-1000 by MTI Instruments Inc. Two probes have been used, models ASP-5HT and ASP-1HT, which have full linear ranges of 5 and 1 mil, respectively. The MTI probes offer a resolution of 0.1% of full linear range meaning a resolution of 0.001 mil for the ASP-1HT and a resolution of 0.005 mil for the ASP-5HT. The main drawback of the ASP-1HT, however, is that the probe must be positioned within 1 mil of the target face, which requires very delicate positioning in the shear stress transducer. The ASP-5HT requires less delicate positioning in the shear stress transducer, at the expense of some decrease in probe resolution.

Another company by the name of Capacitec, Inc. manufactures capacitive proximity probes that offer a resolution of 0.01% of the full linear range, meaning that a probe with a 20 mil full linear range has a resolution of 0.002 mil. Although the resolution of the 20 mil Capacitec probe is only half as much as the 1 mil MTI probe, the full linear range of the Capacitec probe is 20 times greater than the MTI probe, so that the positioning of the Capacitec probe in the shear stress transducer is much easier than with the MTI probe. The Capacitec probe can thus be placed anywhere within 20 mils of the target face, which allows a greater scope for the deflection of the probe end of the transducer beam. With this in mind, the Capacitec capacitance probe was chosen over the MTI probe.

The specific type of probe used was a model HPT-40/105 with a sensor O.D. of 0.040in, a guard O.D. of 0.105in, and a 0.735in 10-32 UNF threaded length. Two of these probes were utilized in this research work; one for each shear stress transducer. Two 4100 ReVA board basic single channel amplifiers, a 4100-C clock driver card, and a 4004-P115 4 slot rack with 15V power supply completed the system. It should be noted that the HPT-40/105 probes and 4100 ReVA board amplifiers are non-standard equipment that

Capacitec, Inc. had in its stock and was willing to sell at reduced prices since they had been custom built for another customer. The probes can operate at temperatures ranging from -73° C to 205° C and are connected with 0.063in 100% fully shielded coaxial cables with 10-32 microdot connectors. The 205° C maximum temperature is a limitation of the cable and not of the probe, whose temperature can exceed 250° C, beyond which the sensor insulator begins to melt. Refer to Appendix D for the Capacitec product literature.

3.5. Temperature Control

In order to ensure good temperature control of the slit die rheometer, several heaters were strategically placed in the already crowded slit die which was well insulated to prevent large temperature variations within the rheometer. Two Watlow Firerod cartridge heaters were inserted in the top half of the slit die along the length of the die, a Watlow Thincast platen heater was attached to the bottom half of the slit die, and two Watlow mica band heaters were fitted around the shear stress transducers.

Automatic temperature controllers were initially used but were eventually rejected due to the on-off nature of their operation, i.e. the heating was either one hundred percent on or one hundred percent off. This manifested itself through short bursts of heat from each heater, which resulted in a strong temperature dependence on time. The capacitance probe response reflected this effect to the point where it acted much like a temperature probe due to the expansion and contraction of transducer components as the temperature cycled. The use of a more sophisticated temperature control system could have solved this problem, but a quicker and cheaper solution was devised.

Manually operated Variac controllers were used to set the heating rates. With Variac controllers the feedback element of the control loop is the human operator. Thus, by carefully experimenting with different settings and monitoring the temperature at various locations of the rheometer, a desired temperature can be established.

An essential factor in temperature control is insulating the element whose temperature is to be controlled. However, since this was a research apparatus, it was anticipated that it must very often be entirely disassembled and reassembled. With this in mind, a portable and removable insulation system was designed. The basic concept was a "sandwich" configuration in which the two shells of the housing could be clamped together

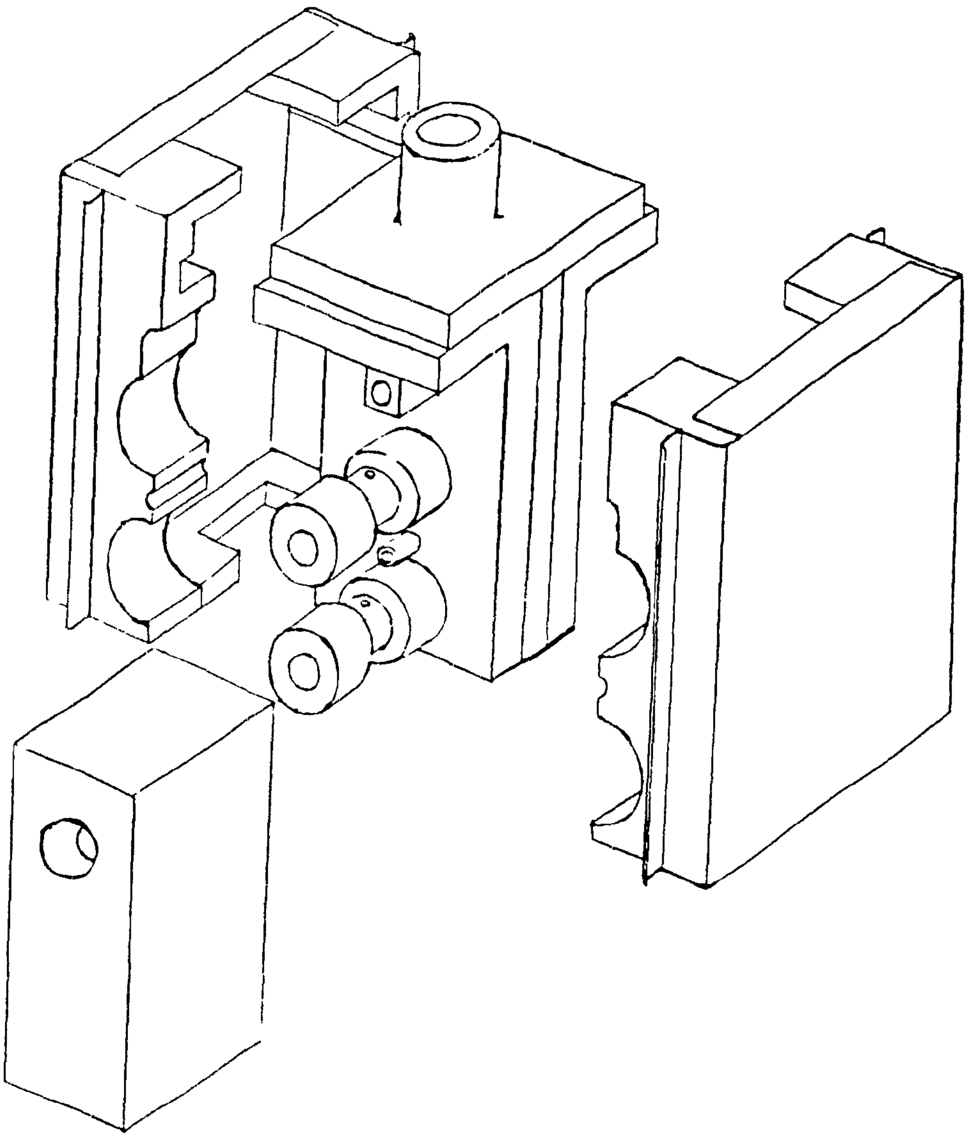

Fig.3.17: Schematic Assembly of Rheometer and Insulative Housing

encompassing the rheometer, ensuring easy removal and installation of the insulation. Therefore, the insulation of the rheometer consisted of two large pieces of maranite insulation cut to fit snugly around the slit die rheometer, coated with a high temperature paint on its inner surface, and attached to a formed sheetmetal covering to protect the fragile insulation. A third piece was then constructed in a similar fashion, except with fiberglass insulation, to insulate the tops of the shear stress transducers (refer to Fig 3 17).

3.6. Data Acquisition

Originally, a data acquisition program was written in Turbo C for a DT2808 A/D converter board to be used in conjunction with an IBM compatible computer system However, this particular program did not allow for real time graphic output, a necessity when evaluating the operation of a system of this type, and it was not utilized for this developmental work. Outputs from the capacitance probe amplifiers were instead directed to a Cole-Parmer, two-channel, strip chart recorder. This provided a convenient method for the real time evaluation of the performance of the transducers

CHAPTER 4

EXPERIMENTAL EVALUATION

A high density polyethylene blow molding resin (Dupont Canada Sclair 56B), used previously and characterized by Hatzikiriakos and Dealy (4,10) in their sliding plate and capillary rheometer studies, was chosen as the material to be used for the evaluation of the newly developed slit die rheometer. The operating temperature chosen was 180°C, since Hatzikiriakos and Dealy (4,10) had used this temperature. They observed power law viscosity behavior and found the power law exponent, **n**, to be 0.44, and the power law coefficient, **K**, to be 0.0178 $MPa\text{-}s^{0.44}$.

4.1. Experimental Procedure

The two shear stress transducers are referred to as $\mathbf{SST_A}$ and $\mathbf{SST_B}$. The upstream position is referred to as position $\mathbf{Z_1}$ and the downstream position, $\mathbf{Z_2}$ (refer to Fig. 4.1). The two capacitance probes are referred to as $\mathbf{P_1}$ and $\mathbf{P_2}$.

4.1.1. Preliminary Observations

Probe $\mathbf{P_1}$ was inserted into $\mathbf{SST_A}$ at position $\mathbf{Z_2}$, and probe $\mathbf{P_2}$ was inserted into $\mathbf{SST_B}$ at position $\mathbf{Z_1}$. Each of the transducers was then calibrated to yield identical signals for a given shear stress The plunger speed was increased until there was a noticeable response from the shear stress transducers.

In placing the shear stress transducers into their positions, it was noted that placing $\mathbf{SST_A}$ into position $\mathbf{Z_2}$ resulted in such a tight fit that full deflective freedom of the active

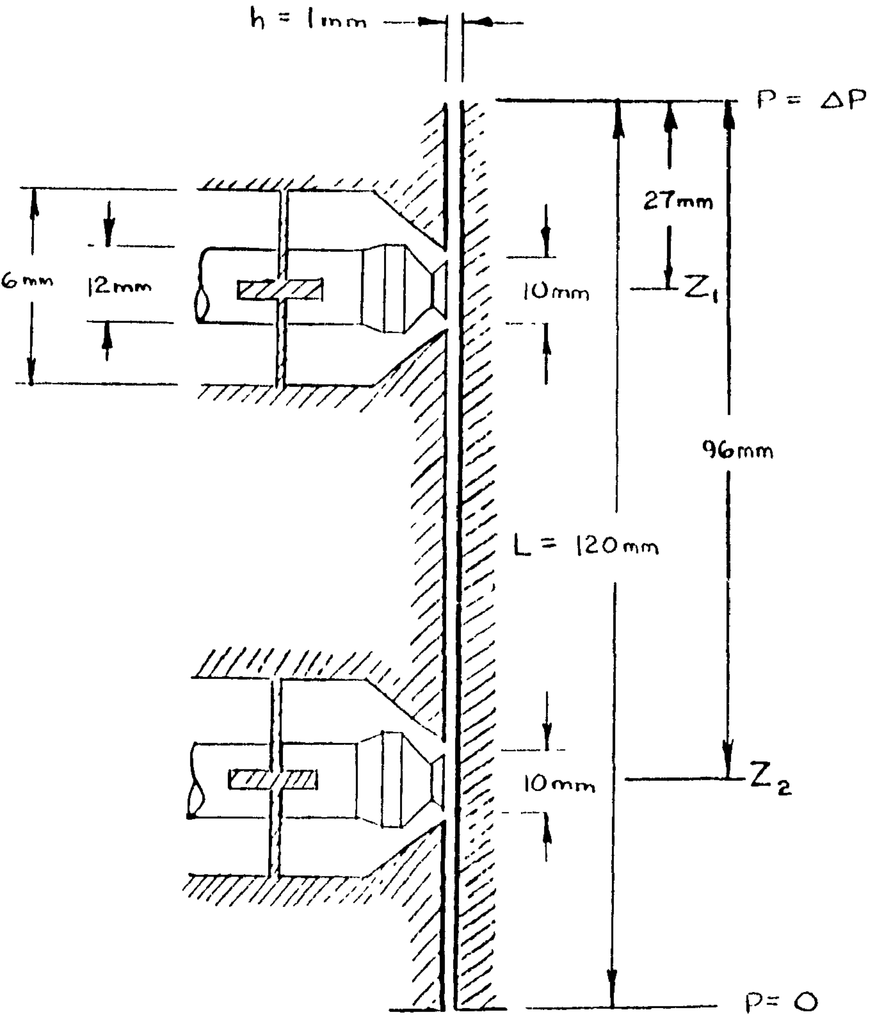

Fig. 4.1: Diagram of $\mathbf{Z}_1$ and $\mathbf{Z}_2$ Positions and Pressure Distribution in Slit Die Rheometer

face was likely to be hindered. This tightness can be attributed to a minor dimensional difference between the two transducers. In any event, it was found that $\mathbf{SST}_A$ was unresponsive at position $\mathbf{Z}_2$.

$\mathbf{SST}_B$ installed at position $\mathbf{Z}_1$, although responsive, did not respond as predicted from the calibration. The response was always lower than the predicted response based on a power law relationship and the calculated shear stress at the wall. Also, below a certain plunger speed, **SST**$_B$ actually exhibited a negative response, meaning that the beam deflected in the direction **opposite** to the applied shear stress (refer to Fig. 4.2).

In order to assure that the two capacitance probes had the same response, probe **P**$_1$ was placed into **SST**$_B$, and probe **P**$_2$ was placed into **SST**$_A$. There was no difference in the outputs after this switch, indicating that the capacitance probes were not the source of the unexpected behavior.

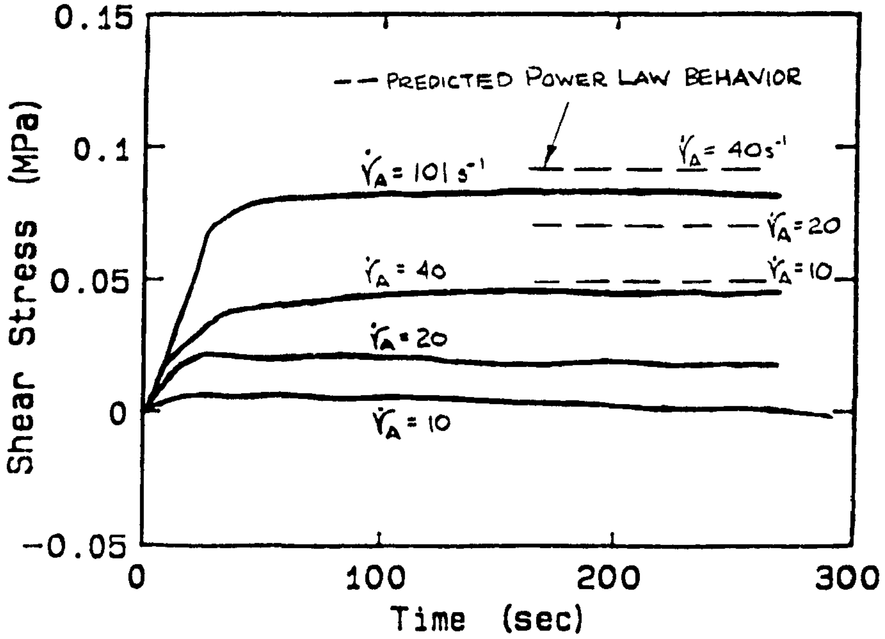

Fig. 4.2: Response of **SST**$_B$ in Position **Z**$_1$

4.1.2. Transducer Response

On the basis of the preliminary observations, for purposes of transducer evaluation $\mathbf{SST_A}$ was placed at position $\mathbf{Z_1}$ and $\mathbf{SST_B}$ at position $\mathbf{Z_2}$. It was found that both $\mathbf{SST_A}$ and $\mathbf{SST_B}$ yielded measurable responses as shown in Figs. 4.3 and 4.4. By comparing Figures 4.2 and 4.3, we see that when either transducer is installed at position Z_1 the responses have similar shapes, although the magnitudes are different. By contrast, the response form of $\mathbf{SST_B}$ at position Z_2 exhibited a characteristic initial peak and then decreased to a much a lower plateau. It should be mentioned as well that $\mathbf{SST_B}$, installed at position Z_2, was always the first to respond. Beyond a certain plunger speed, $\mathbf{SST_A}$ at the Z_1 position yielded a negative response, but at a higher plunger speed than when $\mathbf{SST_B}$ was installed at Z_1. The responses exhibited in every case were repeatable.

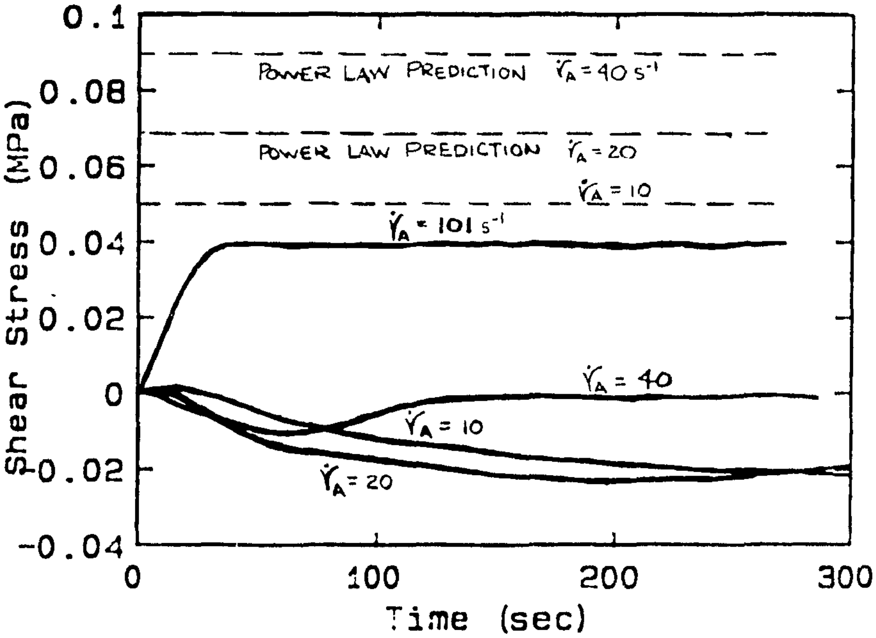

Fig. 4.3: Response of $\mathbf{SST_A}$ at $\mathbf{Z_1}$

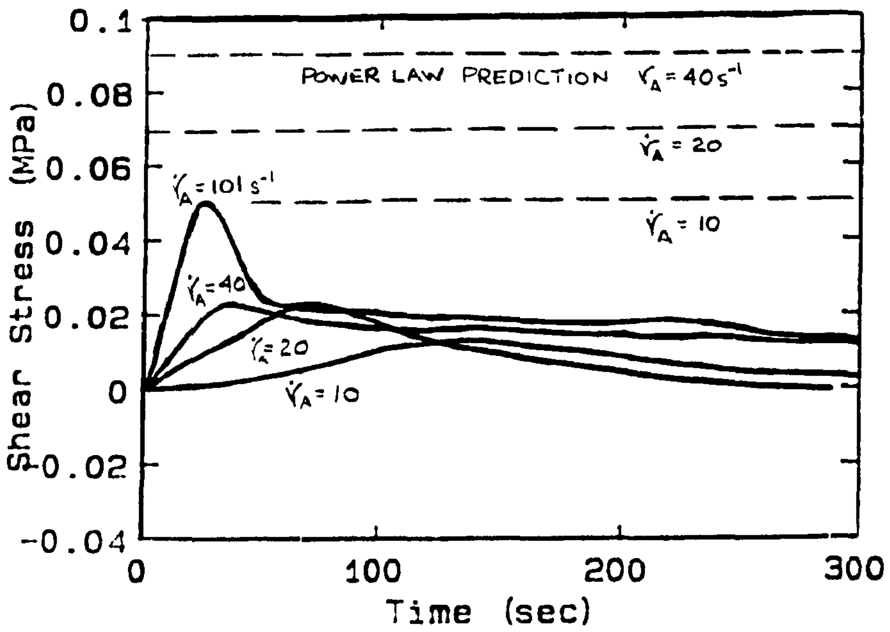

Fig.4.4: Response of $\mathbf{SST_B}$ at $\mathbf{Z_2}$

4.2. Evaluation of Operation

Careful examination of the data led to the hypothesis that the large pressure gradient present in the slit affects the operation of the shear stress transducers. One indication of such an effect is that both shear stress transducers were calibrated to respond in the same way to a given shear stress, but the response curves of both transducers in the $\mathbf{Z_1}$ position, while similar in shape, are very different in magnitude. This suggests that a dissimilarity in the details of construction of the two transducers is magnified by the pressure effects. Since the same pressure effects should exist for both shear stress transducers at a given position, the only reason the magnitude of their responses should differ is that one shear stress transducer is affected more than the other by the same pressure effect. In other words, it appears that a small dissimilarity in the machining of the two transducers is amplified by the pressure effect.

The second factor suggesting pressure effects is that $\mathbf{SST_B}$ in position $\mathbf{Z_2}$ responds with a characteristic peak and then decreases to a much lower plateau. This same shear stress transducer responded in a quite different manner when installed in the Z_1 position The major difference between the response of the two positions is the magnitude of the pressure. As mentioned earlier, when $\mathbf{SST_B}$ was installed at Z_2 it was always the first to respond. Since the magnitude of the pressure acting normal to the wall is much smaller than that at position $\mathbf{Z_1}$, it appears that there is a delay before these pressure effects stabilize at position $\mathbf{Z_2}$.

Nevertheless, although the pressure effects at positions Z_1 and Z_2 were different in intensity, the response at both locations was in the opposite direction from the shear stress acting on the active face of the shear stress transducer Having concluded that important pressure effects are present, it remained to determine how these pressure effects could counteract the force due to the shear stress imposed on the active face of the transducer

It should be noted that the only effects due to pressure observed with the previous shear stress transducer designs at McGill were normal thrust effects in which the pressure itself caused an axial deflection of the transducer beam, as discussed in Section 3 2 Since this effect was taken fully into account in designing the disk-bar shear stress transducer it was not considered likely that this was the cause of the anomalous responses

After considering the types of applications used previously at McGill, it was noted that the shear stress transducers previously developed had all been used for drag flows in which there was no significant pressure gradient. Thus, the primary applied load on the active face of the shear stress transducer was from a drag flow transmitted from either a sliding plate or a rotating drum (27). A shear stress transducer had never been used in poiselle flow, or pressure driven flow, in which a substantial pressure gradient exists. It was concluded that the pressure effects exhibited by the shear stress transducers in this slit die rheometer might be the result of the large pressure gradient existing across the active face of the shear stress transducer.

However, calculations suggested that this effect is not due directly to the pressure gradient at the active face but to the pressure gradient acting on the disk element of the disk-bar shear stress transducer transmitted to it by the polymer filling the lower transducer cavity. Since a pressure gradient exists across the active face, a pressure gradient also exists across the disk element of the shear stress transducer. This gradient is believed to play a significant role in the response of the transducer, since it causes a torque opposite to that produced by the applied shear stress.

Determining the exact contribution of the torque induced by the pressure gradient to the transducer response would require a major analytical effort, which is beyond the scope of this thesis A rough approximation, however, can be made by considering a simple model of the situation. Consider a pressure drop, **ΔP**, acting over the length of the slit die rheometer as shown in Fig. 4.1 Recalling that the length of the slit channel is 120mm and the diameter of the active face of the shear stress transducer is 10mm, the pressure gradient across the active face of the shear stress transducer is 1/12 of the overall pressure drop across the length of the slit die, or **ΔP**/12. If we consider a no-flow situation, we can assume that this same pressure gradient exists across the disk element of the shear stress transducer. Thus, the resulting torque on the transducer induced by the pressure gradient across both the disk element and the active face can be calculated and compared with the torque induced by the pressure gradient across the active face alone (refer to Fig. 4.5). By representing the shear stress in terms of the overall pressure drop across the length of the slit die [Equation (2.3)], the ratio of the torque imposed by the pressure gradient to that

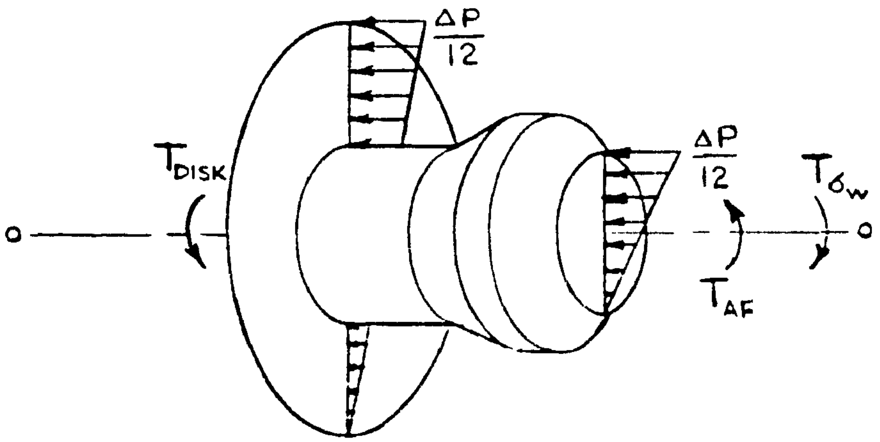

Fig. 4.5: Pressure Gradient Across the Shear Stress Transducer

imposed by the shear stress on the active face can be calculated Thus, let us define the following ratios:

$$\phi_A = \frac{\text{torque produced by pressure gradient acting on active face}}{\text{torque produced by shear stress}} \tag{4.1}$$

$$\phi_D = \frac{\text{torque produced by pressure gradient on disk element}}{\text{torque produced by shear stress}} \tag{4.2}$$

After substituting the appropriate parameters, ϕ_A is found to be about -0.4. Based on this analysis, the response of the shear stress transducers should always be positive. The ratio of the total torque due to the pressure gradient to that due to the shear stress is $\phi_A+\phi_D$, which is found to be about -7.4. This implies that the response would always be negative. As mentioned earlier, both positive and negative transducer responses are obtained. This suggests that the calculation of ϕ_D leads to an overestimate of the pressure gradient effects on the shear stress transducer response It is apparent that the pressure transmitted to the disk element of the shear stress transducer by the polymer filling the lower transducer cavity does not have a simple relation to the pressure gradie. : existing across the active face of the shear stress transducer A detailed simulation of the slow flow occurring inside the lower transducer cavity would be necessary to find this relation. However, the simple model does show the significant effect a pressure gradient can have on the performance of the shear stress transducer.

Although the torque due to the pressure gradient may not be the only factor affecting the operation of the shear stress transducers of the new slit rheometer, it is believed to be the primary factor Another factor that should be taken into consideration is the drag force due to the flow of molten polymer in and out of the lower transducer cavity due to the existence of the pressure gradient This effect, however, is considered to be less significant than the torque due to the pressure gradient since the flow through the lower transducer cavity is only a tiny fraction of the polymer flow through the slit channel. A three dimensional fluid flow simulation could be performed to determine not only the extent of fluid flow in the lower transducer cavity but the pressure gradient across the disk element of the shear stress transducer. However, this is beyond the scope of this thesis

CHAPTER 5

CONCLUSIONS AND RECOMMENDATIONS

Although the successful operation of the new slit die rheometer was compromised by the performance of the new disk-bar shear stress transducer, the new rheometer still holds great promise in characterizing the wall shear stress behavior of a polymer melt However, before work can proceed with this rheometer a new shear stress transducer that is unaffectable by any type of pressure effects must be developed

The new disk-bar design, although affected by what appear to be pressure gradient effects, is thought to be well suited for use in a drag type flow in which there is a large wall normal stress but no substantial pressure gradient. This is the situation in the in-line rheometer developed at McGill to monitor the rheological behavior of polymer melts as they are extruded (26). In this rheometer, a shear stress is imposed on the melt by a rotating drum which draws the polymer into a thin gap in which a shear stress transducer is installed. The amount of shearing is controlled by the speed of the rotating drum, and the rheological behavior of the melt stream can thus be monitored In this device, the magnitude of the pressure gradient along the length of the shearing gap is much smaller than the magnitude of the pressure acting normal to the wall to cause an axial deflection of the transducer beam. It was to account for this effect that the disk-bar shear stress transducer was originally designed.

The pressure **gradient** effect was unanticipated because a shear stress transducer had **never** been used in a pressure driven flow. Through experience comes wisdom The results of the present experiments show that a new concept is necessary to develop a shear stress transducer capable of operation when there are very large pressure gradients present.

If the observed effects are the effect of flow within the cavity, this could be remedied by sealing the lower transducer cavity and thus preventing the polymer melt from entering. In order to accomplish this, a silicone elastomer could be injected into the lower transducer cavity and then cured in position. The silicone elastomer would remain solid at normal process temperatures but remain flexible enough to allow movement of the shear stress transducer beam A disadvantage of this scheme, however, is that the elastomer could degrade after extended use at high temperatures. Another factor to be considered is the effect the elastomer would have on the response of the transducer. The damping effect could be greater than that of the molten polymer. Nevertheless, this arrangement is worth trying in future research

However, as stated previously, it is the opinion of the author that the flow effects of polymer within the lower transducer are not as significant as the torque due to pressure gradients in this rheometer. This pressure gradient would still be transmitted to the disk element through either a silicone elastomer or by the molten polymer. At the present time there is no obvious solution to this problem.

It was stated in Chapter 4 that in order to determine the effect of a pressure gradient on shear stress transducer performance an extensive numerical simulation would need to be performed. However, this is not thought to be a fruitful direction in which to proceed. It is the opinion of the author that an entirely new design is needed.

The progression of shear stress transducer design was described in Chapter 3. Let us consider the state at which shear stress transducer technology stands Since the decision to use capacitive methods to measure transducer response, it has always been necessary to prevent polymer from making contact with the capacitance probe. Hence, the disk spring element served not only as an elastic element but as a seal as well. However, this disk element seems to be at the root of the pressure effects witnessed in the present work. To eliminate this disk element, capacitance may have to be abandoned as a method of displacement measurement. The selection of an alternative measurement method is thus the primary concern of this conceptual design exercise.

An attractive alternative to capacitive measurement is piezoelectricity. This phenomenon involves the production of an electrical potential difference across the major crystallographic axes of a quartz crystal whenever a stress is imposed upon it and causes it to deform. This deformation is in the order of nanometers. Thus, not only does it require only a minute deformation to produce a signal, but it is quite sensitive and is used most often in oscillatory or vibratory tests. Under constant deformation, however, its response decays, a decrease on the order of one percent of full-scale in 10^3 sec at ambient temperature. At elevated temperatures, however, the decay rate is much higher

It has been found, however, that by translating the crystallographic axes with respect to the principal axes these temperature effects can be nearly eliminated This technique was developed and patented (U.S. Patent NO. 4,148,530) by a Swiss company, Kistler Instrumente, A.G., and involves cutting the crystal at a certain rotation of angle away from the principal axes. The primary efforts of the Company have been to develop high temperature pressure transducers. This may provide a viable alternative to the method of capacitive measurement

The temptation at this point would be to develop a radically new shear stress transducer. Instead of abandoning the present state of shear stress transducer technology, however, we should benefit from the experience gained at McGill in shear stress transducer design. It seems ironic to recognize that the one existing shear stress transducer design that seems mechanically unaffectable by pressure effects is the one used previously for applications in which there is no applied pressure, i.e. the cantilever design

It may be feasible to combine the technology developed by Kistler and the technology developed at McGill to produce the first piezoelectric shear stress transducer. Kistler manufactures a type of diaphragmless pressure transducers that are used in monitoring compressive stresses on solid structures (much like a force transducer). By placing this type piezoelectric transducer in contact with the cantilever transducer beam, the shear stress on the active face could be monitored with almost no deflection of the beam itself. A conceptual design of such a transducer is provided in Fig. 5.1. By placing three piezoelectric transducers 120° apart from each other, the shear stress transducer can be made omni-directional and the applied shear stress on the active face can always be resolved. The shear stress transducer would then also be unaffected by **any** type of pressure effects making it an ideal design to be implemented with the newly developed slit die rheometer The author plans to pursue this concept in full detail in doctoral research at McGill University.

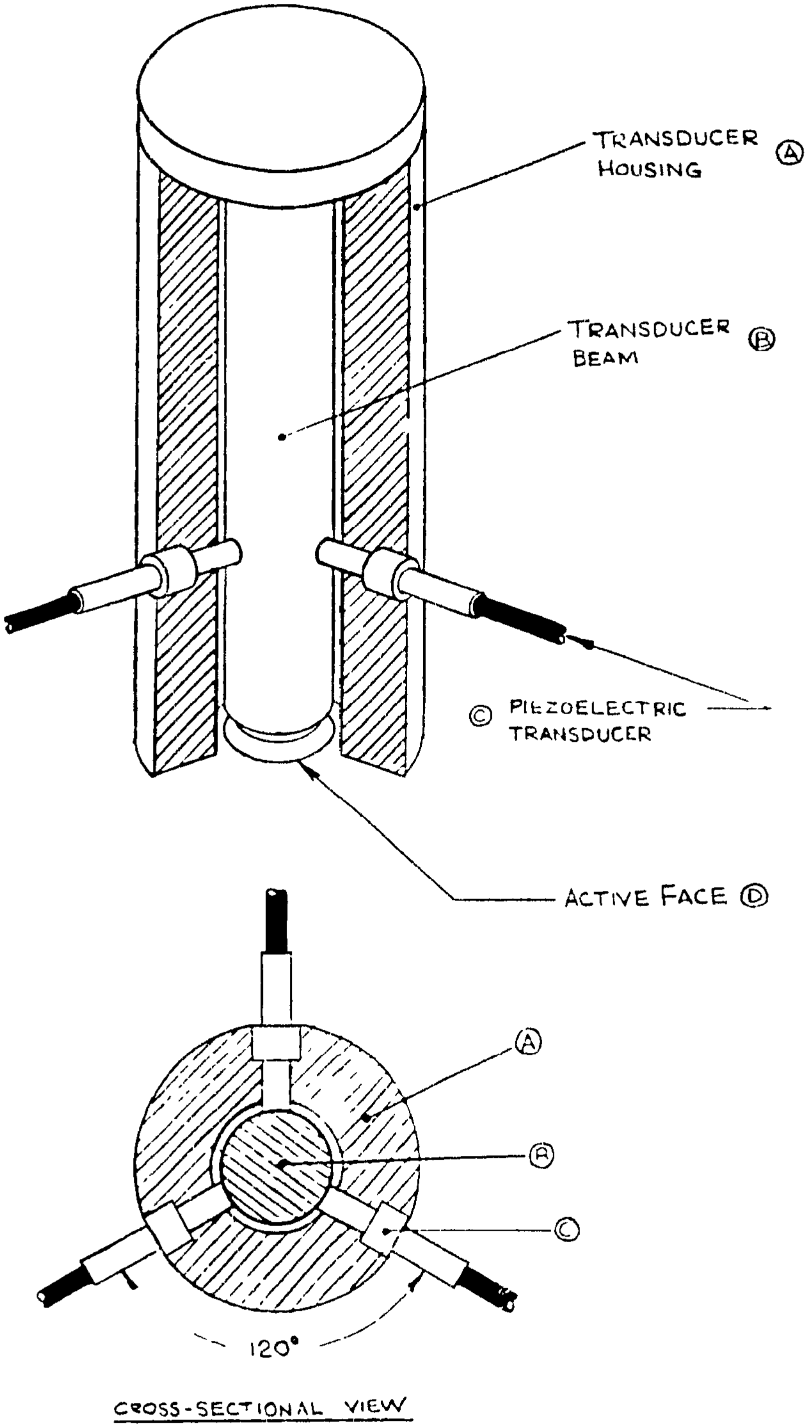

Fig. 5.1: Conceptual Design of Piezoelectric Shear Stress Transducer

REFERENCES

(1) Vinogradov, G.V. and L.I.Ivanova, **Rheol. Acta**, 6, 209-222 (1967)

(2) Ramamurthy, A.V., **J. Rheol.**, 30(2), 337-357 (1986)

(3) Atwood, B.T. and W.R.Schowalter, **Rheol. Acta**,28,134 (1989)

(4) Bagley, E.B., **J. Applied Physics**, 29, 109 (1958)

(5) Beaufils, P., **Intern. Polym. Proc.**, IV, 78 (1989)

(6) Becker, J., **Inter. Polym. Proc.**, VI, 318 (1991)

(7) Lupton, J.M. and J.W.Regester, **Polym. Eng. Sci.**, Oct, 235-45 (1965)

(8) Kraynik, A.M. and W.R.Schowalter, **J. Rheol.**, 25(1), 95-114 (1981)

(9) Vinogradov, G.V. and L.I.Ivanova, **Rheol. Acta**, 7, 243-254 (1968)

(10) Hatzikiriakos, S.G. and J.M.Dealy (submitted to **J. Rheol.**, 1991)

(11) White, J.L. et al., **J. Rheol.**, 35(1), 167-189 (1991)

(12) Laun, H.M., **Rheol. Acta**, 22, 171-185 (1983)

(13) Laun, H.M. and H.Schuch, **J. Rheol.**, 33, 119 (1990)

(14) Hatzikiriakos, S.G and J.M.Dealy, **J. Rheol.**, 35, 497 (1991)

(15) Mooney, M., **J. Rheol.**, 2, 210 (1931)

(16) Lau, H.C. and W.R.Schowalter, **J. Rheol.**, 30(1), 193-206 (1986)

(17) Vinogradov, G.V., **Rheol. Acta.**, 23, 46 (1984)

(18) Lin, Y.H., **J. Rheol.**, 29, 605 (1985)

(19) Ramachandran and Christianson, **J. Non-Newt. Fl. Mech.**, 13, 21 (1983)

(20) Han, C.D.,Rheology in Polymer Melt Processing, Acad. Press, N.Y. (1976)

(21) Dealy, J.M., **Rheol. Acta.**, 21, 475-477 (1982)

(22) Giacomin, A.J , PhD Thesis, McGill University (1987)

(23) Samurkas, T., PhD Thesis, McGill University (1992)

(24) Nelson, B.I., PhD Thesis, McGill University (1992)

(25) Young, W.C., Roark's Formulas for Stress & Strain, 6th ed., McGraw-Hill, NY (1989)

(26) Orbey, N., PhD Thesis, McGill University (1983)

(27) Dealy, J.M., Melt Rheology and Its Role in Plastics Processing, Von Nostrand Reinhold Company,NY (1990)

APPENDIX A

DISK-BAR SST DESIGN PROGRAM

```
10 CLS
100 REM **************************************************************
110 REM *                                                            *
120 REM *                    Author: Martin L. Sentmanat             *
130 REM *                                                            *
140 REM *                Department of Chemical Engineering          *
150 REM *                        McGill University                   *
160 REM *                                                            *
170 REM *  Program Description:                                      *
180 REM *                                                            *
190 REM *  This program was written to aid in the design of a new shear  *
200 REM *  stress transducer incorporating the concepts of the existing  *
210 REM *  torsion bar and disk spring models for rheometric use in high *
220 REM *  pressure applications. The program involves the use of    *
230 REM *  superposition in order to model the behavior of the torsion   *
240 REM *  bar and disk spring united into a single unit. The concept    *
250 REM *  essentially resembles a ribbed, or webbed, disk spring shear  *
260 REM *  stress transducer. This webbing is incorporated not only to   *
270 REM *  promote unidirectional rotation of the transducer beam, but   *
280 REM *  as a support mechanism under high pressure situations to     *
290 REM *  prevent significant axial deflections.                    *
300 REM *                                                            *
310 REM **************************************************************
320 REM
330 REM
340 REM
350 REM *** It should be noted that most of the following relationships
360 REM     and definitive equations were derived from models taken from
370 REM     Roark & Young's "Formulas for Stress and Strain" (1989).
380 REM     The following models were used:
390 REM     - From Chapter 7, Art. 7.1, Beams; Flexure of Straight Bars
400 REM           Concentrated intermediate load, left end guided, right
410 REM           end fixed (ref.no. 1b) p.100
420 REM     - From Chapter 9, Art. 9.2, Torsion
430 REM           Solid rectangular section (ref.no. 4) p.348
440 REM     - From Chapter 10, Art. 10.2, Flat Plates
450 REM           Annular plate with a uniform annular line load, outer
460 REM           edge fixed, inner edge guided (Case no. 1f) p.402
470 REM     - From Chapter 10, Art. 10.2, Flat plates
480 REM           Central couple on an annular plate with a fixed outer
490 REM           edge (trunnion loading), trunnion fixed to the plate
500 REM           (Case no. 21b) p.435
510 REM     - From Chapter 10, Art. 10.2, Flat Plates
520 REM           Annular plate with a uniformly distributed pressure
530 REM           outer edge fixed,inner edge guided (Case no. 2f) p.406
540 REM     - From Chapter 7, Art. 7.1, Beams; Flexure of Straight Bars
550 REM           Deflectionof elastic straight beam with a distributed load
560 REM           left end guided, right end fixed (Case no. 2b) p.103
610 REM     From these four equations (two equations for axial deflections,
620 REM     two equations for torsional deflections), two equations were
630 REM     developed (one for total axial deflection, one for total torsional
640 REM     deflection) in terms of the thickness of the plate,t, and in terms
650 REM     of the cross sectional height of the torsion bar,h, the two
660 REM     unknowns (technically there are three unknowns with the inclusion
670 REM     of the cross sectional width,b, but if an aspect ratio of h to b,
680 REM     phi, is assumed, b can be put in terms of h, and thus the number
690 REM     of unknowns is reduced to two, h and t). These two equations
700 REM     were then solved for h and t simultaneously, knowing the desired
710 REM     maximum axial and torsional deflections apriori.
720 REM
```

```
730 REM
740 REM
750 REM
1000 INPUT "Enter the maximum axial deflection (mm):",DELA
1005 PRINT
1010 INPUT "Enter the maximum deflection at the probe (mm):",DELT
1015 PRINT
1020 INPUT "Enter the aspect ratio (phi):",PHI
1025 PRINT
1050 REM
1100 DIAM=10!*.001
1110 AL=30!*.001
1120 PL=80!*.001
1130 OD=25!*.001
1140 ID=12!*.001
1150 DELA=DELA*.001
1160 DELT=DELT*.001
1170 PRES=96!*1000000!
1180 MAX=.4*1000000!
1190 DELMIN=.000127*.001
1200 EE=1.95E+11
1210 G=7.5E+10
1220 ALPH=.1411
1230 BETA=1.3708
1235 PI=3.14159265359#
1240 V=.3
1250 A=OD/2!
1260 BB=ID/2!
1270 L=(OD-ID)/2!
1280 AB=A/BB
1290 BA=BB/A
1300 AR=PI*DIAM^2/4!
1310 C2=.25*(1!-BA^2*(1!+2!*LOG(AB)))
1320 C5=.5*(1!-BA^2)
1330 C8=.5*(1!+V+(1!-V)*BA^2)
1340 L3=BA/4!*((BA^2+1!)*LOG(AB)+BA^2-1!)
1350 L5=.5*(1!-BA^2)
1360 L6=BA/4!*(BA^2-1!+2!*LOG(AB))
1370 L9=BA*(.5*(1!+V)*LOG(AB)+.25*(1!-V)*(1!-BA^2))
1372 L11=1!/64!*(1!+4*BA^2-5!*BA^4-4!*BA^2*(2!+BA^2)*LOG(AB))
1375 L14=1!/16!*(1!-BA^4-4!*BA^2*LOG(AB))
1380 GAMM1=(C2*L6)/C5-L3
1385 GAMM2=(C2*L14/C5-L11)
1390 ZETA=1!/PHI
1400 PSI1=ZETA^3/16!*(16!/3!-3.36*ZETA*(1!-ZETA^4/12!))
1410 PSI2=EE/(12!*(1!-V^2))
1420 F=.005
1430 OM1=F*L^4/(2*EE*ZETA)
1440 OM2=L^3/(EE*ZETA)
1445 OM3=L/(PSI1*G)
1450 MU1=1!/A^4
1460 MU2=PI*ID/A^3
1470 N1=PRES
1480 N2=(PRES+.25*MAX)*AR
1490 N3=MAX*AR*AL*PL
1500 CHI1=ALPH/(OM3*EE)
1510 CHI2=N3*OM3/DELT
1520 SIG1=OM1*PSI2*MU1/GAMM2
1530 SIG2=OM2*PSI2*MU2/GAMM1
1540 PHI1=2!-2!*CHI1*SIG1
```

```
1550 PHI2=2!-2!*CHI1*SIG2
1560 KAP1=CHI1*CHI2*SIG1
1570 KAP2=CHI1*CHI2*SIG2
1580 AAA=PHI1*PHI2
1590 BBB=PHI1*KAP2-PHI2*KAP1-(N1*OM1*PHI2+N2*OM2*PHI1)/DELA
1600 CCC=KAP1*KAP2-(N1*OM1*KAP2+N2*OM2*KAP1)/DELA
1610 PPI=(-BBB+(BBB^2-4!*AAA*CCC)^(.5))/(2!*AAA)
1620 H=PPI^(.25)
1630 T=((N3*OM3/(DELT*PPI)-2!)*ALPH*PPI/(OM3*EE))^(1!/3!)
2050 REM
2080 REM
3000 REM
3010 REM
3020 REM
5000 REM     Description of significant variables:
5010 REM     ____________________________________________________
5020 REM
5030 REM     Mt = Moment required to deflect the torsion bar the angle
5040 REM          corresponding to the maximum deflection at the probe
5050 REM          (N-m)
5060 REM     Md = Moment required to deflect the disk the same angle
5070 REM          as the torsion bar (N-m)
5080 REM     Ft = Force required to deflect the torsion bar axially by
5090 REM          DELA (N)
5100 REM     Fd = Force required to defect the disk axially by the same
5110 REM          distance DELA (N)
5120 REM
5130 REM
6000 MT=(MAX*AR*AL)/(2!+EE*T^3/(H^4*PSI1*G*ALPH))
6010 MD=((L*EE*T^3)/(H^4*PSI1*G*ALPH))*MT
6020 REM
6030 I=ZETA/12!*H^4
6035 D=EE*T^3/(12*(1!-V^2))
6040 REM
6050 FT=(PRES+.25*MAX)*AR/(2!+D*L^3*PI*ID/(12!*A^3*EE*I*GAMM1))
6060 FD=FT*D*L^3*PI*ID/(12!*A^3*EE*I*GAMM1)
6070 WB=PRES/(2!+(T^3*F*L^4*PSI2/(2!*EE*ZETA*A^4*GAMM2*H^4)))*F
6080 REM
6090 REM
7000 BEND=FT*L/2!*H/2!/I+WB*L^2/6!*H/2!/I
7010 REM
7020 SHEAR=3!*MT/(8!*(H/2!)*(H/2!/PHI)^2)*(1!+.6095*ZETA+.8865*ZETA^2-1.8023*ZET
A^3+.91*ZETA^4)+1.5*(FD+FT+WB*L)/(ZETA*H^2)
7030 REM
7050 MIN=DELMIN*(2!+EE*T^3*L/(PSI1*H^4*G*ALPH))*PSI1*H^4*G/(PL*AL*L*AR)
8000 INPUT "Do you want output to go to printer (Y/N)?",ANS$
8010 IF ANS$="Y" THEN GOTO 14000
10000 PRINT
10010 PRINT
10020 PRINT "                         Transducer Data                              "
10030 PRINT "_____________________________________________________________________"
10040 PRINT
10050 PRINT "Maximum measured shear stress:          (MPa) ",MAX*.000001
10055 PRINT "Minimum measured shear stress:          (MPa) ",MIN*.000001
10060 PRINT "Maximum bending stress in bar:          (MPa) ",BEND*.000001
10065 PRINT "Maximum shear stress in bar:            (MPa) ",SHEAR*.000001
10070 PRINT "Maximum melt pressure:                  (MPa) ",PRES*.000001
10100 PRINT
10120 PRINT "Maximum axial deflection:                (mm) ",DELA*1000!
10130 PRINT "Maximum deflection at probe:             (mm) ",DELT*1000!
```

```
10140 PRINT "Minimum deflection at probe:                  (mm) ",DELMIN*1000!
10145 PRINT "Maximum active face deflection:               (mm) ",DELT*1000!*AL/PL
10150 PRINT "Minimum active face deflection:               (mm) ",DELMIN*1000!*AL/PL
10155 PRINT
10160 PRINT "Active face diameter:                         (mm) ",DIAM*1000!
10170 PRINT "Disk outside diameter:                        (mm) ",OD*1000!
10180 PRINT "Disk inside diameter:                         (mm) ",ID*1000!
10460 PRINT "Disk thickness:                               (mm) ",T*1000!
10470 PRINT "Torsion bar cross-sectional height:           (mm) ",H*1000!
10480 PRINT "Torsion bar cross-sectional width:            (mm) ",ZETA*H*1000!
10500 PRINT "Lever lengths - Active face end               (mm) ",AL*1000!
10510 PRINT "                Probe end                     (mm) ",PL*1000!
11000 GOTO 15000
14000 LPRINT
14010 LPRINT
14020 LPRINT "                         Transducer Data                              "
14030 LPRINT "______________________________________________________________________"
14040 LPRINT
14050 LPRINT "Maximum measured shear stress:               (MPa) ",MAX*.000001
14055 LPRINT "Minimum measured shear stress:               (MPa) ",MIN*.000001
14060 LPRINT "Maximum bending stress in bar:               (MPa) ",BEND*.000001
14065 LPRINT "Maximum shear stress in bar:                 (MPa) ",SHEAR*.000001
14070 LPRINT "Maximum melt pressure:                       (MPa) ",PRES*.000001
14100 LPRINT
14120 LPRINT "Maximum axial deflection:                     (mm) ",DELA*1000!
14130 LPRINT "Maximum deflection at probe:                  (mm) ",DELT*1000!
14140 LPRINT "Minimum deflection at probe:                  (mm) ",DELMIN*1000!
14145 LPRINT "Maximum active face deflection:               (mm) ",DELT*1000!*AL/PL
14150 LPRINT "Minimum active face deflection:               (mm) ",DELMIN*1000!*AL/P
L
14155 LPRINT
14160 LPRINT "Active face diameter:                         (mm) ",DIAM*1000!
14170 LPRINT "Disk outside diameter:                        (mm) ",OD*1000!
14180 LPRINT "Disk inside diameter:                         (mm) ",ID*1000!
14460 LPRINT "Disk thickness:                               (mm) ",T*1000!
14470 LPRINT "Torsion bar cross-sectional height:           (mm) ",H*1000!
14480 LPRINT "Torsion bar cross-sectional width:            (mm) ",ZETA*H*1000!
14500 LPRINT "Lever lengths - Active face end               (mm) ",AL*1000!
14510 LPRINT "                Probe end                     (mm) ",PL*1000!
15000 END
```

```
                        Transducer Data
_______________________________________________________________

Maximum measured shear stress:          (MPa)        .4
Minimum measured shear stress:          (MPa)        3.366667E-03
Maximum bending stress in bar:          (MPa)        95.97648
Maximum shear stress in bar:            (MPa)        148.3202
Maximum melt pressure:                  (MPa)        96

Maximum axial deflection:                (mm)        5.000001E-04
Maximum deflection at probe:             (mm)        .015
Minimum deflection at probe:             (mm)        .000127
Maximum active face deflection:          (mm)        .005625
Minimum active face deflection:          (mm)        4.7625E-05

Active face diameter:                    (mm)        10
Disk outside diameter:                   (mm)        26
Disk inside diameter:                    (mm)        12
Disk thickness:                          (mm)        1.003385
Torsion bar cross-sectional height:      (mm)        17.11858
Torsion bar cross-sectional width:       (mm)        3.229921
Lever lengths - Active face end          (mm)        30
                Probe end                (m          80.00001
```

APPENDIX B

THE SLIT DIE

Part	Qty.	Description	Drawing No.
SD001	1	Bottom Half of Slit Die AISI 420	001 002 003
SD002	2	Shims for 1 mm Gap AISI 420	004
SD003	1	Top Half of Slit Die AISI 420	005 006 007 008 009 010
SD004	4	Mounting Bolts for Flange SPEC: 3/8" - 16 UNC x 1" Socket Head Flat Steel Alloy	
SD005	8	Die Assembly Bolt SPEC: 3/8" - 16 UNC x 2" Socket Head Cap Steel Alloy	
SD006	8	Mounting Bolts for SST's SPEC: 1/4" - 28 UNF x 2" Socket Head Cap Steel Alloy	
SD007	1	Locking Cap Adaptor for Thermocouple SPEC: 3/8" - 24 UNF STD	
SD008	1	15000 psi Pressure Transducer	009A
SD009	1	Mounting Flange for Capillary Rheometer	011 012
SD010	4	Reinforcement Bolts for Mounting Flange SPEC: 3/8" - 16 UNC x 1 1/2" Socket Head Cap Steel Alloy	

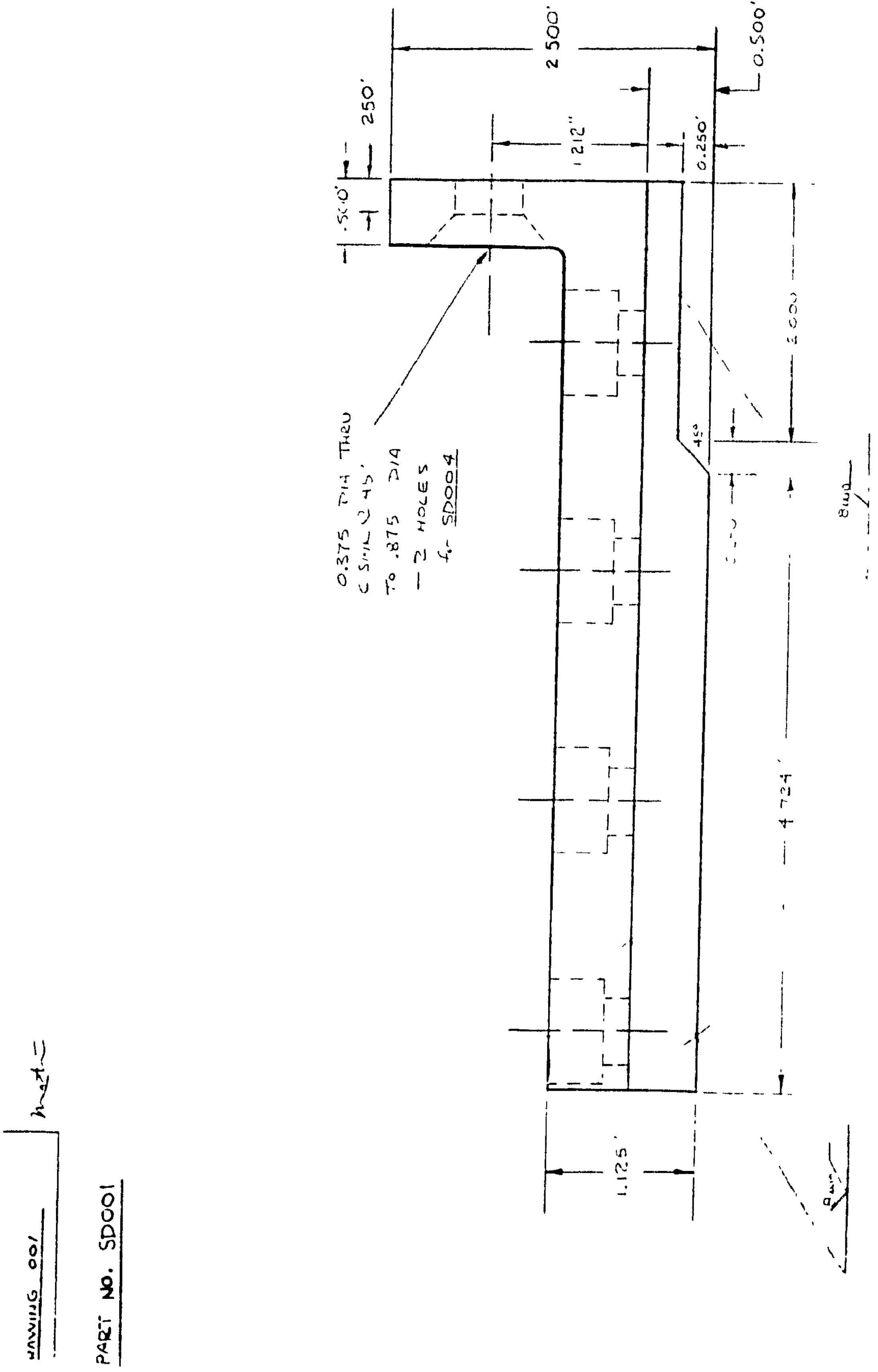
2.500"
0.500"
.250"
1.212"
0.250"
.500"
2.000
45°
4.724"
1.125"
0.375 DIA THRU
C SINK 2 45°
TO .875 DIA
— 2 HOLES
f.r SD004
DRAWING 001
PART NO. SD001
mat =

RAWING 002 | Sheet -

PART NO. SD001

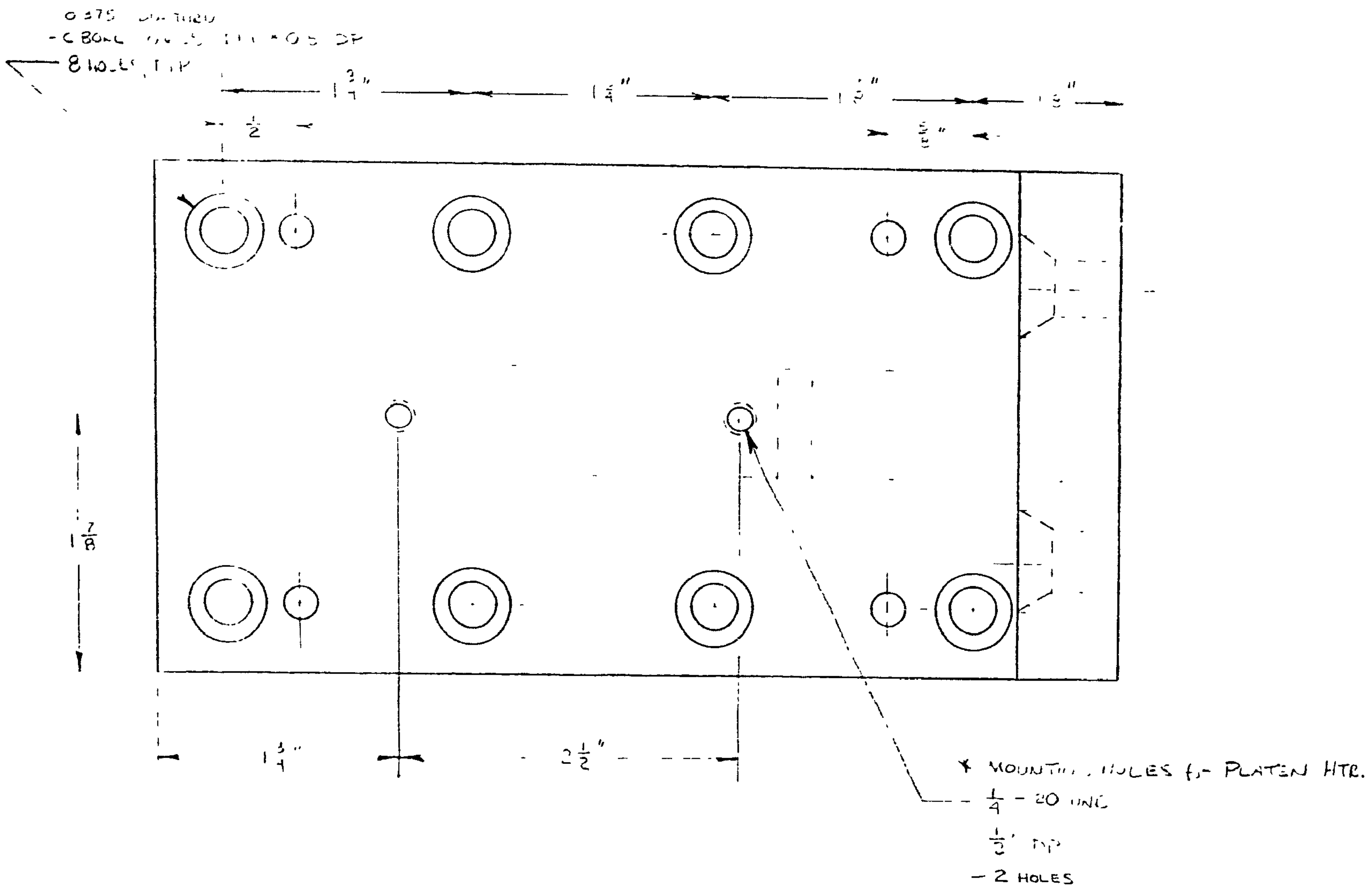

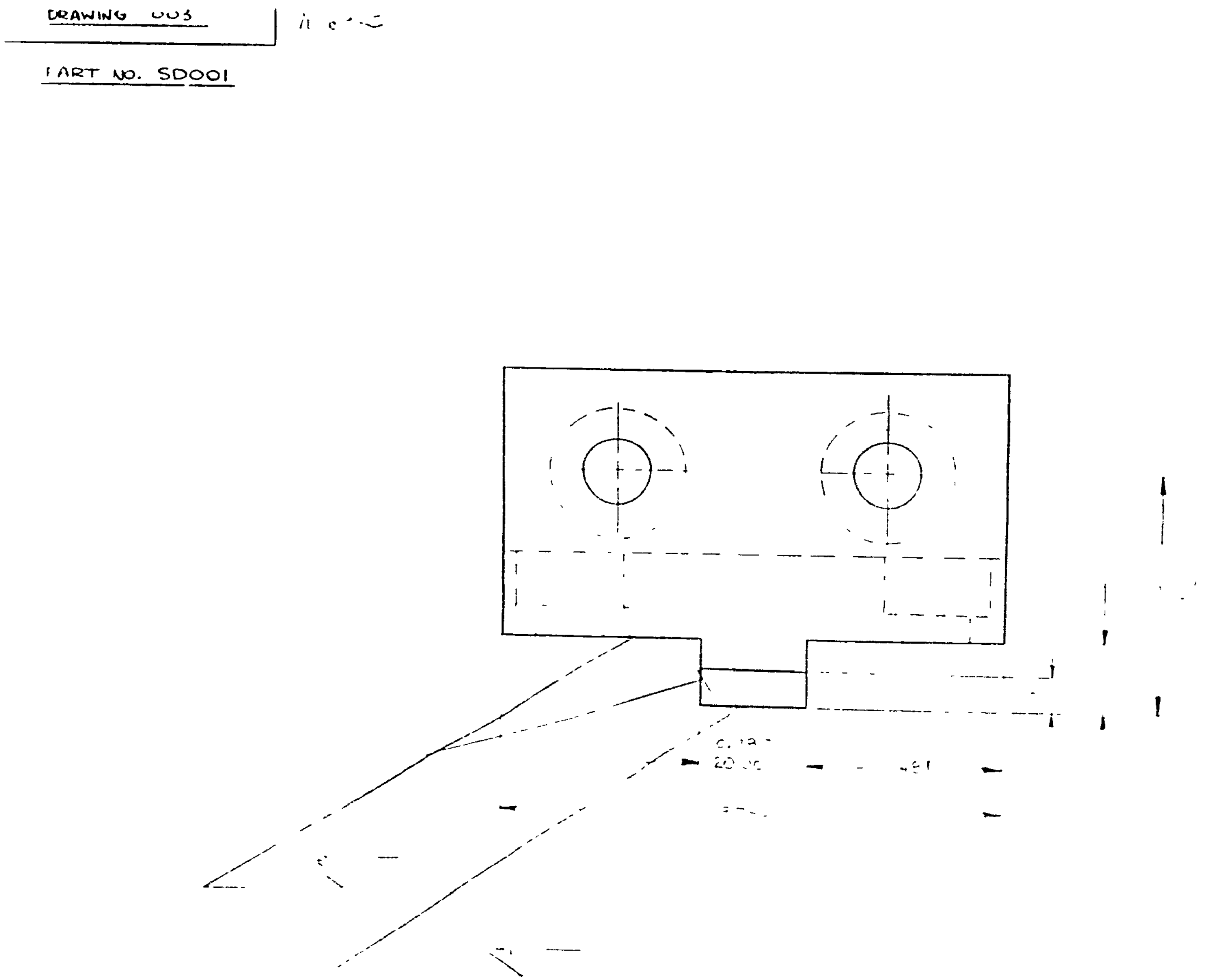
DRAWING 003
PART NO. SD001

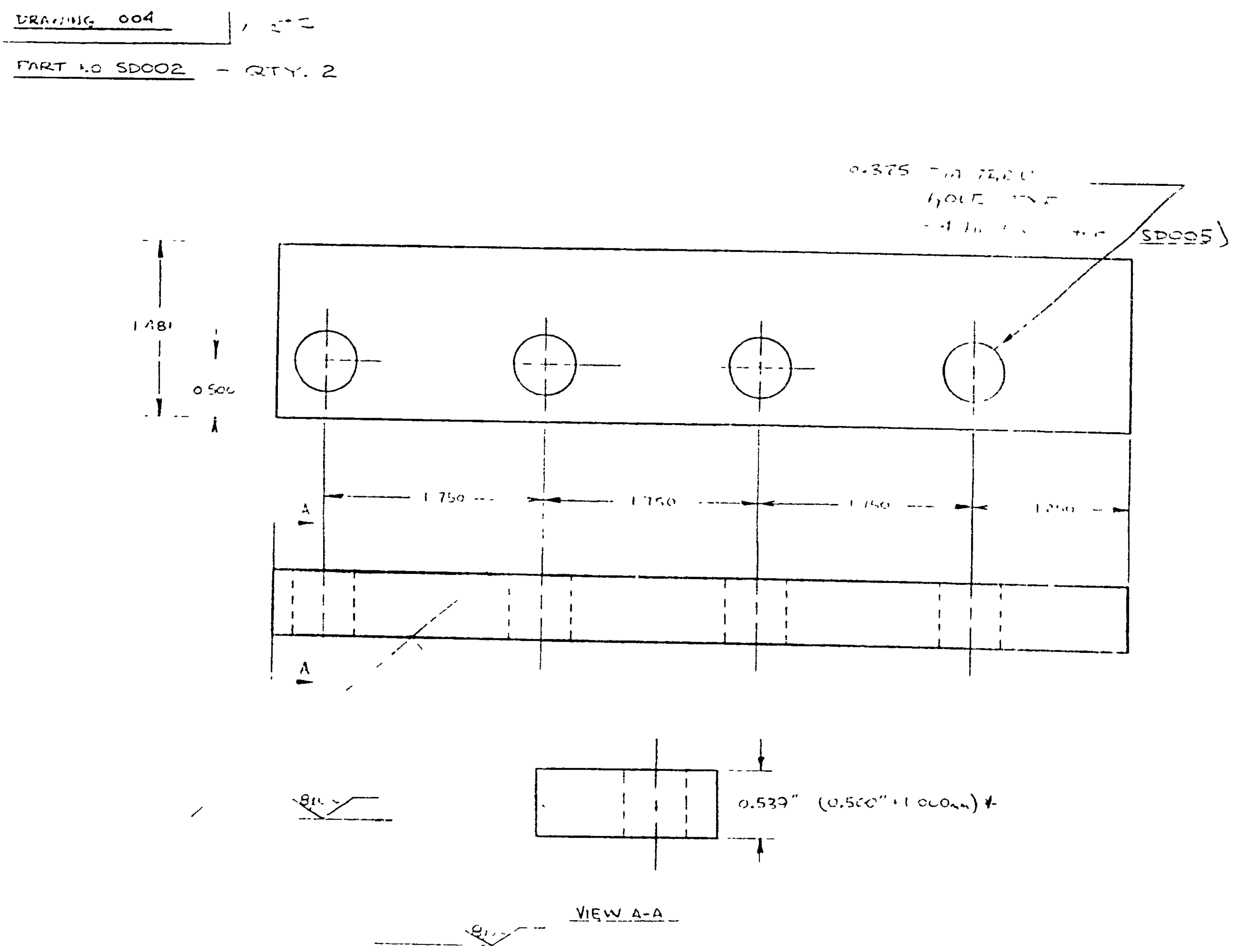
DRAWING 004
PART NO SD002 - QTY. 2
0.375 [illegible]
HOLE [illegible]
SD005)
1.481
0.500
1.750
1.750
1.750
1.250
A
A
0.539" (0.500" + 1.000mm)
VIEW A-A

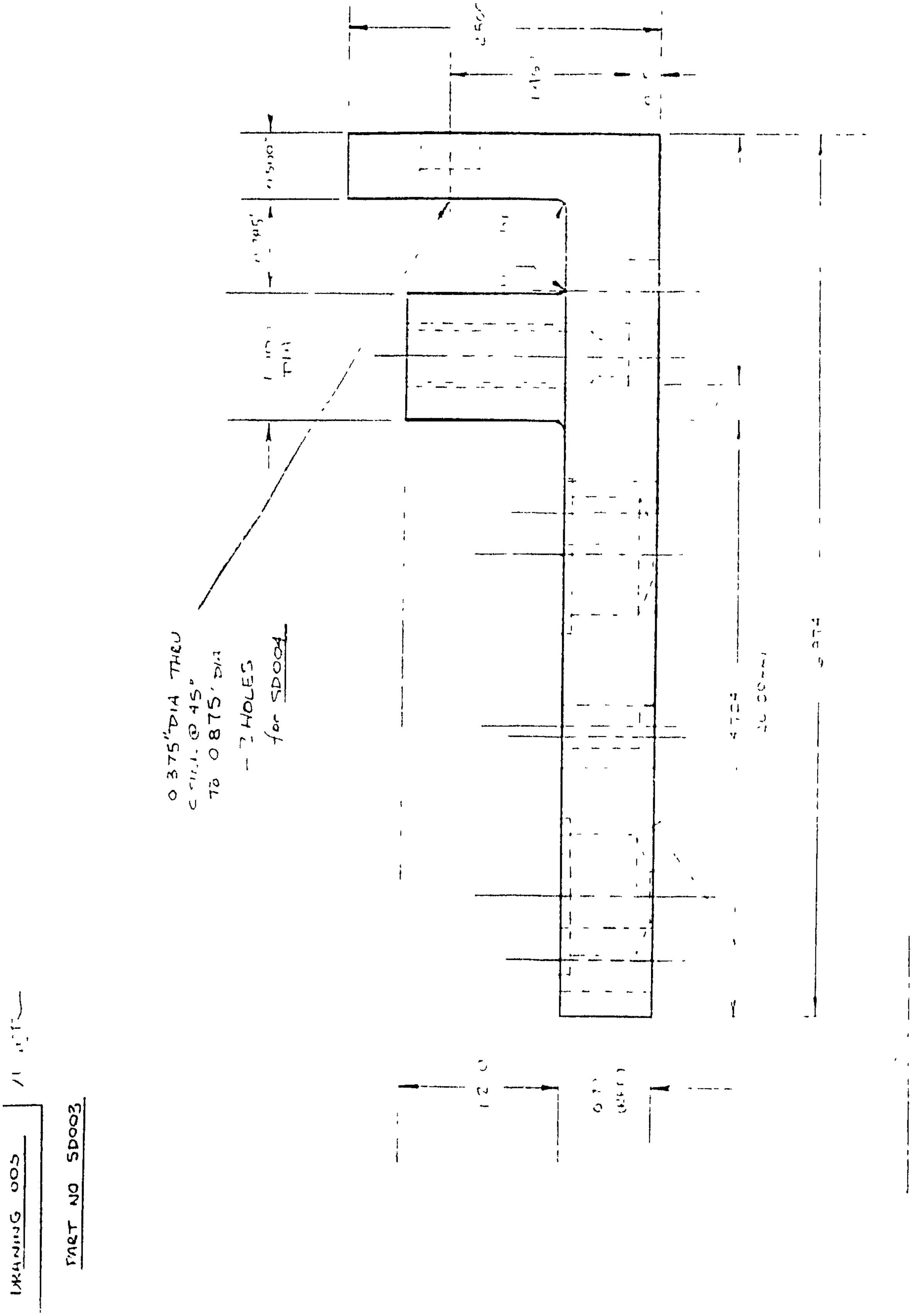
0.375" DIA THRU
C'SINK @ 45°
TO 0.875' DIA
— 2 HOLES
for SD004
DRAWING 005
PART NO SD003

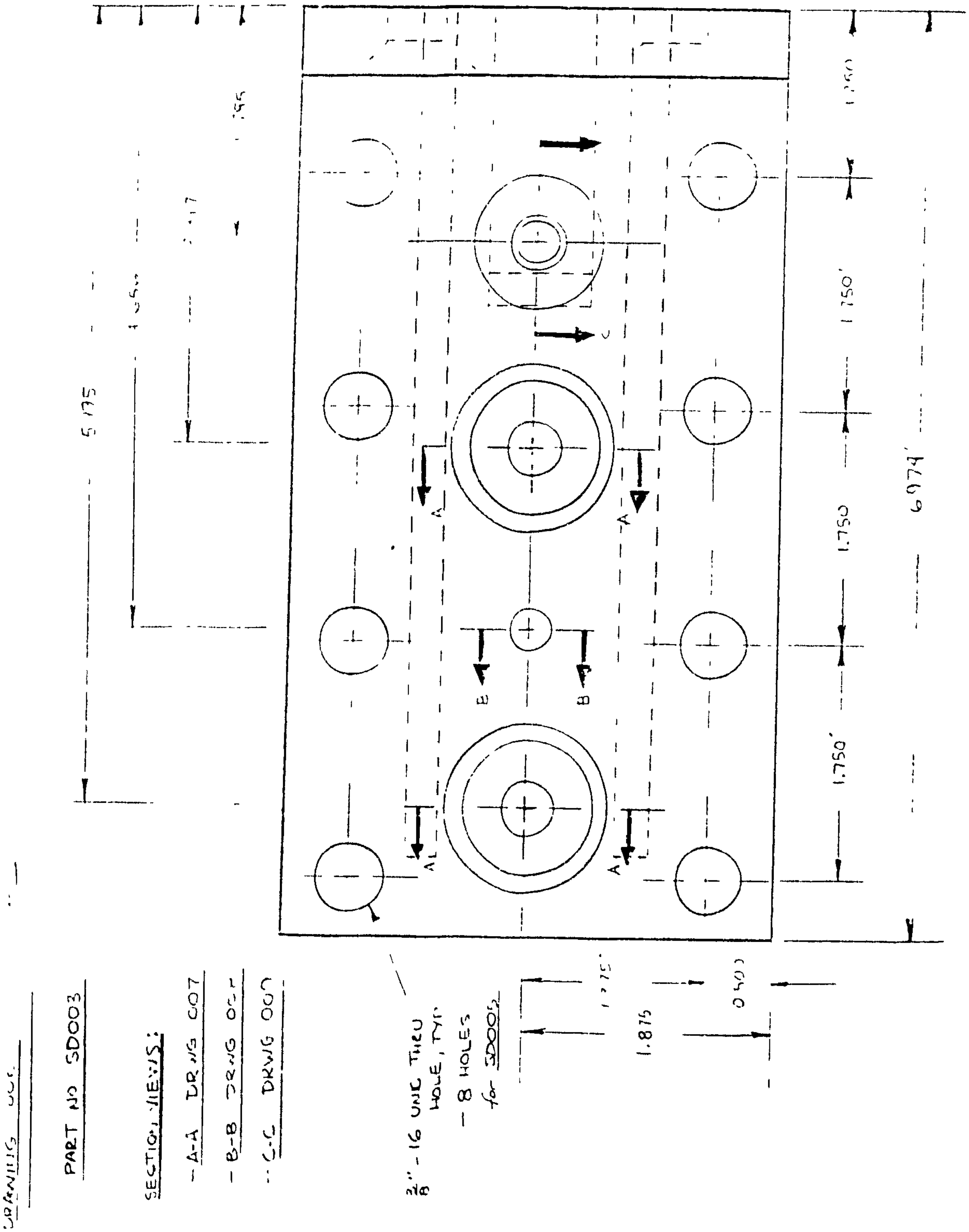
DRAWING
PART NO SD003
SECTION VIEWS:
- A-A DRWG 007
- B-B DRWG 008
- C-C DRWG 009
3/8" - 16 UNC THRU HOLE, TYP. - 8 HOLES for SD005
5.175
1.750
1.750
1.750
6.974
1.875
A
B
C

DRAWING 007

SECTION VIEW A-A

— SHOWS PRESS TRANSDUCER MOUNTS

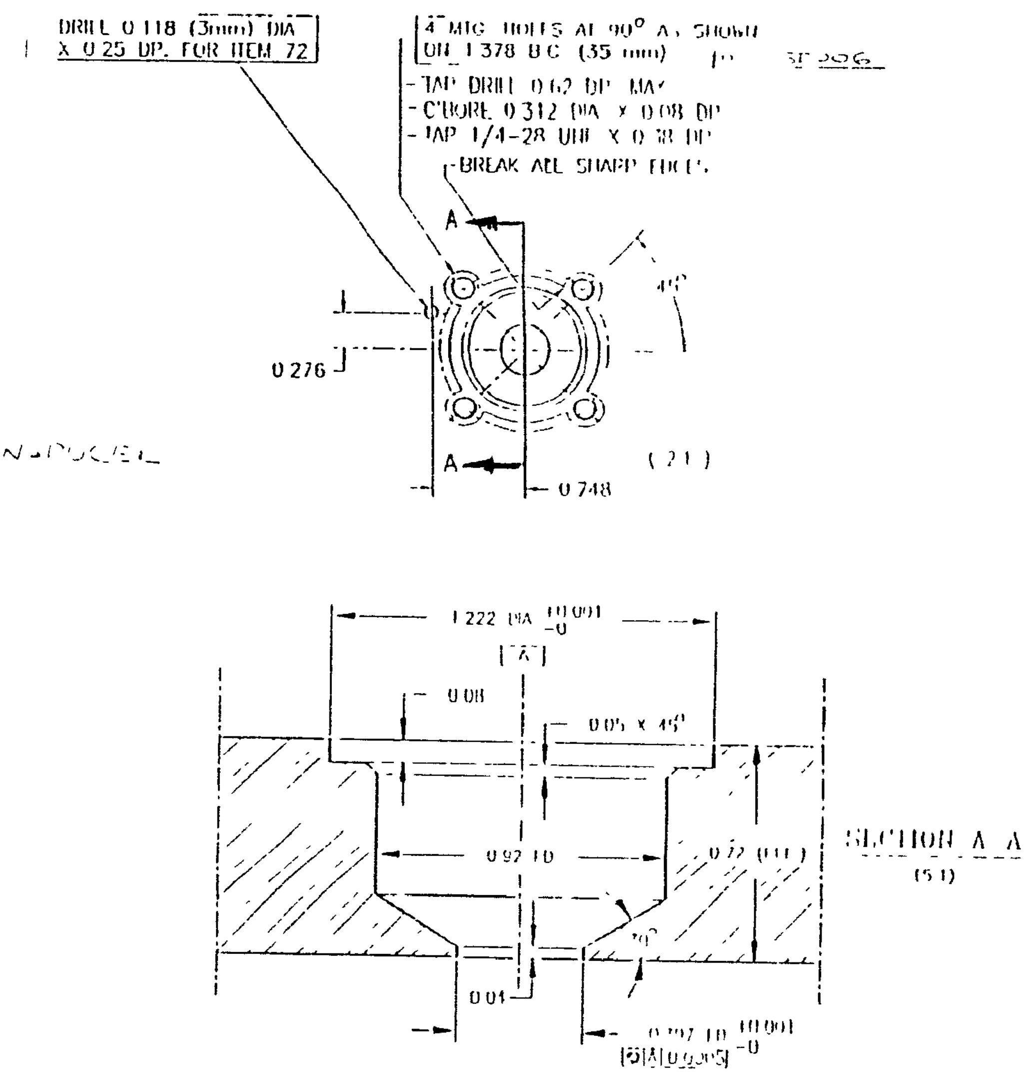

DRAWING 008 | 1/1

SECTION VIEW B-B

— THERMOCOUPLE MOUNT

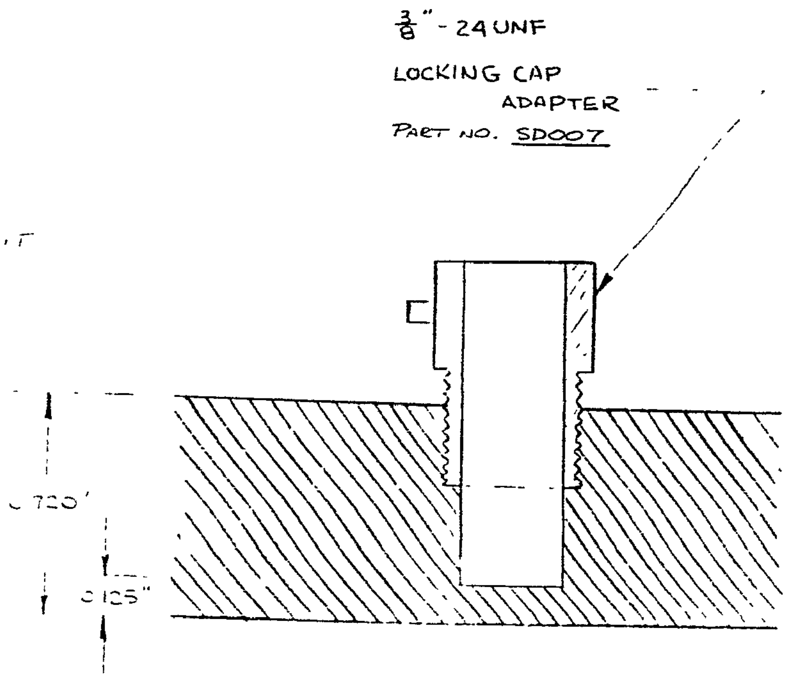

DRAWING 009

SECTION VIEW C-C

- PRESSURE TRANSDUCER MOUNT
- SEE FOLLOWING PAGE for PRESSURE TRANSDUCER DIMENSIONS

PART NO. SD008

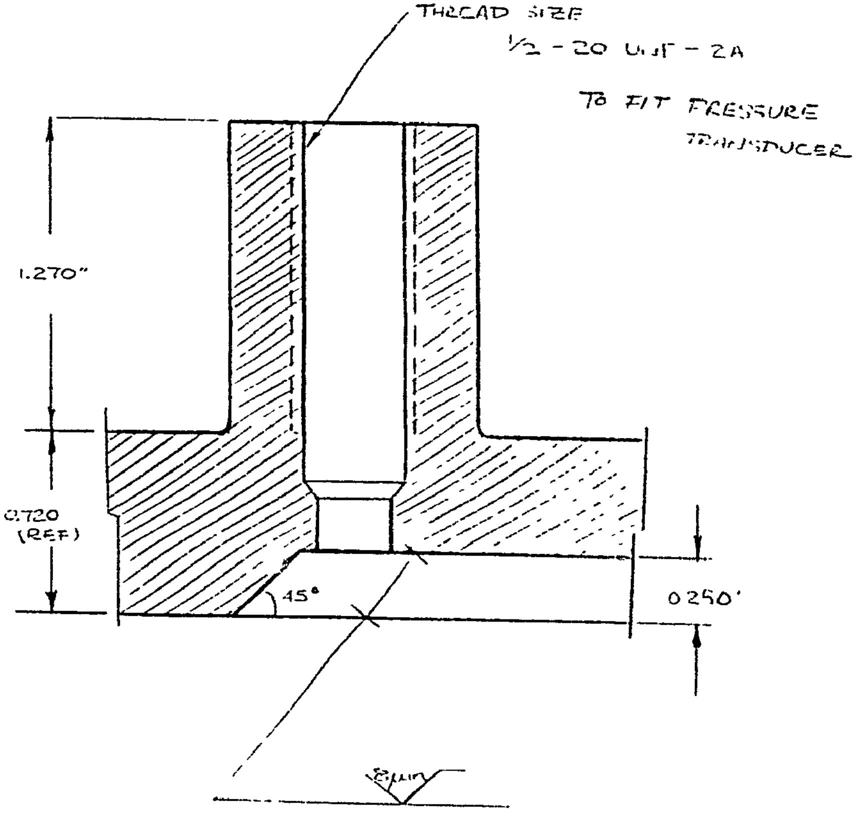

PLASTIC MELT PRESSURE TRANSDUCER MODEL GT76/GT77

SPECIFICATIONS

STANDARD PRESSURE RANGES	0-1000, 0-1500, 0-3000, 0-5000, 0-10,000, 0-15,000
OPERATING TEMPERATURE	0° to 750°F (Diaphragm)
SENSITIVITY	3.0 MV/V nominal (open circuit)
NOMINAL RESISTANCE	350 ohms
NON-LINEARITY	±1.0% of full scale, max. (B.S.L.)
HYSTERESIS	1.0% of full scale, max.
REPEATABILITY	0.1% of full scale, max.
THERMAL ZERO SHIFT	0.01% of full scale/°F nominal
THERMAL SENSITIVITY SHIFT	0.01% of full scale/°F nominal
OVERLOAD	150% Rated range
EXCITATION VOLTAGE	5-12 Volts DC or AC (RMS), 15 Volt max.

	A	B	C
GT-76	6 in. 152.4 mm	9.5 in. 241.3 mm	0.5 in. 12.7 mm
GT-77	12 in 304.8 mm	15.5 in 393.7 mm	0.625 in. 15.88 mm

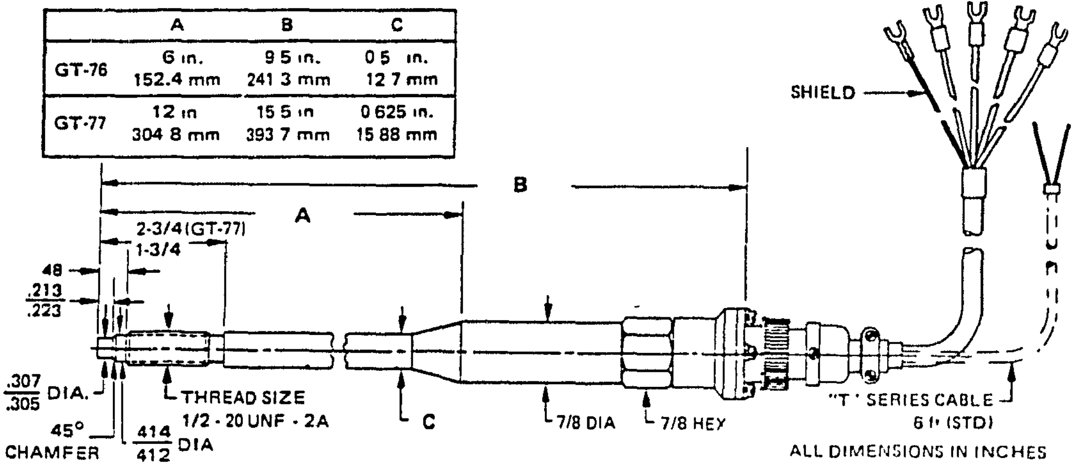

ALL DIMENSIONS IN INCHES

GENERAL INFORMATION

The Model GT76, or GT77, transducer is supplied with a 6-foot, 4 conductor shielded cable with Cannon WK6-21C mating connector and spade lug terminations.

This pressure transducer does not require special installation; in mounting, do not torque transducer greater than 20 foot-pounds.

Nominal impedance of the type J thermocouple is 5.0 ohms (with 6-foot leads).

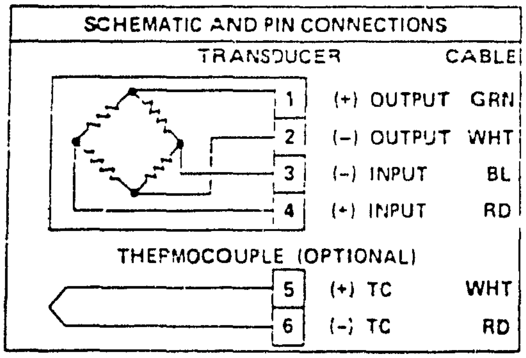

SCHEMATIC AND PIN CONNECTIONS

TRANSDUCER		CABLE
1	(+) OUTPUT	GRN
2	(–) OUTPUT	WHT
3	(–) INPUT	BL
4	(+) INPUT	RD

THERMOCOUPLE (OPTIONAL)

5	(+) TC	WHT
6	(–) TC	RD

Gentran inc. 1290 Hammerwood Avenue • Sunnyvale, CA 94089 • Phone 408/734-5060

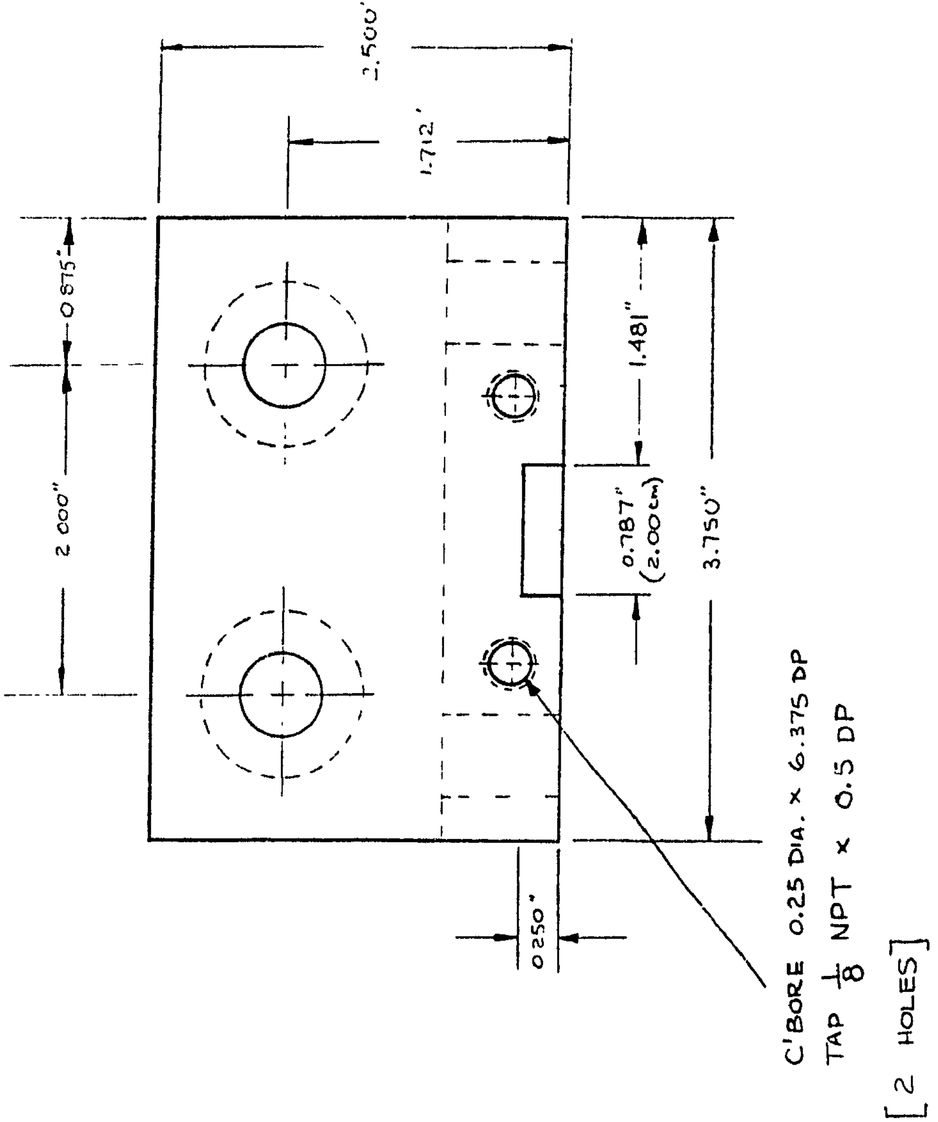

DRAWING

PART NO SD003

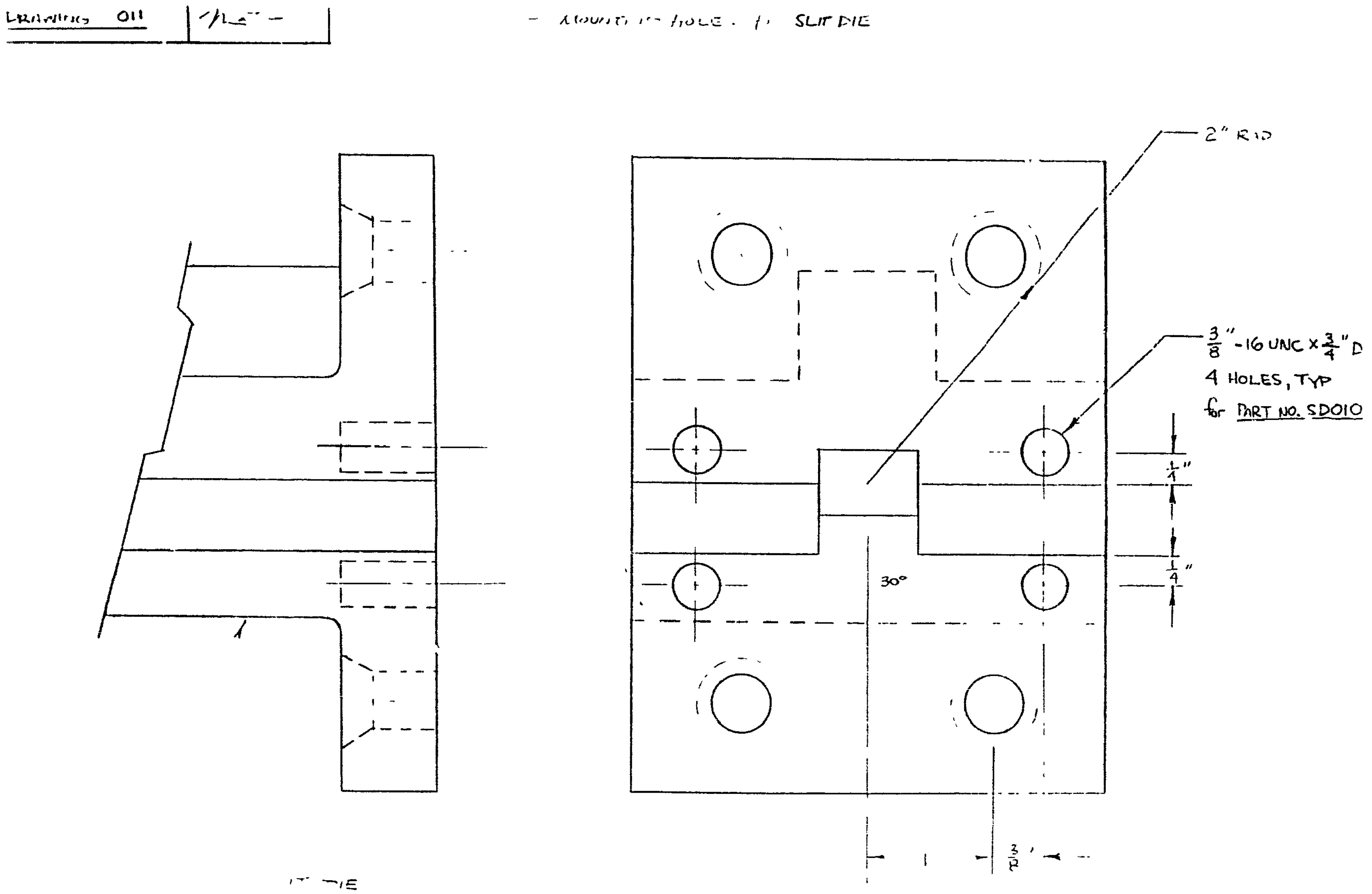
DRAWING 011
SLIT DIE
2" RAD
3/8"-16 UNC x 3/4" D
4 HOLES, TYP
for PART NO. SDO10
1/4"
1/4"
30°
3/8'

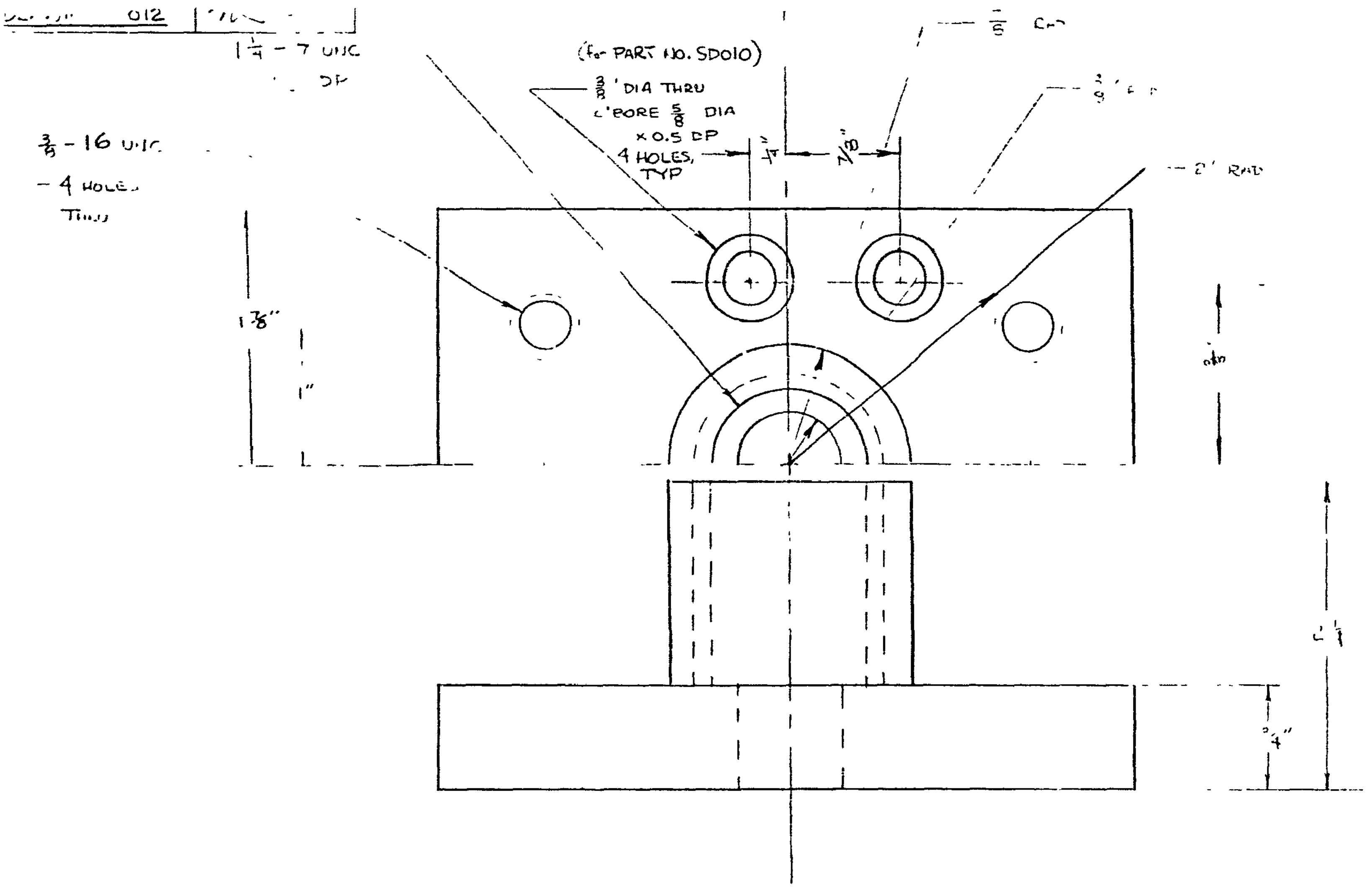

PART NO. SD009 — MOUNTING FLANGE for CAPILLARY/RHEOMETER [illegible] AND SLIT DIE

APPENDIX C

THE DISK-BAR SST

Part	Qty.	Description	Drawing No.
		SST Assembly	001
SST001	2	Disk-Bar SST	002
SST002	2	SST Housing	003
SST003	2	Mounting Sleeve for Capacitance Probe	004
SST004	2	Probe Target	005
SST005	2	Active Face SST Head	006
SST006	2	Locking Set Screw for SST Head	007
SST007	2	Locking Cap Adaptor for Thermocouple SPEC: 3/8" - 24 UNF STD	

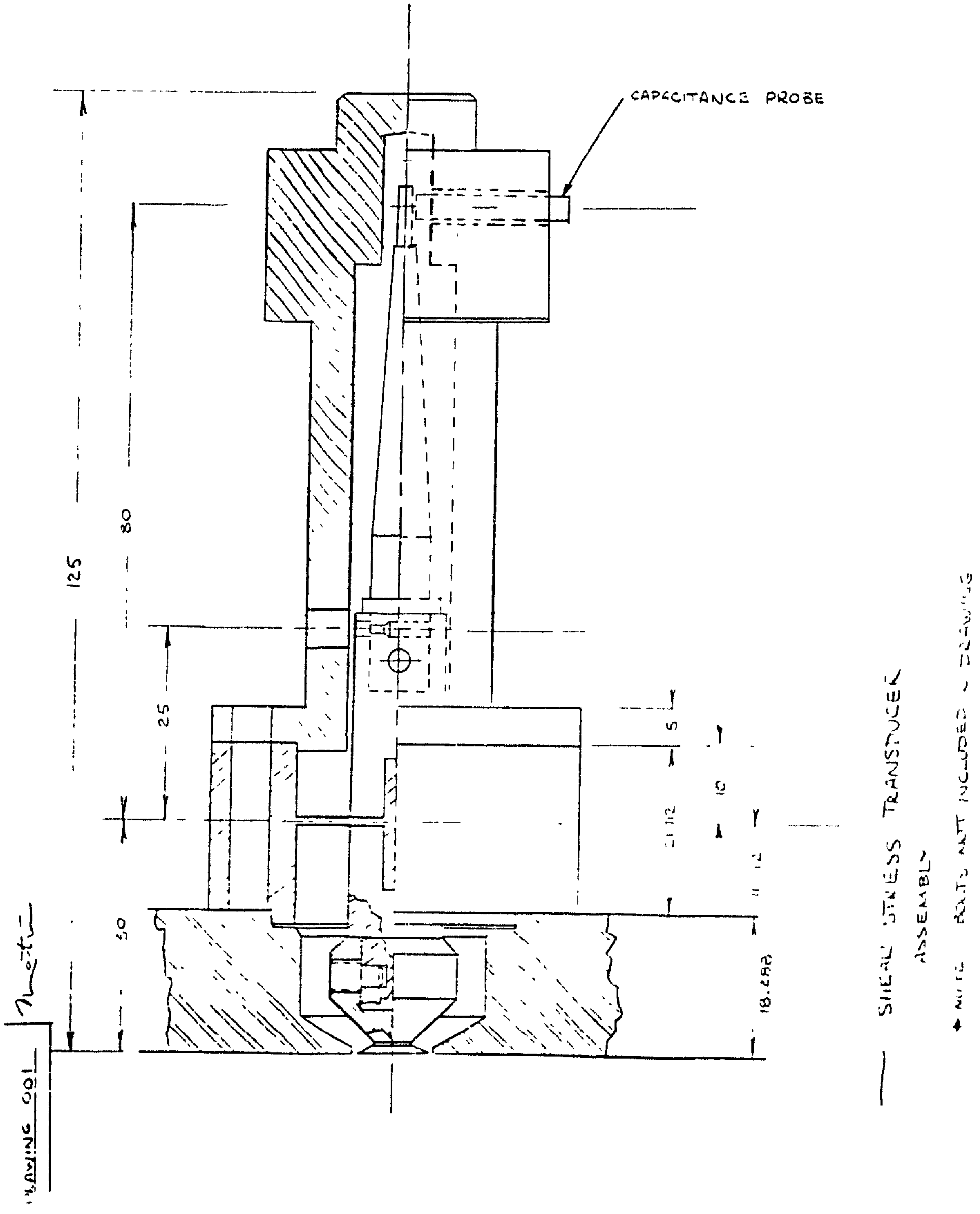
CAPACITANCE PROBE
125
80
25
30
5
10
12
18.288
SHEAR STRESS TRANSDUCER
ASSEMBLY
NOTE BOLTS NOT INCLUDED IN DRAWING
DRAWING 001

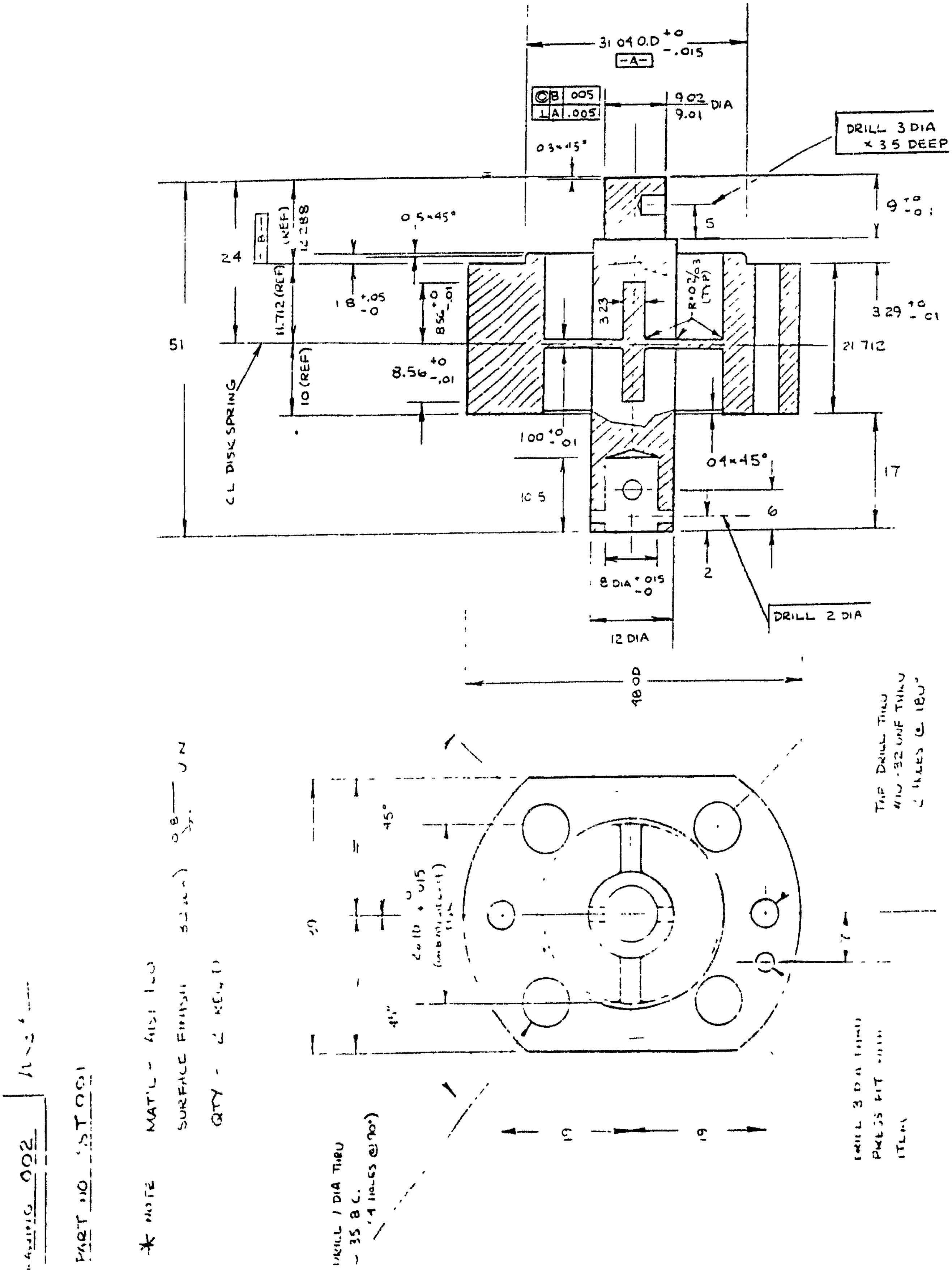
31.04 O.D +0 -.015
-A-
⌾ B .005
⊥ A .005
9.02 / 9.01 DIA
0.3×45°
DRILL 3 DIA × 3.5 DEEP
9 +0 -0.1
5
0.5×45°
24
-B-
12.288 (REF)
11.712 (REF)
1.8 +.05 -0
8.56 +0 -.01
3.23
R.02/.03 (TYP)
3.29 +0 -.01
21.712
51
CL DISK SPRING
10 (REF)
8.56 +0 -.01
1.00 +0 -.01
0.4×45°
17
10.5
6
2
8 DIA +.015 -0
DRILL 2 DIA
12 DIA
48 OD
TAP DRILL THRU #10-32 UNF THRU 2 HOLES @ 180°
45°
=
39
20.10 +0 .015
45°
7
19
19
DRILL 7 DIA THRU 35 B.C. (4 HOLES @ 90°)
DRILL 3 DIA THRU PRESS FIT WITH ITEM
DRAWING 002
PART NO SST001
* NOTE MAT'L - AISI
SURFACE FINISH
QTY - 2 REQ'D

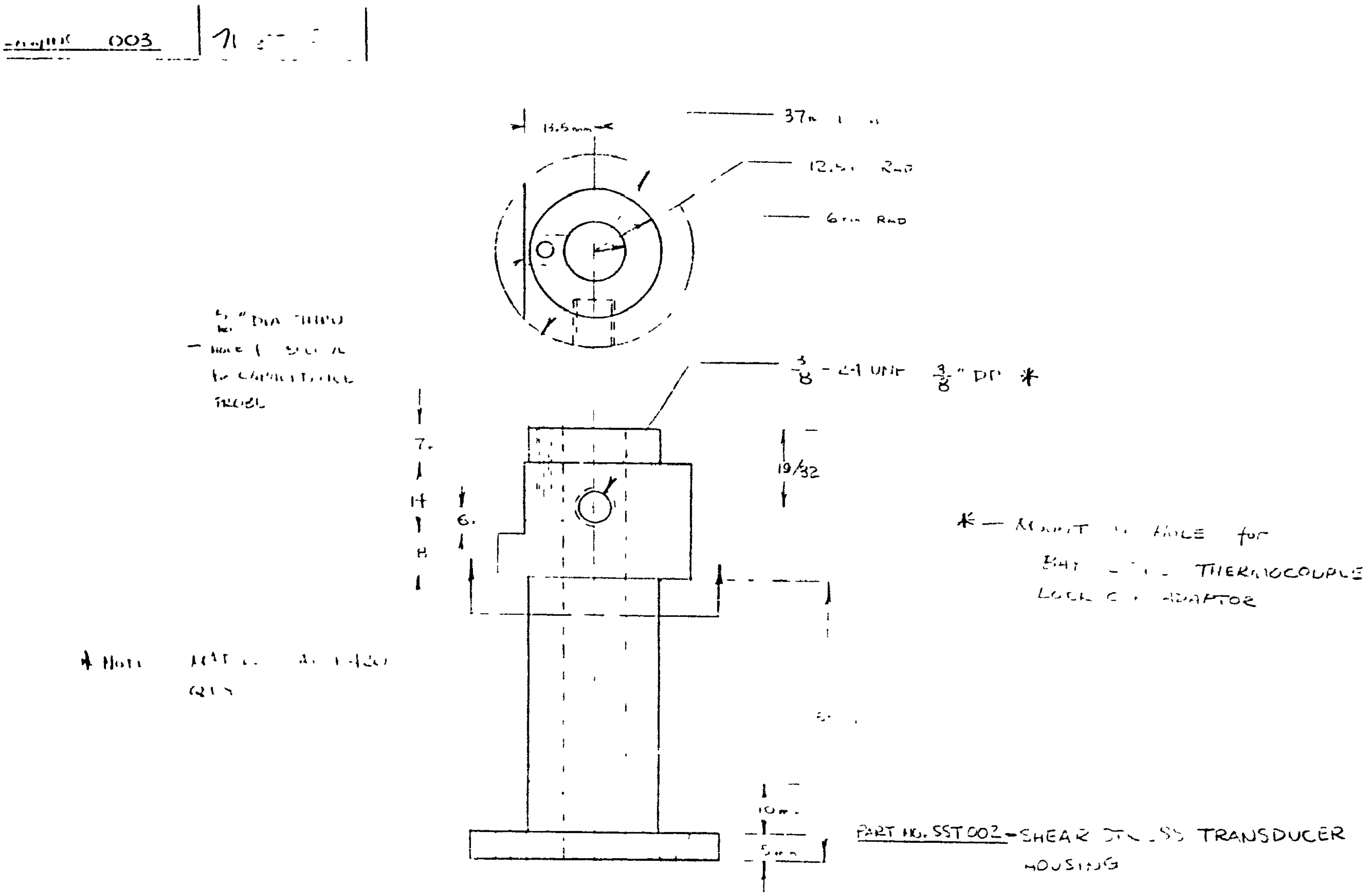
003
37
13.5mm
12.5 RAD
6mm RAD
3/8 - 24 UNF 3/8" DP *
19/32
7.
14
6.
8
10mm
5mm
" DIA THRU HOLE
CAPACITANCE PROBE
* — MOUNT HOLE for THERMOCOUPLE ADAPTOR
PART NO. SST 002 — SHEAR TRANSDUCER HOUSING
* Note
QTY

RAWING 004

* NOTE : MAT'L - AISI 420
QTY - 2

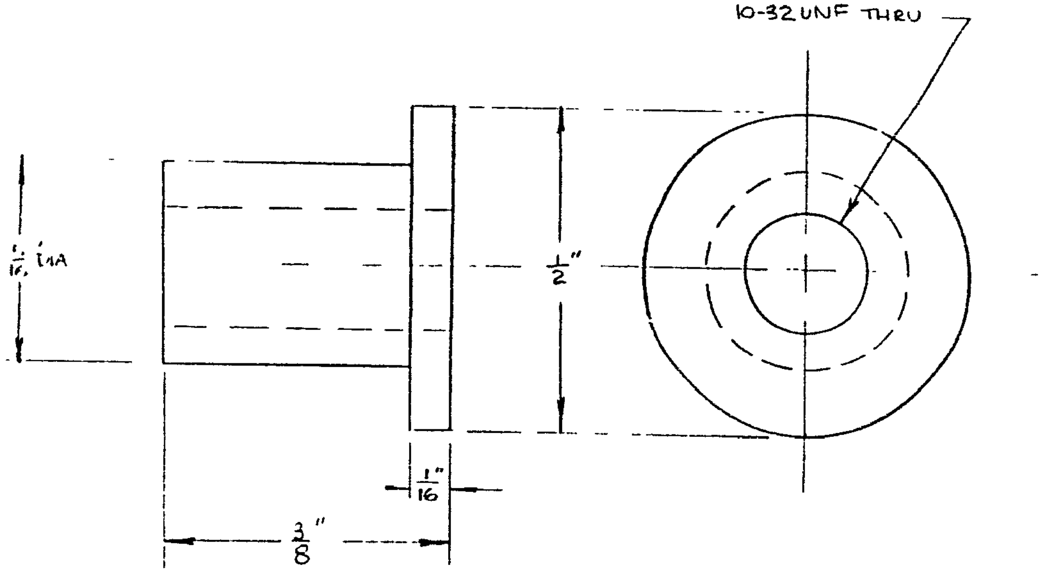

PART NO. SST 003 — MOUNTING SLEEVE for CAPACITANCE PROBE

DRAWING 005

— NOTE: QTY' - 2 REQ'D

PART NO SST004 — PROBE TARGET

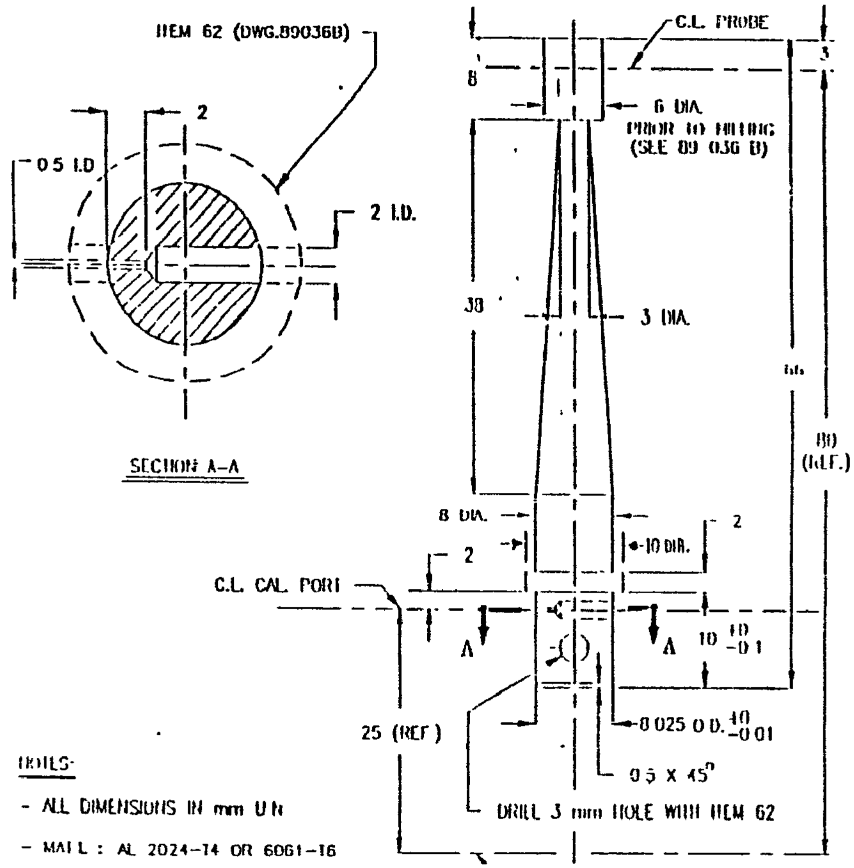

DRAWING 006

- NOTE: QTY - 2 REQ'D

PART NO. SST005 - ACTIVE FACE SST HEAD

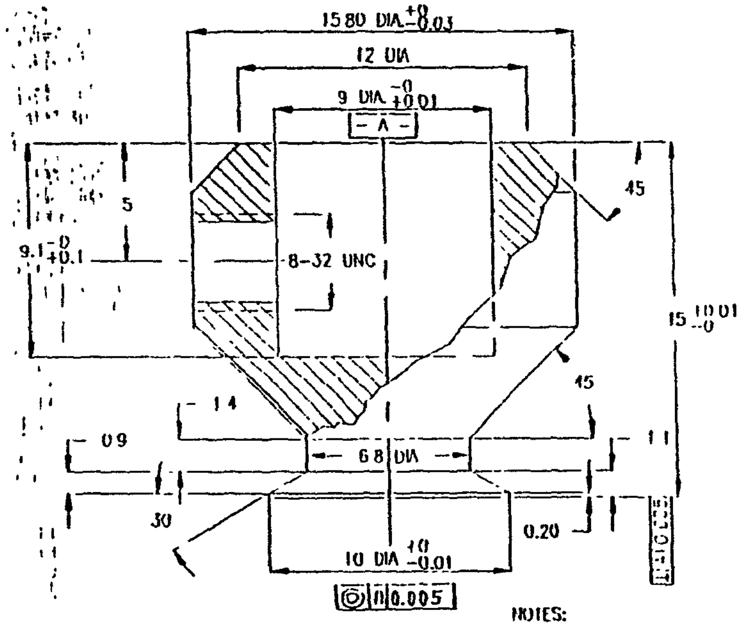

NOTES:
- ALL DIMENSIONS IN mm U.N.
- MAT'L : AISI 420 OR 17-4 PH
- SURFACE FINISH : (32μin.) $\overset{0.8}{\checkmark}$ U.N.

DRAWING 001

— NOTE : QTY - 2 REQ'D

PART NO. SST006 — LOCKING SET SCREW for SST HEAD

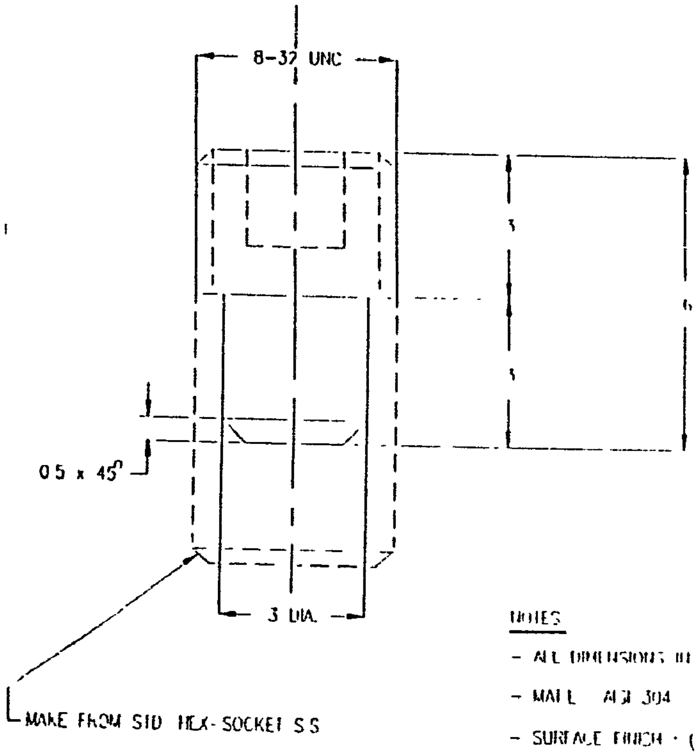

NOTES

- ALL DIMENSIONS IN mm [illegible]
- MAT'L AISI 304
- SURFACE FINISH · (32μm) 0.5

APPENDIX D

CAPACITEC PRODUCT LITERATURE

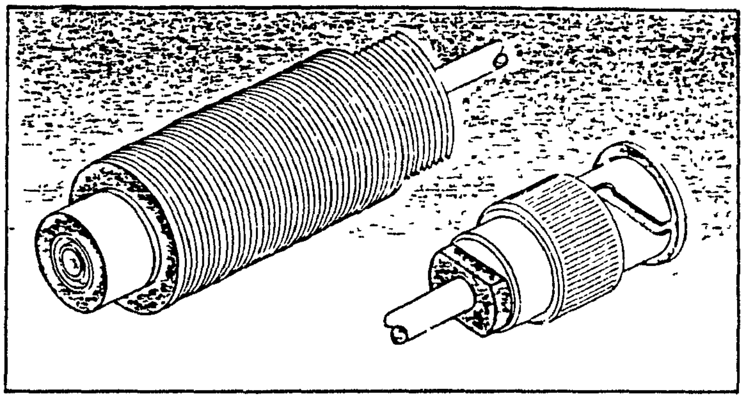

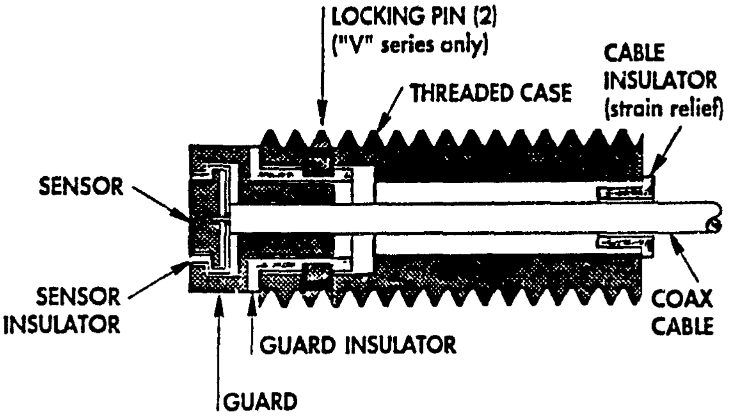

HPT SERIES THREADED PROBES

Similar to the HPC Series the threaded probes allow mounting into a drill and tapped hole, or bracket where more limited access is available. The probe is held in place with a mating nut (optional) and may be rotated for fine axial positioning.

NOTES: (cont'd)

5. Millimeter dimensioned probes are available.

6. Maximum of 2000 pF cable capacitance load.

7. Sensor must be calibrated with final length of cable for stated results

*

HPT - 40	HPT - 75	HPT - 150	HPT - 375	HPT - 500
		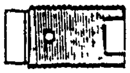	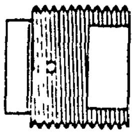	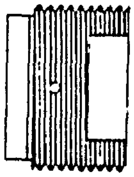
SENSOR OD: 0.040 (1.016)	SENSOR OD: 0.075 (1.905)	SENSOR OD: 0.150 (3.810)	SENSOR OD: 0.375 (9.525)	SENSOR OD: 0.500 (12.70)
CASE OD: 0.187 (4.750)	CASE OD: 0.250 (6.350)	CASE OD: 0.375 (9.525)	CASE OD: 0.750 (19.05)	CASE OD: 1.000 (25.40)
LINEAR RANGE: 0.020 (0.508)	LINEAR RANGE: 0.050 (1.270)	LINEAR RANGE: 0.100 (2.540)	LINEAR RANGE: 0.250 (6.350)	LINEAR RANGE: 0.375 (9.525)
THREAD SIZE: 10 - 32 UNF	THREAD SIZE: 1/4 - 28 UNF	THREAD SIZE: 3/8 - 24 UNF	THREAD SIZE: 3/4 - 16 UNF	THREAD SIZE: 1 - 12 UNF

RANGE SPECIFIED IN INCHES (MILLIMETERS)
THREAD SIZE DEFINED AS FIRST NUMBER = DIAMETER (3/8), SECOND NUMBER THREADS PER INCH (24)

EXAMPLE: **HPT-150A-A-L2-5-M**

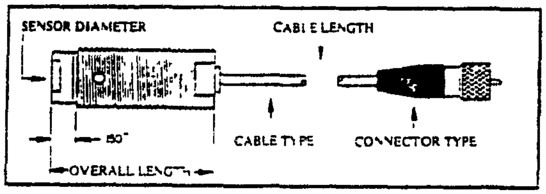

PROBE ORDERING FORMAT

HPX -	**XXX** -	**X** -	**X** -	**XX** -	**XX** -	**X**
CASE STYLE	SENSOR DIAMETER	PROBE LENGTH	OPERATING TEMPERATURE	CABLE TYPE	CABLE LENGTH	CONNECTOR TYPE
C - Cylindrical	MILS	A - .500"	A- 32 to 300°F	L2 - 093 coax (E)	FEET ✱←	M - 10-32 Microdot
B - Button	(0254)	B - 625"	(0 to 150°C) ✱←	L3 - 063 coax (E)	(304 8)	B - BNC
T - Threaded	✱→	C - .750" ✱←	E - 100 to 400°F	I2 - 125 coax (E)		
R - Rectangular(optional)		D - .875"	(-73 to 205°C)	N - 125 Inconel Braided (S)		
S - Flat (optional)		E - 1.000"	V - 100 to 1600°F	N3 - .078 Inconel Braided (S)		
		F - 1 250"	(-73 to 871°C)	T - .063 Inconel Solid Sheathed (V)		
		G - 1.500"	S- 100 to 1832°F	(Temperature range)		
		H - 1.750"	(-73 to 1000°C)			
		I - 2.000"	Consult factory			

PROBE THICKNESS
A - .093 (2 36)
B - 065 (1.65)
C - .125 (3 17)

EXAMPLE: **HPB-75B-E-L3-B**

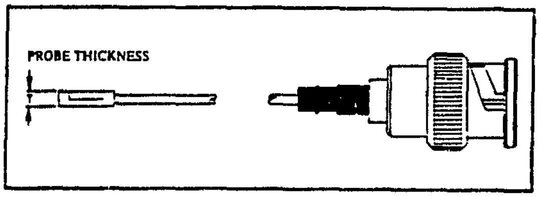

HP PROBE SERIES

Capacitec® non-contact displacement probes are noted for their large linear range versus the small outside diameter of the probe package The sensor component averages the surface it "sees" in front of it (not through the material) and does 95% of the sensing A guard ring adds to the linearity of the sensor by eliminating degrading "side viewing" fringe lines (driven at a maximum potential of 20 volts P-P). A third flexible case component is added on the HPC, HPT and optional on the HPB series probes for use as a desired clamping body All components are electronically isolated from each other by greater than 20 megohms of leakage resistance (at room temperature) for best o[illegible]ion with the instrumentation. A 20 point archived calibration record of voltage output versus nominal displacement is provided standard with every probe.

SPECIFICATIONS

Target Surface Material. Electrically conductive (100 $ohm^{-1} cm^{-1}$) typically or high dielectric constant referenced to grounded surface.

Maximum Range: Approximately the same as the diameter of the sensor element (Minimum range is touch or 0 1% of full scale)

Linearity ±0 2% of full scale value or better with Model 4100-SL, -L, 3200, 3101-SP and 3201-SP.

Repeatability ±0 01% of full scale value with all 4000 and 3000 Series instrument amplifiers. Resolution and repeatability are the same for general comparison

Probe Size 0 025" (0 635 mm) OD to 4 00 (101.6 mm) overall diameter available along with rectangular shaped elements

Cable Type: 99 9% shielded low noise coaxial with driven braided shield (maximum potential 20 volts P-P), 5 feet (1 524 meters) standard 2000pF maximum probe capacitive load

Probe Interchangeability. ±10% of full scale maximum change, ±2% typical.

Probe Material Composition A and E, stainless steel 303, V, Inconel 600, other materials available. (Consult factory)

PROBE ORDERING NOTES

- 21 numbered standard calibrations are available, please specify when ordering. (Consult factory)
- Standard listed ranges are ratios from 0-10 000VDC analog output, but each probe may be calibrated with several range versus sensitivity calibrations. Calibration sensitivity from 0 001VDC/0.001" (.0254) to 10 000VDC/0 001" (0254) are available.
- Range is defined as from touch to full scale reading, ±50% of range = ±10.000 VDC calibration optional.
- Type N and I 2 cable are only available with BNC connector type.
- "B" thickness button probes are only available with Type L3 and T cable.
- "C" thickness button probes are only available with Type I2 and N cable
- -D dip coatings prevent the electronically driven sensor/guard elements from being accidentally earth grounded and shorted

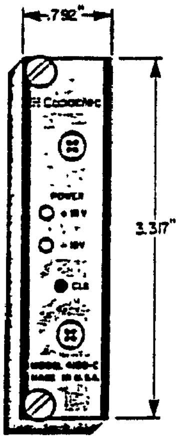

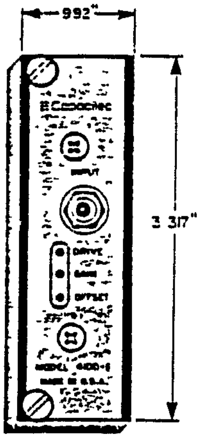

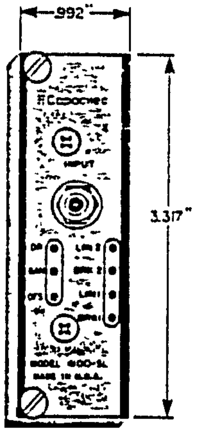

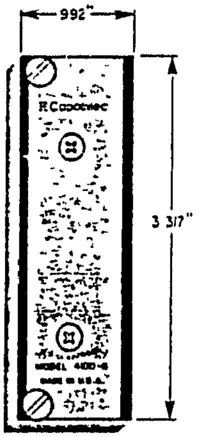

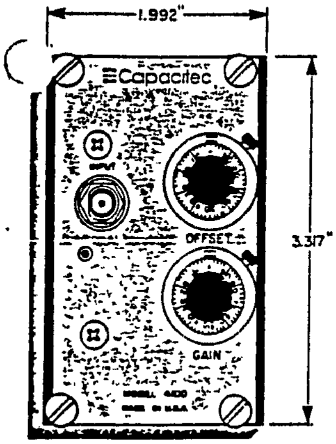

4100: Same as the 4100-S except the screwdriver adjustment pots have been replaced with large counting style offset and gain dials, and a double width front panel of 2.0 inches and ±2% linearity 0.01% repeatability of full scale are typical
(2 slot rack requirement)

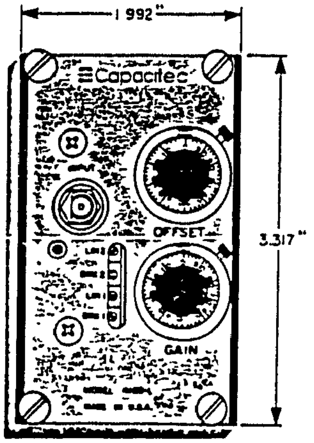

4100-L: Same as the 4100 except that the optional linearization board has been added to yield the same performance as the 4100-SL card but with the convenience of the large adjustment dials ±0.2% linearity and 0.01% repeatability of full scale are typical
(2 slot rack requirement)

NOTE: Instrumentation amplifiers come standard with 232HZ, -3dB frequency response ith 18dB/octave roll-off. Specify options -WB with 3.5kHZ, -3dB or -5WB with 0kHZ, -3dB.

An additional x1 to x6 screwdriver adjustable amplitude control is provided standard on 4100-S, SL, 4100 and -L to have a total of 3 x 6 = 18 V P-P drive amplitude capability.

Model 4100-SL and -L amplifiers have A + B / A - B sums amplifier standard. Consult factory

4100 SERIES AMPLIFIERS

4100-C: A separate clock driver card is required to drive 1 or more amplifier cards. This unit indicates the "on" condition of the ±15 volts DC supply voltage with individual red LED lights and has a x3 amplitude drive adjustment pot for supplying a 15kHZ excitation signal. This control is used to match a required calibration sensitivity to a specific model displacement probe (1 clock, 0.80 wide normally fits in a far right slot)

4100-S: A basic single channel amplifier card with a 1.0 inch rack mountable front panel. A screwdriver implemented offset and gain control is available and ±2% of full scale typical linearity with 0.01% repeatability. It is ideally suited for OEM and high volume multi-point applications where computer interface and possible linearization is available
(1 slot rack requirement)

4100-SL: The same as the 4100-S except that an add on linearization board gives the basic amplifier an enhanced stand alone linearity of ±0.2% accuracy of full scale using only screwdriver adjustable pots. (1 slot rack requirement)

4100-B: A one inch wide blank panel is available to cover any empty slots to prevent damage to internal parts due to dust, dirt and accidental factors

4000 SERIES

The Series 4000 Capacitec® amplifiers and racks were designed to offer the best signal to noise ratio and wide band width response options in a simple modular package. Utilization of individual pins in a 32 pin DIN connector increases reliability for more industrial applications where vibrations are present The small Euro-style 2U size boards have appeal for small portable packaging as well as high (but lightweight) density applications. Similar to the Series 3000 Capacitec® amplifiers in operation (3101-SP, 3200, 3201-SP), when coupled with Capacitec® non-contact displacement probes, they produce a linear output voltage proportional to the gap spacing between the probe and a ground plane. The systems are designed to produce stable and reliable operation with excellent gain and zero stability with respect to changes in ambient temperature Stability is achieved with a digitally derived sine-wave oscillator, having a crystal clock as the frequency reference.

Other special features include synchronous detection, low drift operational amplifiers and a modular preamplifier (PC-201B) and power supply (standard) The units also have an optional linearization board to improve performance by a factor of ten from ±2% to ±0.2% linearity with no outside computer compensated curve fitting and without sacrificing frequency response (to 5kHZ down 3dB) The amplifiers are designed to operate with every probe configuration and all sensitivity ranges by simple recalibration without internal part changes.

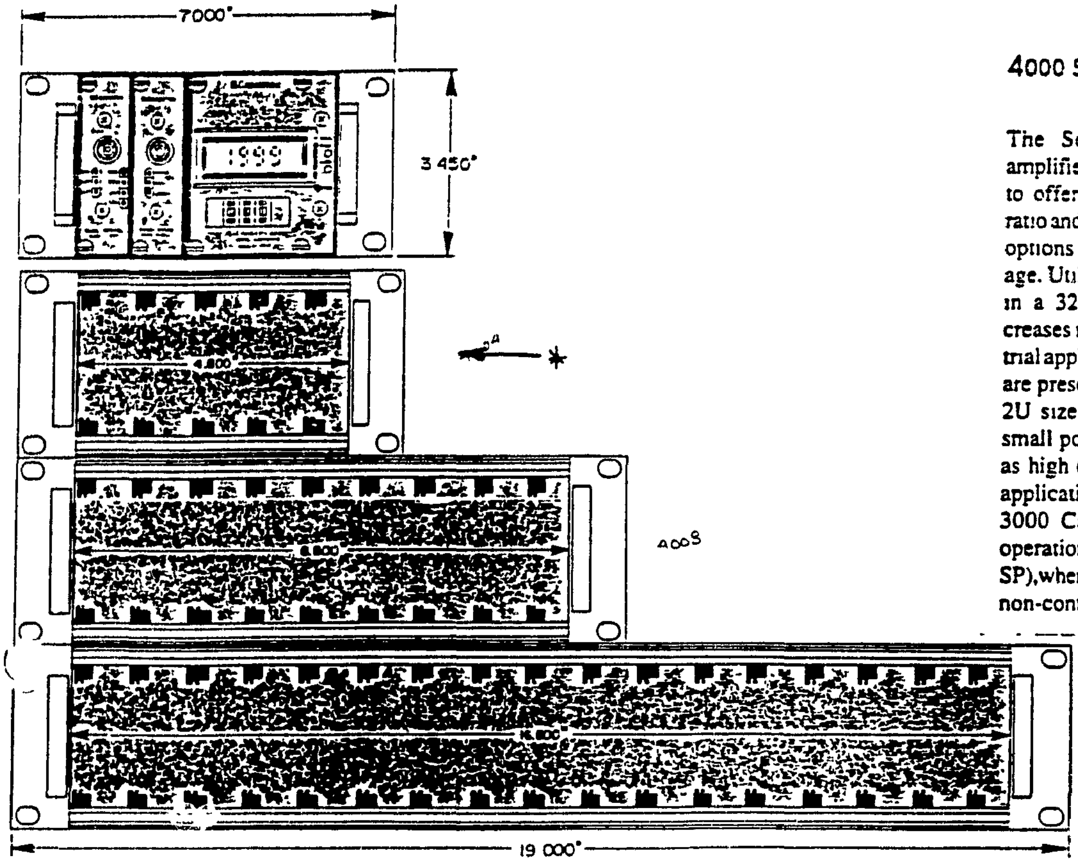

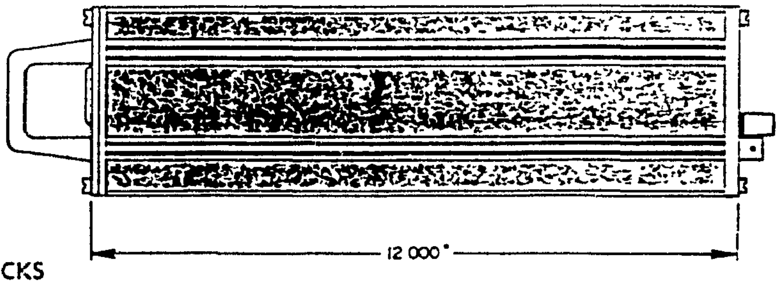

4000 SERIES RACKS

4016-P115: 16 Channel (with 4100-S or 4100 SL), 19 inch rack enclosure with an additional slot for a 4100-C clock driver card A ±15VDC regulated power supply at 850mA is standard to power this unit. (A linear type is preferred for lowest signal to noise performance) The [illegible] as individual 0-10VDC analog outputs as well as [illegible] input/outputs on a mass terminated 50 pin phone style connector for computer or data acquisition interface and option cards An internal AC power supply is available standard by signifying -P115, -P220 or -P240 (AC)

4008-P115: 8 Channel (with 4100-S or 4100-SL) rack closure approximately half the size of the 4016 with the same standard features A ±15VDC regulated power supply at 500mA is standard to power this unit

4004-P115: 4 Channel (with 4100-S or 4100-SL) rack enclosure approximately 5 inches wide with the same standard features but without the 50 pin phone connector A ±15VDC regulated power supply at 350mA is standard to power this unit.

*